Title
Single-molecule studies of DNA dynamics and intermolecular forces

Author
Robertson, Rae Marie

Publication Date
2007

Peer reviewed|Thesis/dissertation

UNIVERSITY OF CALIFORNIA, SAN DIEGO

Single-Molecule Studies of DNA Dynamics and Intermolecular Forces

A Dissertation submitted in partial satisfaction of the
Requirements for the degree Doctor of Philosophy

in

Physics

by

Rae Marie Robertson

Committee in charge:

Professor Douglas E. Smith, Chair
Professor Joseph Goddard
Professor David Kleinfeld
Professor J. Andrew McCammon
Professor Jose Onuchic

2007

The Dissertation of Rae Marie Robertson is approved, and it is acceptable in quality and form for publication on microfilm:

Chair

University of California, San Diego

2007

TABLE OF CONTENTS

LIST OF FIGURES

LIST OF TABLES

ACKNOWLEDGEMENTS

I would like to thank my advisor, Dr. Douglas Smith, for all of his support and guidance, and for trusting me enough to give me freedom and independence in my research. I would like to thank my committee members for all of their advice, support, and encouragement. I would like to thank Ron Larson for all of his help in interpreting my results and understanding polymer theory, and for his genuine interest in my research. I would like to thank Stephan for showing me the ropes around the lab, for guiding me through the first stages of our research, and for always being a friendly face I could count on. I would like to thank Derek and Dorian for their friendship and support, and for wasting a lot of my time watching YouTube in the office. I would like to thank Al Schweitzer for his ingenious technical support. I would like to thank everyone in the UCSD Physics Department for their support and encouragement. I would like to thank all of my family and friends for their love and support. I would especially like to thank my boyfriend Mike for going through every step of this process with me, for always listening to me and understanding me, and for being my best friend. Finally, I would like to thank my parents for their unwavering support, love, and pride, and for encouraging me to pursue my dreams even though they were in California.

Chapter 2, in part, is a reprint of the material as it appears in Macromolecules. Laib, S., Robertson, R. M. & Smith, D. E. *Macromolecules* **39**, 12, 4115-4119 (2006). The dissertation author was the secondary investigator and author of this paper.

Chapter 3, in part, is a reprint of the material as it appears in Proceedings of the National Academy of Sciences. Robertson, R. M., Laib, S. & Smith, D. E. *Proceedings of the National Academy of Sciences U.S.A.* **103**, 19, 7310-7314 (2006). The dissertation author was the primary investigator and author of this paper.

Chapter 4, in part, is a reprint of the material as it appears in Proceedings of the National Academy of Sciences. Robertson, R. M. & Smith, D. E. *Proceedings of the National Academy of Sciences U.S.A.* **104**, 12, 4824-4827 (2007). The dissertation author was the primary investigator and author of this paper.

Chapter 5, in part, is a reprint of the material as it appears in Macromolecules. Robertson, R. M. & Smith, D. E. *Macromolecules* **40**, 9, 3373-3377 (2007). The dissertation author was the primary investigator and author of this paper.

Chapter 6, in part, is a reprint of the material as it appears in Physical Review Letters. Robertson, R. M. & Smith, D. E. *Physical Review Letters* **99**, 12, 126001 (2007). The dissertation author was the primary investigator and author of this paper.

Chapter 7, in part, is a reprint of the material as it appears in Macromolecules. Robertson, R. M. & Smith, D. E. *Macromolecules* **40**, 27, 8737-8741 (2007). The dissertation author was the primary investigator and author of this paper.

VITA

2003 Bachelor of Science with Honors, Georgetown University

2005 Master of Science, University of California, San Diego

2007 Doctor of Philosophy, University of California, San Diego

PUBLICATIONS

Robertson, R. M. & Smith, D. E. Direct measurement of the confining forces imposed on a single molecule in a concentrated solution of circular polymers. *Macromolecules* **40**, 27, 8737-8741 (2007).

Robertson, R. M. & Smith, D. E. Direct measurement of the intermolecular forces confining a single polymer in an entangled polymer solution. *Physical Review Letters* **99**, 12, 126001 (2007).
*highlighted in: Larson, R. G. Going with the flow. *Science* **318**, 5847, 57-58 (2007).
*selected for publication in *Virtual Journal of Biological Physics Research* **14**, 7 (2007).

Robertson, R. M. & Smith, D. E. Self-diffusion of entangled linear and circular DNA molecules: Dependence on length and concentration. *Macromolecules* **40**, 9, 3373-3377 (2007).

Robertson, R. M. & Smith, D. E. Strong effects of molecular topology on diffusion of entangled DNA molecules. *Proceedings of the National Academy of Sciences U.S.A.* **104**, 12, 4824-4827 (2007).

Robertson, R. M., Laib, S. & Smith, D. E. Diffusion of isolated DNA molecules: Dependence on length and topology. *Proceedings of the National Academy of Sciences U.S.A.* **103**, 19, 7310-7314 (2006).

Laib, S., Robertson, R. M. & Smith, D. E. Preparation and characterization of a set of linear DNA molecules for polymer physics and rheology studies. *Macromolecules* **39**, 12, 4115-4119 (2006).

Fuller, D. N., Raymer, D. M, Rickgauer, J. P., Robertson, R. M., Catalano, C. E., Anderson, D. L., Grimes, S. & Smith, D. E. Measurements of single DNA molecule packaging dynamics in bacteriophage lambda reveal high forces, high motor processivity, and capsid transformations. *Journal of Molecular Biology* **373**, 5, 1113-1122 (2007).
*featured as cover story in Nov 9 issue of *Journal of Molecular Biology*

FIELDS OF STUDY

Major Field: Physics

Studies in Granular Media Physics
Professor Jeffrey S. Urbach

Studies in Polymer Physics and Biophysics
Professor Douglas E. Smith

ABSTRACT OF THE DISSERTATION

Single-Molecule Studies of DNA Dynamics and Intermolecular Forces

by

Rae Marie Robertson

Doctor of Philosophy in Physics

University of California, San Diego, 2007

Professor Douglas E. Smith, Chair

DNA molecules were used as a model system to investigate fundamental problems in polymer physics; namely, how molecular length, topology and concentration influence the dynamical properties of polymers. A set of DNA molecules suitable for polymer studies was prepared using molecular biology techniques. Video fluorescence microscopy and single-molecule tracking were used to determine self-diffusion coefficients of DNA molecules. Optical tweezers were used to measure the intermolecular forces confining entangled DNA molecules. Scaling of diffusion with molecular length was in agreement with the Zimm model for dilute solutions of linear and circular DNA, indicating that excluded volume effects

are appreciable for both topologies. Scaling of diffusion with concentration was also determined for the four possible topological combinations of linear and circular molecules: linear DNA diffusing in a solution of linear DNA, linear DNA in circular DNA, circular in circular, and circular in linear. For lower concentrations molecular topology had little effect and scaling was in agreement with that of the Rouse model. As concentration was increased topology played a much larger role and scaling crossed over to that of the reptation model, predicted to describe the dynamics of entangled polymers. The notable exception was the strongly hindered diffusion observed for a circular molecule diffusing in an entangled linear solution, suggesting the importance of constraint release. Using a new experimental approach with optical tweezers, a tube-like field confining a single entangled molecule was measured, in accord with the key assumption of the reptation model. A time-dependent harmonic potential opposed displacement transverse to the molecular contour, and the force relaxations following displacement were composed of three distinct modes. A characteristic tube radius of the entangled solution was also determined, close to the classically predicted value. The dependence of the above findings on molecular topology and concentration was also investigated. In particular, for an entangled solution of circular DNA of the same length and concentration, the confining tube radius was 25% smaller and the longest relaxation time was ~3 times shorter than with linear DNA. For large displacements the confining force for circular DNA was also substantially lower and shorter range than that measured with linear DNA.

Chapter 1

Introduction to Polymers

1.1 A polymer is…

A polymer is a molecule consisting of a chain of repeating subunits known as monomers. There are many naturally occurring biopolymers including DNA, RNA and proteins that are fundamental to living organisms. Polymers also make up many of the materials we encounter everyday, including shampoo, chewing gum, rubber, and petroleum. The lengths of the polymers as well as the environments in which they reside play a large role in determining the properties of these substances.

A polymer is a very complex molecule, and thus in a polymer solution or melt (where no solvent is present) many complex intra- and intermolecular interactions give rise to intriguing non-Newtonian fluid properties unique to polymer solutions. One such property is viscoelasticity. Viscosity, a property of all fluids, is a measure of the resistance of the fluid to deform under stress, or the internal friction of the fluid. Viscous fluids resist deformation linearly with time. Elastic materials, typically solids, deform and relax back to there initial configuration instantaneously. Polymer solutions and melts are unique in that they exhibit both viscous and elastic properties when subject to deformation.

1.2 Universal Properties of Polymers

1.2.1 Universality: A theoretical approach

The chemical structure and size of specific polymers, and the monomers of which each consists, vary widely. However, there are many fundamental properties that all polymers share, and coarse-grained theoretical models have been established whereby one can ignore the detailed atomic structure of the individual monomers making up the polymers (1, 2). The simplest example of such a model is that of the freely-jointed chain. Here, the polymer is divided into N segments of length b, each connected to its neighbor by a freely rotating joint. The unit length or monomer is thus b, termed the Kuhn length, and the contour length of the polymer is defined in terms of the Kuhn length, i.e. $L = Nb$. "Freely-rotating" joints are such that there is no correlation between connected links (no preferred direction), so the polymer can be modeled as a random walk in space with step size b (Figure 1.1). By characterizing all polymers in terms of N and b, comparison between numerous, chemically different polymers is possible. More complex models such as the bead-spring model and the worm-like chain (WLC) model (see section 1.2.2) are examples of corrections to the approximate freely-jointed chain model.

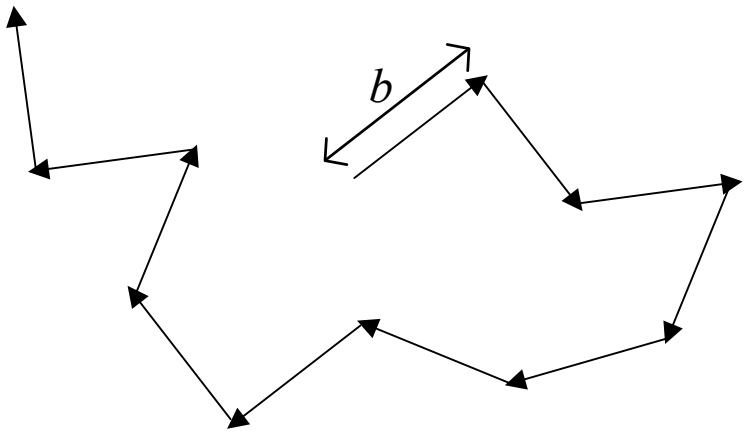

Figure 1.1 Freely-jointed chain model of polymer with Kuhn length (step size) *b*.

1.2.2 Flexibility

The flexibility of a polymer has a large effect on its dynamics, and polymers are typically divided into three classes based on their flexibility: rigid rod, semiflexible and flexible polymers. Flexibility is usually determined by the relative length of the polymer (i.e. the number of monomers *N* making up the polymer) as well as the thickness of the chain compared with its length. Rigid rod polymers (typically $N \cong O(b)$) are essentially stiff filaments, so the intramolecular interactions are simplified because one only has to be concerned with nearest-neighbor interactions. However, the orientation and rotational dynamics of rigid rods are of interest and have been the focus of theoretical and experimental work (1, 3-5).

Flexible polymers, on the other hand, are composed of many Kuhn lengths ($N >> b$), and the freely-jointed chain model can often accurately predict their properties and dynamics. However, with highly flexible polymers one has to take into account both short-range and long-range intramolecular interactions (Figure 1.2), and thus the

polymer cannot always be modeled as a simple random walk. This *excluded volume* effect can be accounted for by modeling the polymer as a *self-avoiding* random walk (SAW). SAW is a random walk with the added constraint that no two polymer segments or joints can occupy the same space.

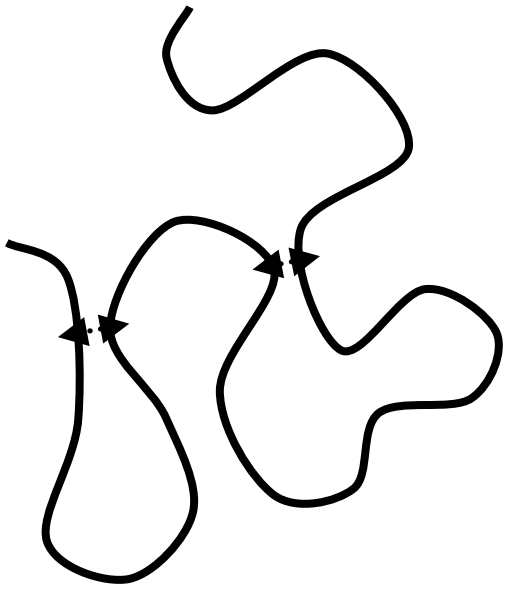

Figure 1.2 A flexible polymer. The dashed arrows indicate the long-range repulsive interactions, collectively termed the excluded volume effect.

Semiflexible polymers lie between rigid rods and flexible polymers, where the freely-jointed chain model begins to break down. More detailed models such as WLC are often better suited for describing the properties of semiflexible chains. In the WLC model the polymer is a continuous bendable entity rather than the discrete jointed segments of the freely-jointed chain model. The relevant length scale, the persistence length P, is the characteristic length over which spatial correlations are still

apparent. At $2P$ all correlations are essentially lost, so this model can be compared to that of the freely-jointed chain by assuming $b = 2P$. While the modeling of short-range interactions is more complicated for semiflexible polymers, one can often ignore long-range intramolecular interactions. DNA is typically classified as a semiflexible chain, however, depending on its length and topology, it can be both a rigid rod and flexible chain as well. This thesis is concerned primarily with flexible chains and unless otherwise noted all discussion will be for flexible polymers.

1.2.3 Radius of Gyration

As mentioned above, the freely-jointed chain model allows one to model a polymer as a random walk in space. Because there is no preferred direction of excursion for the polymer segments (as in all random walks), the average configuration of the polymer is that of a random, sphere-like coil (Figure 1.3). The coil size can be determined from the mean square end-to-end distance of the polymer $\langle R^2 \rangle = Nb^2$, giving us the scaling law $\langle R^2 \rangle^{1/2} \sim N^{1/2} \sim L^{1/2}$. The *radius of gyration* R_G, most often used to describe the size of a polymer coil, is defined as the root mean square distance between *all* pairs of polymer segments (Kuhn lengths) and is related to $\langle R^2 \rangle$ by the relationship $\langle R_G^2 \rangle = (1/6)Nb^2$. Thus, for an isolated, ideal polymer (that modeled by a simple random walk) the radius of gyration is predicted to scale with the length of the polymer as $R_G \sim L^{1/2}$.

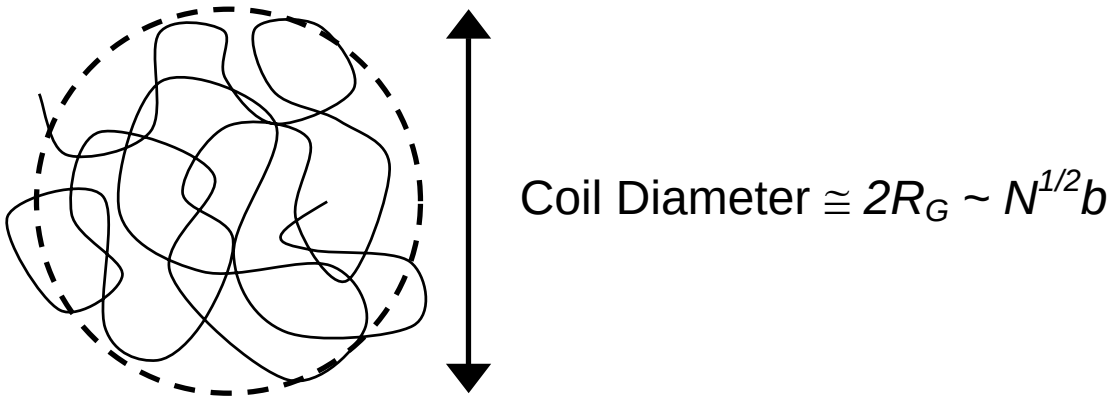

Figure 1.3 Random coil configuration of an ideal polymer.

1.2.4 Topology

Up to this point in the discussion, all polymers were assumed to be linear chains. While most theories and experiments deal with linear chains, polymers are not limited to linear topology. In fact, DNA molecules occur naturally in three topological forms: linear, supercoiled, and relaxed circular (ring conformation with no supercoils). Multiple theories designed for linear polymers have been extended to both circular and branched polymers (6-8), although a consensus on the correct approach to modeling such topologies has yet to be reached. A main focus of this thesis is the differences that arise when altering the topology of a polymer.

1.3 Polymer Solutions

The environment in which a polymer resides plays a critical role in determining its properties and dynamics. Polymers can be dissolved in many types of solvents and the solvent properties and the polymer-solvent interactions affect the

polymer behavior. The ratio of solvent to polymer also strongly alters polymer conformation and dynamics.

1.3.1 Solvent Conditions

Polymers can be dissolved in three classes of solvents defined by the effect of the solvent on the polymer properties. Polymers can also make up melts in which no solvent is present. Good solvent conditions are such that the polymer avoids interactions with itself, causing excluded volume effects to become important. The polymer coil swells as it avoids self-interactions and a SAW best describes its configuration. Poor solvents are such that the polymer avoids interaction with solvent molecules which causes the polymer to pack tightly together (aggregate). A theta solvent is the special condition in which the polymer equally favors interactions with both itself and solvent molecules and thus an ideal random coil (no excluded volume) can describe polymer configuration. All experiments described in this thesis are carried out in good solvent conditions, so the theory discussed will be for such conditions unless otherwise noted.

1.3.2 Concentration Regimes

Polymer solutions are typically divided into three concentration regimes, dilute, semidilute and concentrated, each of which can be described by a different theoretical model. The specific concentration range over which each of these models acts differs from polymer to polymer; however, for each polymer one can determine the concentration at which the polymer coils begins to overlap, defined as $c^* = (3/4\pi)M/N_A R_G^3$ where M is the polymer molecular weight and N_A is Avogadro's

number. Representing concentrations in terms of c^* allows for comparison between concentration regimes of different polymers. The dilute regime ($c < c^*$) is such that the individual polymers are essentially isolated and only the polymer's interaction with itself and the solvent molecules need to be considered. The onset of the semidilute regime occurs when the polymers begin to overlap each other ($c \geq c^*$) in which case the effect of the surrounding polymers (intermolecular interactions) needs to be considered. As the concentration is increased further the molecules become entangled with each other (provided they are of sufficient length). The onset of the concentrated regime occurs when the polymers become well entangled, and the concentration at which this occurs is the *critical entanglement concentration* $c_e > c^*$.

1.3.2.1 Dilute Regime: Zimm Model

In dilute solution individual polymer molecules are very far apart from each other, so intermolecular interactions can be neglected. P. E. Rouse was the first to attempt to describe the dynamics of dilute polymer solutions (9). He modeled the polymer as a string of beads, each separated by a distance b, and considered the Brownian motion of each bead. Here, the motion of any bead is assumed to be due to the force acting on it by the solvent molecules, which simply depends on the friction constant of the bead ($\zeta = 6\pi\eta_s d$ where η_s is the solvent viscosity and d the bead diameter). The only interaction energy term considered is the elastic potential between segments due to the connectivity of the chain. Thus, the Rouse model assumes that the dynamics are governed solely by localized interactions along the polymer.

However, in dilute solution, distant polymer segments of a single polymer can interact with each other by perturbing the solvent molecules. A perturbation of one polymer segment in turn perturbs the surrounding solvent molecules. This perturbation travels through the solvent (induces fluid motion) and affects other polymer segments in the surrounding area. Such indirect intramolecular interactions, mediated by solvent molecules, are termed *hydrodynamic interactions* (HI). B. H. Zimm first introduced a model that took HI into account by extending the Rouse model to include non-localized interactions (10).

Zimm also took into account excluded volume effects, important for flexible polymers in good solvent (the case of interest in this thesis). P. J. Flory was the first to consider excluded volume effects when determining the size of a polymer (11). He did so by introducing a second, repulsive interaction energy term, which gives the scaling law $R_G \sim L^{\nu}$ where $\nu \cong 3/5$ (1). Zimm introduced a similar repulsive interaction term into his model for dilute solution polymer dynamics. The Zimm model predicts that the self-diffusion coefficient D is inversely proportional to R_G, giving us the scaling law $D \sim L^{-\nu}$ with $\nu \cong 0.588$. The exact value is predicted to be $D = 0.203k_BT/(\sqrt{6}\eta_s R_G) = 0.203k_BT/(\eta_s N^{\nu} b)$ (1).

1.3.2.2 Semidilute Regime: Rouse Model

The semidilute regime begins when the polymers start to overlap each other, in which case both the excluded volume effect (repulsive interactions) as well as attractive intramolecular interactions caused by surrounding polymers must be considered. The solution is more homogenous than the dilute case, and the relevant

length scale becomes the *mesh size* of the solution, which is the average spacing between polymer segments (Figure 1.4). For length scales larger than the mesh size the repulsive and attractive interactions exactly cancel with each other giving us once again an ideal polymer coil with $R_G \sim L^{1/2}$.

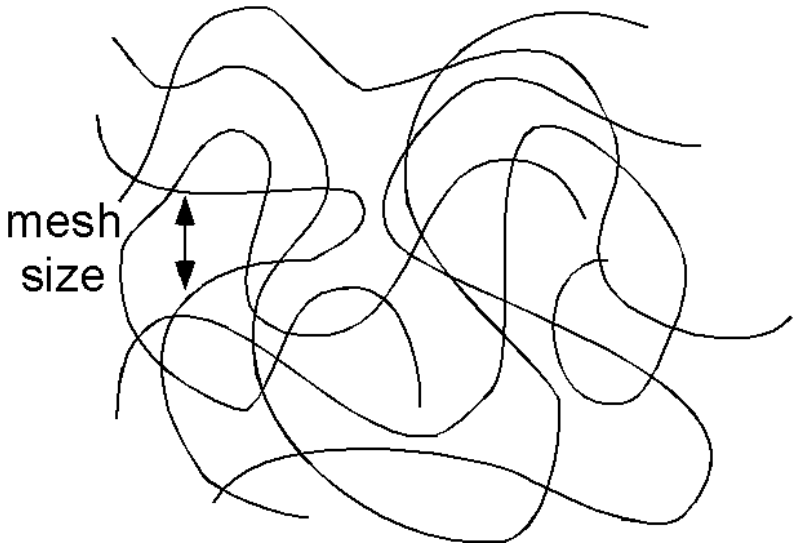

Figure 1.4 Schematic of a semidilute polymer solution. The average spacing between polymers, the *mesh size*, is indicated by the arrows.

The surrounding polymers also act to significantly reduce the effect of HI. Because fluid velocity arising from a point source falls off as $1/\eta_s r$ where r is the distance from the source, in dilute solution, where the fluid is pure solvent, this effect is long range. However, in semidilute solution, for length scales larger than the mesh size, the presence of the polymers must be considered, so η_s becomes the macroscopic viscosity η of the polymeric fluid, which is much larger than that of pure solvent. Because the fluid velocity decreases much faster in semidilute solutions, HI can be

neglected for lengths larger than the mesh size (1). Interestingly, the Rouse model, originally developed for dilute solutions, neglects both excluded volume effects and HI, and thus accurately describes the dynamics in semidilute solutions. The Rouse model predicts the scaling law $D \sim R_G^{-2} \sim L^{-1}$. In this regime the self-diffusion coefficient also depends on the concentration of the solution and the predicted scaling is $D \sim c^{-1/2}$.

1.3.2.3 Concentrated Regime: Reptation Model and Blob Theory

The reptation model, developed by P.G. de Gennes and extended by Doi and Edwards and others, has been extremely successful in describing the dynamics of entangled polymers (1, 2, 12, 13). The key concept of the reptation model is that each polymer is confined to move in a tube-like region parallel to its contour. The molecule can only escape from its tube (and consequently form a new tube) by diffusing "head-first" in a direction parallel to its contour, a process termed *reptation* (Figure 1.5). The reptation model reduces a complex, many-body problem to that of a one body, mean field problem of which the only essential parameter is the *tube radius a*. Numerous scaling laws concerning the dynamics and response of entangled polymers are derived from this model. For example, the scaling of the self-diffusion coefficient with polymer length and concentration is predicted to be $D \sim L^{-2}c^{-7/4}$.

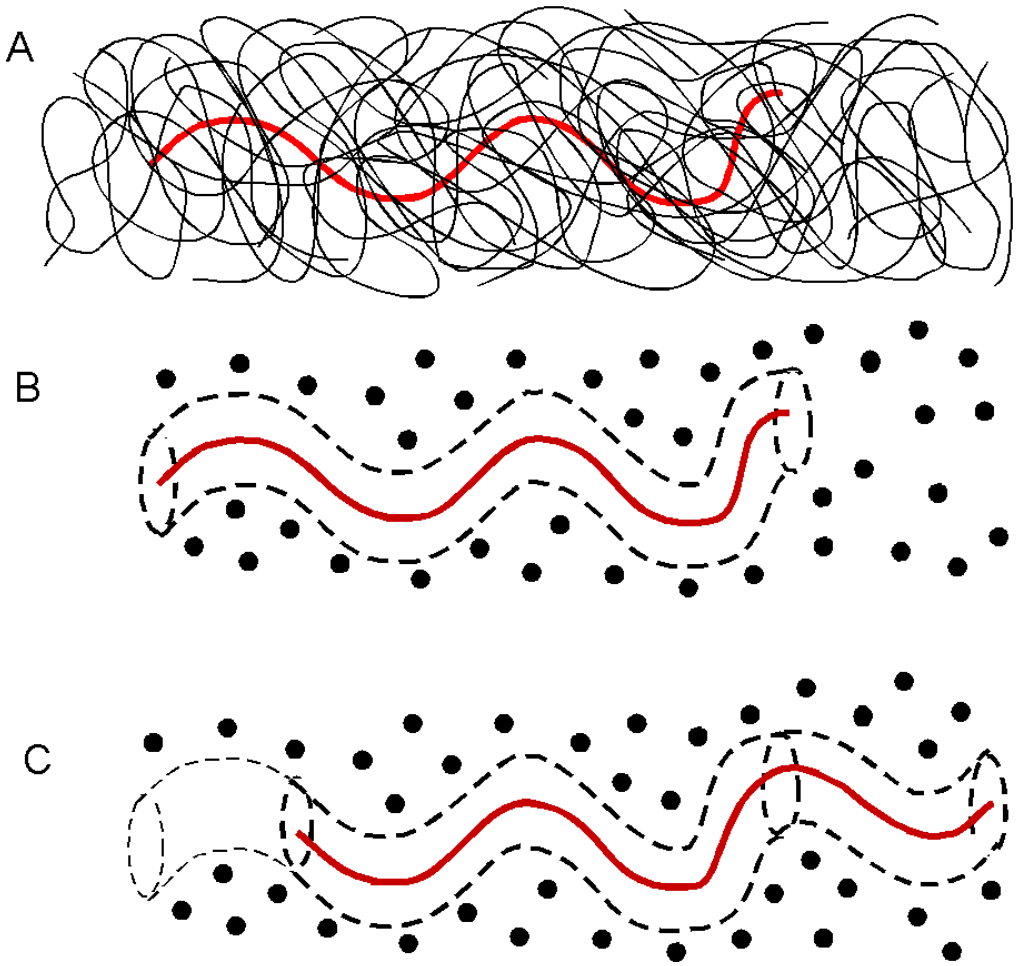

Figure 1.5 Depiction of the reptation model for entangled polymers. **(A)** Schematic of an entangled polymer solution. The polymer of interest is shaded red. **(B)** Theoretically predicted tube, formed by surrounding polymers, that restricts motion transverse to the polymer contour. The black dots represent the constraints formed by the surrounding polymers. **(C)** Reptation of an entangled polymer. As the polymer reptates out of its original tube a new tube is formed as the old one disappears (represented by the thin segment of the tube).

The reptation model was originally designed for polymer melts, and thus did not include solvent interactions. However, "blob" theory successfully extended this model to polymer solutions (12, 14). In the reptation model, the smallest relevant length scale, or unit length, is the monomer size *b*. Blob theory divides each polymer

into "correlation blobs" of size $\xi = R_G(c/c^*)^{-\nu/3\nu-1}$ where $\nu \cong 0.588$ (15). Each blob contains both polymer and solvent, and the blob size is defined as the point at which there is equal probability of finding either segments of the polymer of interest or segments of the surrounding polymers. The unit length becomes ξ rather than b and the solution is modeled as a melt of polymers with monomer size ξ.

1.4 Simulations and Classical Experimental Techniques

Classically, static and dynamic information about polymers and polymeric fluids have been experimentally investigated by examining the bulk properties of the fluid. Simulations, using various methods for modeling the polymers, solvent, molecular interactions, etc., have also played a large role in advancing understanding of polymers and polymeric fluids. Further discussion of these techniques can be found in Reference 2. Recently developed single-molecule techniques, which allow for the direct measurement of molecular conformation and dynamics, will be discussed in Chapter 2.

1.4.1 Rheology

Rheology refers to the study of bulk viscoelastic properties of polymeric fluids by examination of fluid deformation and flow following an applied strain. Shear flows are the most common strain used in rheological measurements. Theories describing the response of polymers to such strains have been extended to predict the bulk fluid properties arising from the molecular response. Thus rheological

measurements can be compared with these theories to infer molecular properties of the polymeric fluids.

A shear flow can be induced by placing a polymeric fluid between two parallel disks with radius *r* and separation *h* and rotating one disk at a set frequency ω relative to the other. The induced stress σ on the fluid, or force needed to rotate the disk at a set strain rate $\dot{\gamma} = \omega r/h$, is measured. While the shear stress induced in a Newtonian fluid is a constant $\sigma = \eta\dot{\gamma}$, in polymer fluids $\sigma(t)$ is time-dependent and can depend on both the strain and strain rate.

A linear response (induced from a small shear strain γ) is such that $\sigma(t)=G(t)\gamma$ where $G(t)$ is the time-dependent relaxation modulus. $G(t)$ is a measure of the relaxation of stress following a strain and is described by a sum of decaying exponentials with distinct relaxation times associated with each. Larger strains can induce a non-linear response in which $G(t)$ becomes dependent on γ as well as $\dot{\gamma}$. The nonlinear response of entangled solutions is predicted to hold important information about the molecular properties and response mechanisms of entangled polymers. One important quantity determined from these measurements is the plateau modulus $G_N^{(0)}$ which is the value of the relaxation modulus at which it becomes time-independent. Entangled polymeric fluids are predicted to exhibit such a plateau over a distinct time scale, and, in principle, the polymer molecular weight (or length) between entanglements as well as the predicted value of the tube radius *a* in the reptation model can be determined from $G_N^{(0)}$.

1.4.2 Light and Neutron Scattering

Scattering experiments exploit the wavelengths and scattering angles of neutrons or laser light to probe the spatial correlations, molecular conformations and dynamics of polymers.

Neutron scattering can determine single-molecule conformations in entangled solutions by replacing the hydrogen atoms of a small amount of the polymers with deuterium during synthesis. Due to the large difference between the scattering cross-sections of hydrogen and deuterium, the conformations of the deuteriated chains can be determined in a highly concentrated melt of mostly non-deuteriated chains. By measuring the scattering angle θ, one can determine the scattering vector $q = \frac{2\pi}{\lambda}\sin\left(\frac{\theta}{2}\right)$. The spatial correlation of the polymer, termed the static structure factor $S(q)$, can be determined from q and the relative distances between chain segments. The radius of gyration can then be determined via the approximate relationship $S(q) \cong 1 - q^2 R_G^2/3$.

A dynamic structure factor can also be determined using neutron spin echo, which exploits the neutron's spin by applying a magnetic field across the sample. The momentum and energy of the scattered neutrons can be measured by examining the spin-rotation, and the time-dependent structure factor can be determined from the Fourier transform of the energy. $S(q,t)$ can provide information about monomer diffusion as well as spatial correlations.

Monochromatic laser light is also used in scattering experiments; however, single-polymer information cannot typically be extracted due to the large wavelength (i.e. spatial resolution) of light compared with neutrons. Therefore, light scattering is only effective for semidilute and dilute solutions with large enough density fluctuations to allow for optical contrast between polymer and solvent.

1.4.3 Simulations

Computer simulation of polymeric fluids is another powerful tool used to investigate polymer conformation and dynamics. An advantage of simulations is the ability to probe short time scale dynamics (i.e. monomer diffusion), inaccessible to many experiments, in order to test the short time scale predictions of classical theories. However, most simulations are unable to also probe time scales comparable to those in most experiments, so direct comparison between experiment and simulation is often not possible. The principal setback for simulations is the inability to efficiently probe a large number of monomers or long time scales which are often needed to effectively model a concentrated polymer solution. Initial simulations, which used simple lattices to represent the space available to the polymers, were unable to accurately imitate an entangled polymer fluid; however, recently, advanced lattice methods such as the bond-fluctuation model have been introduced which more accurately model a polymeric fluid. Real-space (no lattice) molecular dynamics (MD) is another simulation method in which the monomers are beads connected via Hookean springs that interact with each other via Lennard-Jones potentials. Not relying on a lattice has enabled the simulation of highly concentrated polymeric fluids. Brownian dynamics

is yet another method in which physical solvent molecules are replaced by a stochastic force and the polymer is modeled as a bead-spring or bead-rod complex. Coarse-graining out the fast dynamics of the solvent molecules (relative to that of the polymers) enables this method to probe longer time scales important in entangled solutions.

1.5 Conclusions

Polymers are large and complex molecules that come in many different forms. However, all polymers can be related through several universal properties, such as degree of polymerization N, radius of gyration, and flexibility. With models coarse-grained to the Kuhn length, scaling laws can be derived which are applicable to all polymers in a certain regime. Polymeric fluids, which we encounter and rely on everyday, exhibit fascinating behavior that varies based on the properties of the polymers and well as the concentration of the fluid. Much theoretical and experimental effort has been aimed at understanding polymeric fluid behavior and the molecular dynamics that give rise to such bulk properties, and a connection between the macroscopic fluid behavior and the single-molecule dynamics is sought. While much progress has been made in the field over the past ~60 years, many aspects of polymers and polymeric fluids are still not well understood, especially in complicated cases such as entangled fluids and polymers of different topologies.

Chapter 2

Polymer Studies with DNA Molecules

2.1 DNA: A model polymer

DNA is a naturally occurring polymer of great biological importance. In fact, a key motivation for numerous polymer scientists, including pioneers like B. H. Zimm, is the link to DNA (16-18). Over the past few decades DNA has been shown to be a model system for probing fundamental questions in polymer physics (19). Numerous rheological studies as well as single-molecule studies have been carried out on DNA and its behavior has been shown to be akin to that of synthetic polymers (18, 20). Further, DNA stretching experiments have shown that the elasticity of DNA can be accurately described by the WLC model with a persistence length of $P \cong 50$ nm (~150 kilobasepairs (kbp)) (21, 22). Thus, the long DNA molecules ($N > 20$) used in this research can be modeled as flexible polymers with Kuhn length $b \cong 100$ nm.

2.1.1 Advantages to DNA

Beyond the important biological implications, DNA holds several advantages to synthetic polymers as a system for probing fundamental questions in polymer physics. For instance, DNA replication can be used to produce homogeneous samples of *exactly* the same length while synthetic polymer samples often have a distribution of lengths around that desired. In fact, much effort in synthetic polymer studies is devoted to reducing the polydispersity index of the polymers in order to successfully

test polymer theories (which assume homogeneity) and characterize the polymers of interest. DNA topology can also be precisely controlled. For example, supercoiled DNA molecules can be converted to relaxed circular and linear constructs with the use of appropriate enzymes. Studies on synthetic ring polymers, on the other hand, are often hindered by the difficulty of synthesizing a pure sample of ring polymers. During synthesis the rings often become concatenated (linked together) or knotted and linear contaminants are also typically present. Relaxed circular (ring) DNA is prepared by relaxing the supercoils in supercoiled DNA which is initially closed (no free ends) and unknotted. Because there is no step in the conversion that linearizes the DNA (open ends) there is little possibility for the above problematic conformations to occur.

Direct visualization of single molecule conformations and dynamics is possible by staining DNA molecules with fluorescent dyes such as YOYO-I. When blue (480 nm) light is shone on YOYO-I, the dye molecule is excited and emits red (535 nm) light. By using a microscope with a proper set of filters (480 nm exciter filter, 505 nm diachroic mirror, 535 nm emission filter), one can shine purely blue light onto the DNA-dye complex and only allow the red light (that emitted by the dye molecules) coming from the sample to reach the camera. Because the emission intensity of YOYO-I increases over 1000-fold when bound to DNA, only bound molecules will be seen (23). Thus, direct visualization of a single DNA molecule stained with YOYO-I is possible. By using a video camera one can record the real-time dynamics of these molecules. Figure 2.1 is a schematic of the epi-fluorescence setup that I built for the

experiments described in this thesis. While it has been shown that the binding of YOYO-I to DNA increases the contour length and persistence length of DNA by a factor of ~1.35 (24), the number of persistence lengths, elasticity, and conformation of the molecule (those parameters important to polymer studies) remain unchanged upon binding (25, 26).

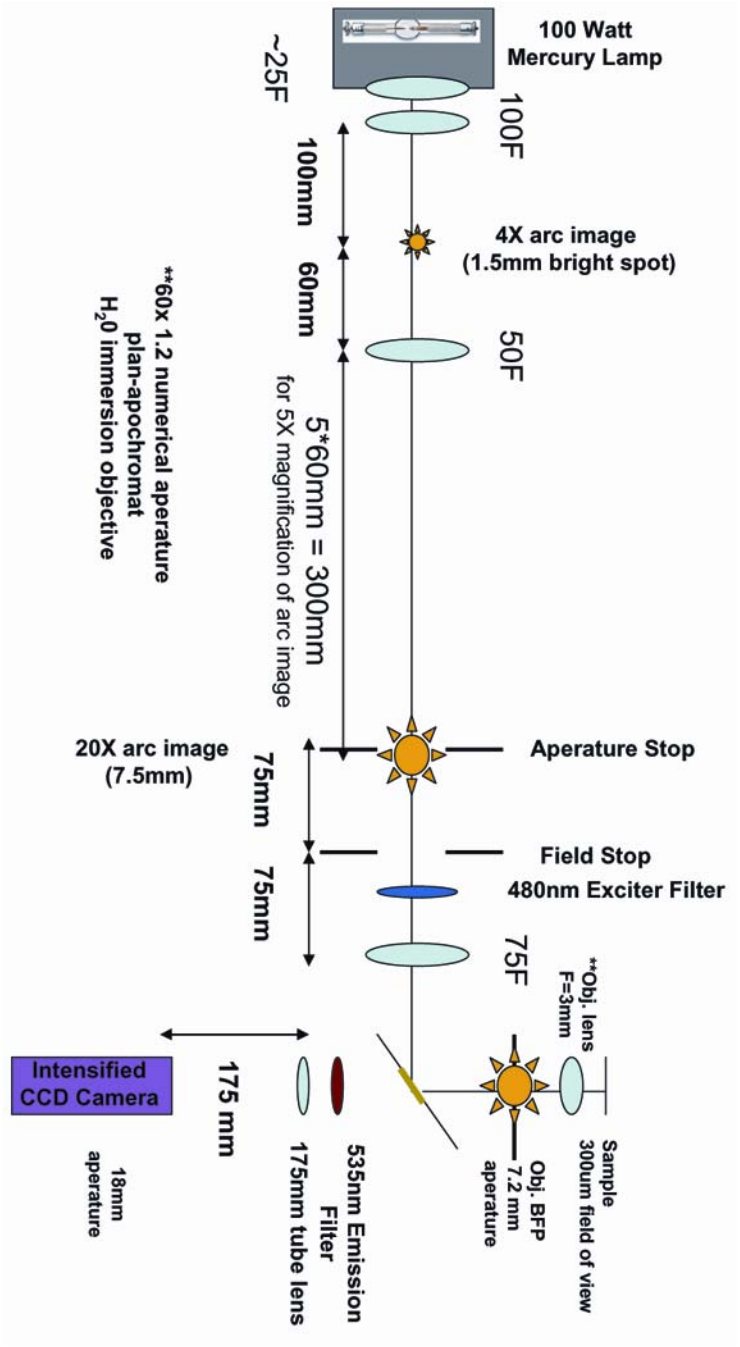

Figure 2.1 Schematic of custom-built epi-fluorescence setup used in thesis work. Placement of optics is such that Kohler illumination is produced. Filter set is designed for visualization of YOYO-I fluorescence.

2.1.2 Single-Molecule Studies

Classically, polymer experiments have been carried out on a large number of polymers and the bulk properties of the fluid have been measured. The individual molecular dynamics then had to be inferred from the fluid properties by relying on theoretical predictions that relate the two. Thus, there was no direct way to test the theoretically predicted behavior of individual polymers. Over the past decade, the development of the single-molecule approach to polymer dynamics, pioneered by S. Chu and others, has allowed for the direct probing of the molecular conformations and dynamics of polymers (27). For example, individual DNA molecules can be directly visualized and manipulated by using video fluorescence microscopy and optical tweezers, respectively. These techniques, which have led to many advances in understanding, are central to the experiments described in this thesis.

Most of the single molecule imaging experiments undertaken to date have examined the dynamics of dilute, isolated DNA molecules. Hydrodynamic deformation and entropic relaxation of single tethered molecules have been studied using optical tweezers (26, 28-30), free diffusion has been studied by single molecule tracking of Brownian motion (24), and the dynamics of molecules in flow has been studied by imaging molecules in various types of miniature fluidic cells (31-33). Only a few of these studies utilized molecules of varying lengths to investigate length dependence, and none required preparation of large quantities of homogeneous, monodisperse DNA samples. Heterogeneous samples, such as randomly ligated λ DNA concatemers, λ restriction fragments, or partly fragmented *E. coli* genomic

DNA, were acceptable for use in these dilute solution studies because the lengths of isolated molecules could be determined during the measurements (24, 31). However, extension of such studies to entangled polymers is preferably done with monodisperse samples (13).

2.1.3 Setbacks

The principal setback in using DNA for polymer studies has been the lack of available DNA molecules suited for such studies. Ideally, a set of molecules covering a wide range of lengths is needed in order to test predicted scaling laws. Highly concentrated DNA solutions are also important for studying the complex molecular dynamics of entangled solutions. Currently, λ and T7 DNA, of ~49 and ~40 kbp, are the only purified samples that are commercially available in the USA in milligram quantities. These samples are quite expensive, especially when one considers that quantities of ~10 mg would typically be desired for entangled polymer dynamics experiments. T2 and T4 DNA, of ~170 kbp, which have been used in a couple of earlier rheology studies (18, 20) are no longer commercially available.

2.2 Preparation of DNA Molecules Suitable for Polymer Studies

To overcome the problem of sample availability, we describe the design and preparation of large quantities (up to tens of milligrams per preparation) of eight different double-stranded DNA constructs ranging in length from ~3 to 300 kbp (~1 to 100 μm in physical contour length). These samples can be prepared by DNA replication using a single consistent method, and any research group can produce exact

copies of these samples by following the protocols described in the Appendix (Section 2.3).

2.2.1 DNA Constructs

We have prepared samples by replication of cloned DNA in *E. coli* using plasmid, fosmid, and bacterial artificial chromosome (BAC) constructs (Table 2.1). Each construct consists of a vector, containing DNA sequences required for replication and conferring antibiotic resistance, and an inserted DNA segment containing cloned DNA sequences. As described below, special effort was required to choose or design these constructs to have certain properties desired for their intended use in polymer physics and rheology experiments. In particular, we sought to prepare a collection of constructs having desired molecular lengths, capability for high yield production, and sequences allowing for preparation of linear molecules. Plasmids are supercoiled DNA molecules, ranging from ~3 to 15 kbp, that can be replicated in bacteria at up to ~500 copies per cell (34). Plasmid vectors are typically ~3-8 kbp, and stable plasmid inserts are typically less than 10 kbp, so these constructs are only useful for producing DNA molecules up to 5 μm (~50*N*), which brackets the small end of what is desired for studies of entangled polymer physics. Commercially available plasmids are only sold in microgram quantities, which are insufficient for direct use in physical experiments. We have thus prepared three plasmid constructs ranging from 2.7 to 11.1 kbp for inclusion in our collection of DNA samples.

To prepare longer molecules, we chose to use fosmid and BAC clones, which were originally developed for use in DNA cloning in genome sequencing projects.

Fosmids are usually ~30-50 kbp while BACs allow for an upper limit as high as ~300 kbp and are designed to replicate at only one or two copies per cell for many generations with high stability (35). While the low copy number confers long-term stability in stock cultures, it also results in much lower yield of DNA. To overcome this problem, we integrated an inducible high-copy number origin of replication (oriV) into the fosmid constructs during cloning and into the BAC constructs by means of DNA transposition (36). The cloned DNA is then replicated at low copy number, which allows for stable maintenance of the clone in stock cultures. However, addition of an inducer (L-arabinose) during DNA preparation boosts replication, which results in significantly higher yields (37).

Table 2.1 Collection of DNA constructs

Name	Size (kbp)	Cutter	Antibiotic resistance
Plasmids			
pUC19	2.7	BamHI	Ampicillin
pYES2	5.9	BamHI	Ampicillin
pPIC9K<TRL5>	11.1	BamHI	Ampicillin
Fosmids			
pCC1FOS25	25	ApaI	Chloramphenicol
pCC1FOS45	45	ApaI	Chloramphenicol
BACs			
CTD-2342K16<*oriV/KAN-2*>	114.8	MluI	Chloramphenicol/Kanamycin
CTD-2609C22<*oriV/KAN-2*>	185.4	MluI	Chloramphenicol/Kanamycin
CTD-2657L24<*oriV/KAN-2*>	289.0	MluI	Chloramphenicol/Kanamycin

2.2.2 DNA Sequences

To convert the DNA to linear form, we sought to use restriction endonucleases that would cut only once in the DNA template. Thus, part of the challenge of this project was to choose or design such constructs. Satisfying this requirement proved to be relatively easy in the case of plasmids due to their short length. We obtained three plasmid constructs from ~3 to 11 kbp that are cut once by BamHI, which is an inexpensive and widely available restriction endonuclease. Two constructs were

simply standard cloning vectors, while the third, pPIC9K⟨TRL5⟩, contained an insert (gene sequence coding for TRL5).

We prepared fosmid constructs by cloning because we were unable to locate any existing constructs that were publicly available, sequenced, and contained a high-copy origin. We therefore cloned fragments of λ DNA using the pCC1FOS vector (38), which contains the oriV origin. Two clones of ~25 and 45 kbp (termed pCC1FOS25 and pCC1FOS45) were identified to have a single ApaI cut site following screening of clones with a battery of restriction enzymes. While many BAC clones are publicly available due to their use in the human genome-sequencing project, we found that most randomly tested BAC sequences did not contain a single-cutting restriction site, or at least one corresponding to an available, suitably inexpensive restriction endonuclease. This situation is easily understood as being due to the long lengths of BACs. Therefore, we screened BAC sequences from a large library at Caltech (CTD library) for suitability by using bioinformatics techniques. In particular, we used sequence alignment software (38) to map sequenced BAC end pairs onto the human genome sequence, which then allowed us to identify several clones that could be cut once by MluI. We then retrofitted these BAC clones with an inducible oriV origin, as described above.

2.2.3 DNA Purification

Detailed, step-by-step protocols for preparing these DNA constructs are given in the Appendix. We sought to devise the simplest protocol that would be sufficient for the intended use of the samples. Our method was modified from various standard

methods in molecular biology. Briefly, cultures of *E. coli* containing the desired DNA clones are grown from frozen stocks, and the cells are lysed via treatment with an alkaline solution. The cloned DNA is re-natured by an acidic detergent solution in which genomic DNA and cellular debris precipitate and are removed by centrifugation. The DNA is then precipitated in cold isopropanol, washed in 70% ethanol, and re-dissolved in aqueous solution at pH 8. The molecules are then converted into linear form by treatment with the appropriate restriction enzyme (Table 2.1). To remove contaminating RNA the sample is treated with RNase A, and proteins are removed by phenol-chloroform extraction followed by dialysis. Finally, the samples are concentrated by a second isopropanol precipitation.

2.2.4 Sample Characterization

We characterized the purified DNA samples by agarose gel electrophoresis, UV absorption spectroscopy, colorimetric protein-dye binding assays, and single molecule fluorescence imaging. We found that purifying DNA from 3 L of bacterial culture is a quite feasible scale for a small laboratory and typically yields ~10-30 mg of DNA, with ~70-90% recovery of that obtained in the initial lysis step. Following the final isopropanol precipitation, we re-dissolved the DNA at concentrations ranging from ~1 to 10 mg/ml. We determined the concentration of our samples by gel electrophoresis with ethidium bromide staining and comparison against a standard of known concentration (λ DNA from New England Biolabs). As ~0.5 mg/ml of λ DNA is the threshold for observing entanglement effects (39), a yield of tens of milligrams is a sufficient quantity for many types of rheology measurements.

Following the initial extraction and precipitation of the cloned DNA, we find, as anticipated, that most of the molecules are in the supercoiled form or in a combination of the relaxed circular and supercoiled forms. As illustrated in Figure 2.2, the molecules may be converted into the linear form by digestion with the appropriate restriction endonuclease. We have carried out titrations in order to estimate the minimum amount of enzyme required, rather than simply using an excess, because the restriction enzyme is the most expensive reagent needed in the preparation. Although an often stated rule of thumb in molecular biology is that ~1 unit of enzyme is recommended for digestion of ~1 μg of DNA in a typical reaction, we found that it was possible to use significantly less enzyme. By using siliconized tubes, keeping the DNA concentrated, avoiding serial dilution of the enzyme, and extending the reaction time to 6 hours, we found that complete cutting could be obtained with as little as 0.1 units of enzyme per μg of DNA. This approach further lowers the cost of each preparation.

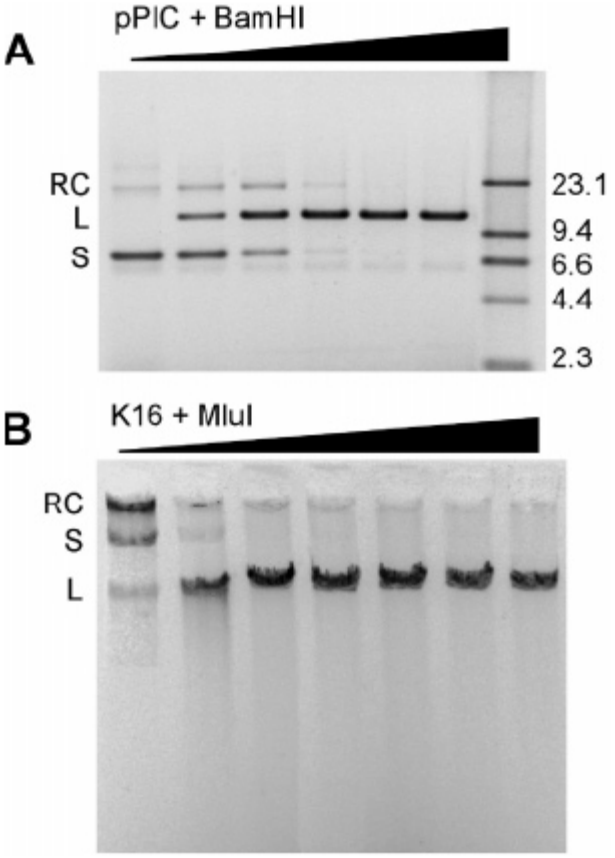

Figure 2.2 Agarose gel electrophoresis showing conversion of DNA constructs to linear form. Bands corresponding to molecules in the supercoiled circular, relaxed circular, and linear forms are indicated by the labels S, RC, and L, respectively. **(A)** Cleavage of the plasmid clone pPIC9K⟨TLR5⟩ at one recognition site by BamHI. Gel lanes (from left to right) show DNA incubated with increasing amounts of enzyme (0, 0.02, 0.06, 0.17, 0.5, and 1.5 units of BamHI per μg of DNA) at 37 °C for 6 h. **(B)** Cleavage of the BAC clone K16 at one recognition site by MluI. Gel lanes (from left to right) show DNA incubated with increasing amounts of enzyme (0, 0.03, 0.1, 0.3, 1, 3, and 10 units of MluI per μg of DNA) at 37 °C for 6 h. Samples were run on a 0.8% agarose gel in 1X TAE buffer at 3 V/cm (DC) for 3 h and stained with ethidium bromide.

As the DNA was extracted from bacteria, the purity of the final sample is an important issue. UV spectroscopy indicated an absorbance peak at 260 nm and $A_{260}/A_{280} \cong 2$, which are characteristic of pure double-stranded DNA (34). Successful

removal of contaminating proteins was also assessed more sensitively by using a colorimetric protein-dye binding assay (Micro BCA protein assay, Pierce Biotechnology). This assay indicated a low residual protein contamination of only ~2 μg of protein per mg of DNA. Successful removal of contaminating RNA is shown in Figure 2.3. We titrated the RNase to determine the amount needed to fully digest the RNA. Highly purified RNase A, certified to be free of DNase activity, is available but is prohibitively expensive given the scale of our preparation. We therefore chose to use an inexpensive preparation of RNase A from bovine pancreas (Fisher Scientific). While we found that this RNase preparation causes degradation of the DNA, we found that this problem was eliminated by preheating the RNase A to 80 °C for 20 min (Figure 2.3).

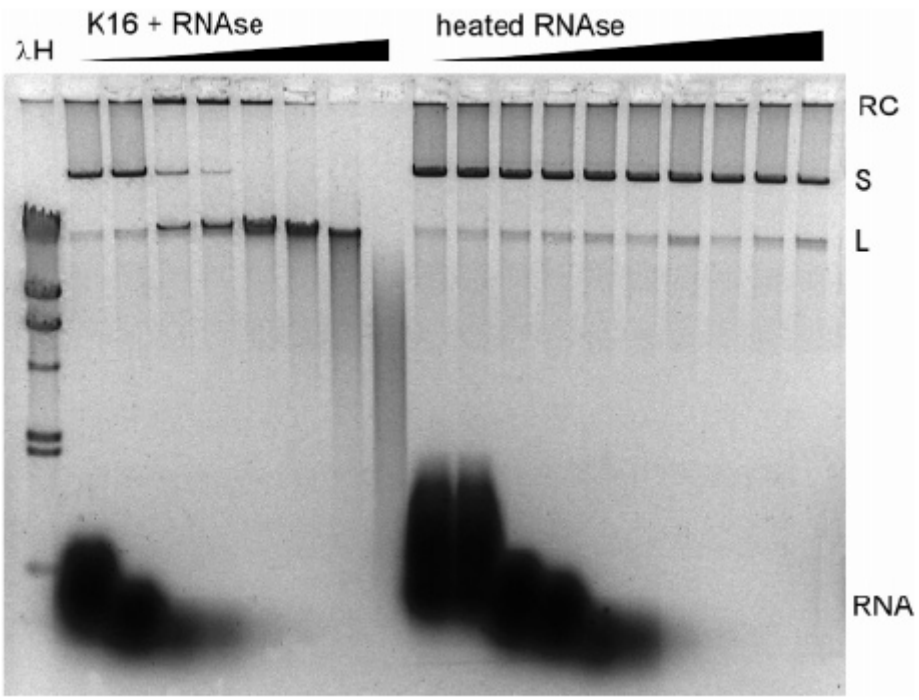

Figure 2.3 Removal of contaminating RNA from the K16 BAC DNA sample as determined by gel electrophoresis. Bands corresponding to molecules in the supercoiled circular, relaxed circular, and linear forms are indicated by the labels S, RC, and L, respectively. Far left lane: λ DNA HindIII (λH) digest used as a molecular weight standard. Lanes 2-9: samples following incubation with increasing amounts of RNase A (0.3, 1, 3, 10, 30, 100, 300, 1000 ng of RNase per μg of DNA) for 1 h at 37 °C. Lanes 10-19: samples following incubation with increasing amounts of RNase A (0.3, 1, 3, 10, 30, 100, 300, 1000, 3000, and 10000 ng of RNase per μg of DNA) after the enzyme was preheated to 80 °C for 20 min. Note the suppression of DNA degradation obtained with the preheated RNase. The gel was run as in Figure 2.2.

We also tested the amplification in yield obtained by induction of the oriV origin of replication that we included in our constructs. As shown in Figure 2.4E, we found that cultures grown with 0.01 to 0.1% (w/v) of L-arabinose produce a gain of at least 10-fold in the DNA yield. Based on our gel electrophoresis and fluorescence microscopy results, there was no effect on the quality of the DNA prepared following

induction with L-arabinose. This amplification method is thus valuable for preparing the desired large quantities of DNA. The cost of the reagents needed to prepare one batch of DNA by our protocol is ~$20-80 (US), with the greatest expense being for MluI. By comparison, purchase of an equal amount of λ DNA is ~10-50 times more expensive and limits one to studying only one particular length molecule.

Gel electrophoresis measurements were done to confirm that the sizes of the constructs corresponded to the expected DNA sequence lengths. As shown in Figure 2.4A, the linearized plasmid DNA constructs were clearly resolved using constant voltage (DC) agarose gel electrophoresis. While the linear form of fosmids and BACs can be easily distinguished from the supercoiled or relaxed circular forms by DC gel electrophoresis, it is not possible to size linear DNA constructs by this method because molecules longer than ~30 kbp have nearly the same mobility in DC electrophoresis. Therefore, we used pulsed field gel (PFG) electrophoresis with contour-clamped homogeneous electric fields (40) to confirm the sizes of the fosmid and BAC constructs (Figure 2.4B-D).

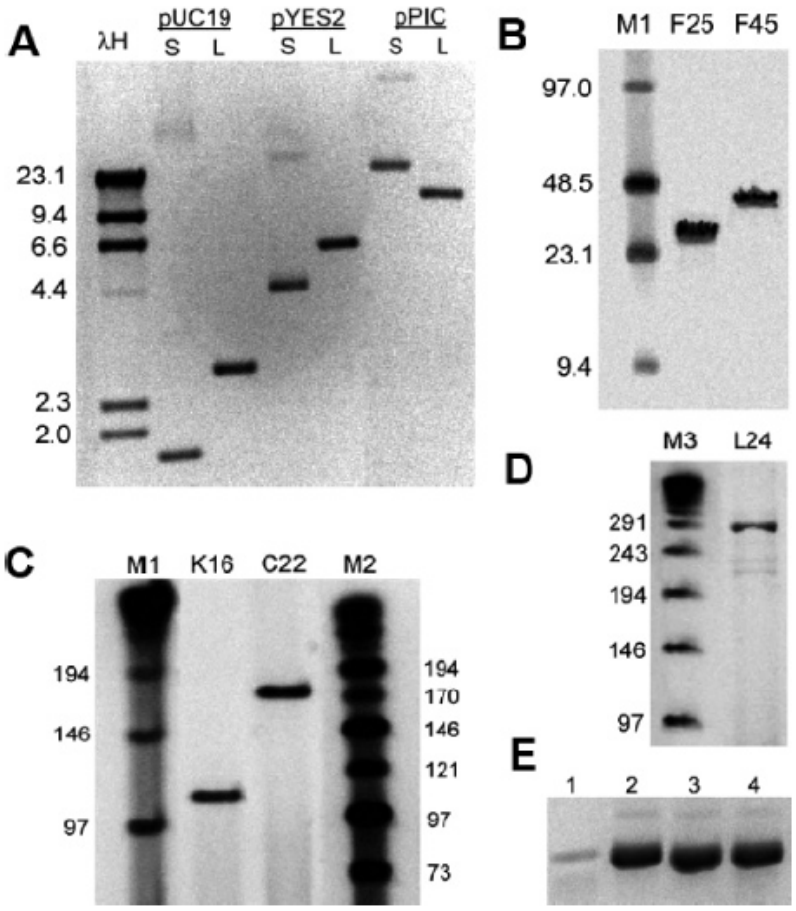

Figure 2.4 Analysis of linearized DNA by agarose gel electrophoresis. DNA sizes are listed in kbp. **(A)** Plasmid DNA samples. Far left lane: λH digest used as a molecular weight standard. Subsequent lanes show indicated plasmid DNA samples in supercoiled (S) and linear (L) form following digestion with BamHI. The gel was run as in Figure 2.2. **(B)** Fosmid DNA samples. Far left lane: low range PFG marker (M1). Subsequent lanes show FOS25 and FOS45 DNA samples after linearization with ApaI. Samples were run on a 1% agarose gel in a cold room (5 °C) in 0.5X TBE buffer in a pulsed field gel system with clamped homogeneous electric fields at 200 V for 15 h. Field switch times were ramped from 1 to 15 s, and the gel was stained with ethidium bromide. **(C)** BAC DNA samples. Far left lane: M1. Lanes 2 and 3: indicated BAC clones retrofitted with the ⟨oriV/KAN-2⟩ transposon. Far right lane: midrange PFG marker (M2). The gel was run as in (B). **(D)** L24 BAC DNA sample. Far left lane: λ ladder PFG marker (M3). The gel was run as in (B), but for 24 h with switch times ramped from 1 to 25 s. **(E)** Electrophoresis gel of FOS45 showing the gain in sample yield upon induction of the oriV origin of replication. Lane 1 is a control culture with no inducer added; lane 2 contains 1/1000 volume of Copy Control reagent; lanes 3 and 4 contain 0.1% and 0.01% (w/v) L-arabinose. The gel was run as in (A).

To substantiate our gel electrophoresis results for the sizes of our constructs and to test that the prepared DNA molecules could be used in the same manner that λ DNA has been used in previous single molecule experiments, we labeled the DNA samples with YOYO-I and imaged them at high magnification in an epi-fluorescence microscope (detailed in Figure 2.1). Protocols used for labeling and imaging are given in the Appendix. As shown in Figure 2.5, single molecules of the plasmid, fosmid, and BAC constructs could be easily visualized, and individual samples of molecules appeared to be homogeneous. We observed that the areas of the images monotonically increased with expected size, pCC1FOS45 (expected to be ~45 kbp) was roughly the same size as λ DNA (48.5 kbp), as expected, and no difference in the quality of our samples was detected compared to the commercially prepared λ DNA. We did not quantify the image sizes because measuring sizes of such bright, compact moving objects imaged with an intensified video camera is known to be inaccurate because of blooming artifacts in the camera, diffraction effects, and out-of-focus effects which have been discussed previously (40).

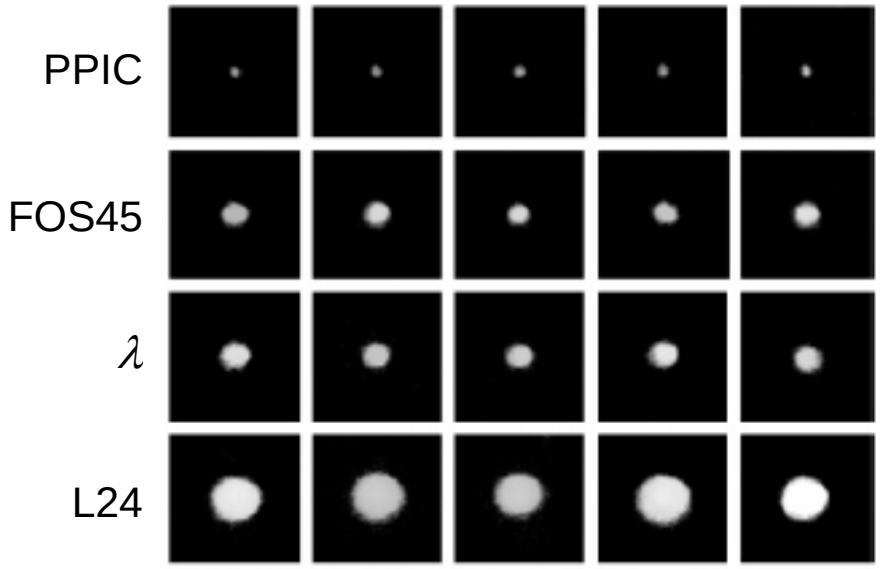

Figure 2.5 Fluorescence microscopy images of YOYO-I-labeled DNA molecules. Snapshots of five randomly chosen molecules are shown, including examples of a linearized plasmid (pPIC), fosmid (FOS45), and BAC (L24). Images of λ DNA purchased from New England Biolabs are shown for comparison. Each image covers a 12 μm by 12 μm field of view.

2.2.5 Conclusions

The samples described and characterized here will facilitate the extension of single polymer dynamics experiments to the case of entangled polymers and comparison with bulk rheology measurements. Having a wide series of molecular lengths will allow for examination of scaling laws and changes in polymer solution dynamics during the crossover from the dilute to the entangled regimes. The length range of constructs we have prepared is an ideal range that spans the entanglement molecular weight of DNA and allows for ample investigation of the length and concentration dependence of DNA dynamics in the dilute, semidilute, and concentrated regimes.

2.3 Appendix

Below we describe our protocols for preparing DNA samples from the prepared bacterial strains. The cultures may be stored as glycerol stocks at –80 °C for at least several years and used at any time to produce DNA samples.

Preparation of Reagents:
1. Add 12.5 g of LB broth powder and 0.5 L of purified deionized water to each of six 2 L baffled Erlenmeyer flasks. Cover the tops of the flasks with aluminum foil and sterilize in a steaming autoclave at 121 °C for 30 min.

2. Prepare 1 L of Suspension Buffer in a pyrex bottle by adding 50 ml of 1M tris buffer, pH 8 and 20 ml of 0.5 M EDTA to 930 ml of purified water. Sterilize in a steaming autoclave at 121 °C for 30 min.

3. Prepare 1 L of Alkaline Lysis Buffer by dissolving 8.0 g of NaOH in 950 ml purified water and adding 50 ml of 20% SDS solution, or prepared using SDS powder. Filter the solution through a 0.2 μm sterile filter unit.

4. Prepare 1 L of Neutralization Buffer in a pyrex bottle by dissolving 295 g potassium acetate in 500 ml of purified water. Adjust the pH to 5.5 by adding in glacial acetic acid as needed (~110 ml) and then adjust the volume to 1 L by adding purified water. Sterilize in a steaming autoclave at 121 °C for 30 min.

5. After the LB broth has cooled to room temperature add the following to each flask:
For Plasmids: 1 ml of 50 mg/ml ampicillin dissolved in water (final concentration of 100 μg/ml).
For Fosmids: 0.5 ml of 12.5 mg/ml chloramphenicol dissolved in ethanol and 0.5 ml of 10% (w/v) L-arabinose (final concentration of 0.01% w/v).
For BACs: 0.5 ml of 12.5 mg/ml chloramphenicol, 0.5 ml of 50 mg/ml kanamycin in water (final concentration of 50 μg/ml), and 0.5 ml of 10% (w/v) L-arabinose.

Growth of the Bacterial Culture:
1. Using a sterile pipette tip scrape off a small amount (~10 μl) of bacteria from a frozen glycerol stock carrying the desired DNA construct and add this to each flask.

2. To grow the bacterial culture to saturating density place the flasks on an orbital shaker at 37 °C and shake at 200 rpm for 16 to 20 h. The culture should be very cloudy (opaque).

3. To pellet the bacteria pour 1.5 L of the culture into six 250 ml centrifuge bottles. Centrifuge these bottles at 5000 x g (5000 rpm) for 8 min in a centrifuge. Pour off the liquid, add the remainder of the culture to the bottles, and centrifuge again for 10 min.

After pouring off the liquid one should have a wet pellet of ~1 to 4 g in each bottle. Use of more than 4 g in the DNA extraction protocol is not recommended. The bottles may be stored at –20 °C for up to a week or one may continue the protocol directly.

Cell Lysis and DNA Extraction:

1. Add 42 ml of Suspension Buffer to each bottle, incubate for 10 min at room temperature, and then tap the bottle against a hard rubber surface to break up the pellets (until the solution appears uniformly cloudy).

2. Add 42 ml of Alkaline Lysis Buffer to each bottle and mix by gently inverting six times to lyse the bacteria. DNA will be released and will be denatured into single-stranded form. From this point on one must be gentle in handling to not damage the DNA. Allow the lysis to continue for 5 min at room temperature.

3. Add 42 ml of Neutralization Buffer (pre-chilled on ice) to each bottle and mix by gently inverting each bottle six times to re-nature the cloned DNA. The *E. Coli* genomic DNA is too large to renature and precipitates along with cellular debris. Incubate this solution for 30 to 60 min on ice. A white precipitate should form.

4. Mix by gently inverting the bottles four times. Centrifuge the bottles at 16,000 x g (10,000 rpm) at 4 °C for 25 min to pellet out the unwanted precipitate. Immediately following the centrifugation gently pour the solutions through a fine mesh tea strainer into clean 250 ml centrifuge bottles.

5. To precipitate the DNA fill each bottle to the top with cold (–20 °C) isopropanol while gently swirling. Mix gently by inverting four times and incubate at –20 °C overnight.

6. Centrifuge the bottles at 16,000 x g (10,000 rpm) at 4 °C for 25 to 40 min to pellet the DNA. Small yellow-white chunks should be visible at the bottom of the bottle. Pour off the liquid through a tea strainer (helpful for catching the pellet in case it comes loose).

7. Add 30 ml of 70% (v/v) ethanol in water and gently wash the pellet by inverting the bottle five times and incubate 5 to 10 min. This step helps remove salt and isopropanol from the pellet. Centrifuge at 16,000 x g (10,000 rpm) for 10 min to bring the pellet back to the bottom of the bottle and then pour off the liquid through a fine mesh tea strainer without disturbing the pellet.

8. Dry the pellet by gently blowing compressed air into each bottle for 1-2 min such that the ethanol is mostly removed but the pellet is still slightly moist (do not dry it completely). To dissolve the DNA add 6 ml of TE buffer, pH 8 (10 mM Tris-HCl, 1 mM EDTA, pH 8) to each bottle and rock them gently at ~0.5 Hz for 10 min at room

temperature on a rocker. Place the samples in a refrigerator (at ~4 °C) overnight to dissolve further.

9. Rock the bottles again gently at ~0.5 Hz for 10 min at room temperature and then gently pour the contents equally into a 50 ml centrifuge tube. To recover residual DNA from the bottles add an additional 1 ml of TE buffer to each bottle and rock the bottles again gently at ~0.5 Hz for 10 minutes at room temperature and then gently pipette out the solution with a wide bore pipette tip. Centrifuge the sample at 12,000 x g (10,000 rpm) for 10 min to pellet any un-dissolved material. Pour the clarified solution into a clean 50 ml centrifuge tube.

DNA linearization and RNA digestion:

1. Analyze the sample by agarose gel electrophoresis to determine the concentration of the sample. Run a series of dilutions of the sample and a series of dilutions of λ DNA (~0.1 to 1 μg per lane) as a standard.

2. To digest contaminating bacterial RNA add ribonuclease A to a final concentration of 0.3 μg RNase per mg of DNA. First heat the RNase A to 80°C for 20 min (to inactivate residual DNase activity).

3. To convert the molecules into linear form first add 1/10 volume of the appropriate 10x reaction buffer and the appropriate restriction enzyme for the DNA construct (Table 2.1) to 0.1 to 0.5 units of enzyme per μg of DNA. This digestion is done simultaneously with the RNase digestion for 6 h at 37 °C.

DNA Purification and Concentration:

1. To remove contaminating proteins and lipids (working under a fume hood and wearing chemical-resistant gloves and apron) divide the sample into two 50 ml centrifuge tubes (~20 ml each) and add 20 ml of phenol/chloroform/isoamyl alcohol (25:24:1 mixture, preequilibrated to pH 8 with Tris buffer) to each tube. Gently invert the tubes about 15 times to form a white, opaque emulsion between the two immiscible fluids.

2. Centrifuge for 20 min at 12,000 x g (10,000 rpm) and carefully pipette off the top, aqueous phase containing the DNA into a clean 50 ml centrifuge tube, while avoiding any material at the interface.

3. Carefully pour the DNA solution into one or two lengths of dialysis tubing (Spectra/Por Biotech CE membrane, 300 kd molecular weight cutoff, 16 mm flat width or larger), clamp each with universal closures, and immerse them in a 5 L plastic beaker of TE buffer in a cold room or refrigerator while gentle stirring with a magnetic stirrer for >3 h. Then change to 5 L of fresh buffer and continue dialysis overnight. When finished, transfer the solution into 50 ml tubes.

4. To precipitate the DNA add 1/25 volume of 5 M NaCl (final concentration of 0.2 M). Mix gently by inverting 4 times then add an equal volume of cold isopropanol (–20 °C) and mix gently by inverting 5 times. Incubate at –20 °C for 2 to 24 h.

5. Centrifuge for 20 min at 12,000 x g (10,000 rpm) and then pour off the liquid through a tea strainer, retaining the DNA pellets.

6. Add 10 ml of 70% (v/v) ethanol in water and gently wash the pellet by inverting the tube 5 times and incubate 5 to 10 min. Centrifuge at 12,000 x g for 10 min and then pour off the liquid through a fine mesh tea strainer without disturbing the pellet.

7. Dry the pellet by gently blowing compressed air into each tube for 1-2 min, such that the ethanol has mostly evaporated but the pellet is still slightly moist (do not dry it completely). To dissolve the DNA at the desired concentration add the desired volume of TE buffer (supplemented with 10 mM NaCl) (typically ~500 µl to 2 ml) and rock them gently at ~0.5 Hz for 30 min at room temperature. Place the samples in a refrigerator (at ~4 °C) to dissolve further.

Fluorescence Labeling:

1. Prepare TE10β buffer by adding NaCl to 10 mM and 4% volume of β-mercaptoethanol to standard TE buffer.

2. Dilute a small amount of the DNA solution in a 1.7 ml microcentrifuge tube to 10 µg/ml in TE10β buffer and gently mix the DNA sample by slowly pipetting up and down through a wide-bore pipette tip. To mix, pipette liquid off the bottom of the tube and pipette it back out while making a swirling motion. Repeat the mixing about 10 times.

3. Add 2 µl of YOYO-I dye (stock concentration of 1 mM) to 198 µl of TE10β buffer.

4. Add 386 µl of TE10β and 4 µl of the diluted dye in a 1.7 ml microcentrifuge tube. Vigorously mix this solution and then gently add 10 ml of the 10 µg/ml DNA. Note that the basepair to dye ratio is ~4:1 and the DNA concentration is ~0.25 ng/µl.

5. Gently mix the DNA sample by slowly pipetting up and down through a wide-bore tip as described in Step 2.

6. Incubate sample in the dark at room temperature for ~1-2 h. For best results labeled DNA should not be used for longer than ~10 h.

7. To visualize the DNA molecules with a fluorescence microscope dilute the sample by ~1/100 to 1/1000 in TE10β buffer.

8. To mitigate fluorescence photobleaching, add 10 μg/ml catalase, 100 μg/ml glucose oxidase, and 30% (w/w) glucose and incubate the sample for 15 to 20 min in a sealed chamber in order to scavenge dissolved oxygen.

2.4 Acknowledgements

Chapter 2, in part, is a reprint of the material as it appears in Macromolecules.

Laib, S., Robertson, R. M. & Smith, D. E. *Macromolecules* **39**, 12, 4115-4119 (2006).

The dissertation author was the secondary investigator and author of this paper.

Chapter 3

Diffusion of Isolated DNA Molecules: Dependence on Length and Topology

3.1 Abstract

The conformation and dynamics of circular polymers is a subject of considerable theoretical and experimental interest. DNA is an important example as it occurs naturally in different topological states, including linear, relaxed circular, and supercoiled circular forms. An important fundamental question is how the diffusion coefficients D of isolated polymers scale with molecular length L and how D varies for different topologies. Here, diffusion coefficients for relaxed circular, supercoiled, and linear DNA molecules, ranging in length from ~6 to 290 kbp, were measured by tracking the Brownian motion of single molecules. A topology-independent scaling law $D \sim L^{-\nu}$ was observed with $\nu_L = 0.571 \pm 0.014$, $\nu_C = 0.589 \pm 0.018$, and $\nu_S = 0.571 \pm 0.057$ for linear, relaxed circular, and supercoiled DNA, respectively, in good agreement with the scaling exponent $\nu \cong 0.588$ predicted by renormalization group theory for polymers with significant excluded volume interactions. Our findings thus provide evidence in support of several theories that predict an effective diameter of DNA much greater than the Debye screening length. In addition, the measured ratio $D_{Circular}/D_{Linear} = 1.32 \pm 0.014$ was closer to the value of 1.45, predicted using renormalization group theory, than the value of 1.18 predicted by classical Kirkwood

hydrodynamic theory. This ratio also agreed very well with a value of 1.31 predicted when incorporating a recently proposed expression for the radius of gyration of circles into the Zimm model.

3.2 Introduction

While many eukaryotic genomes are linear, prokaryotic genomes and most cloned DNA constructs are circular (41). Indeed, a commonly stated motivation for theoretical calculations on circular polymers is that they may be applicable to understanding the behavior of DNA. However, four of the five previously reported studies on the diffusion of circular polymers have employed synthetic polymers, and only two of these, both using synthetic polymers, examined the dependence of D on molecular length. The dependence of D on length for relaxed circular DNA has never been measured. Here we examine linear, relaxed circular, and supercoiled DNA molecules covering a wide range of lengths (~6 to 290 kbp).

For long linear polymers in a good solvent, where excluded volume effects are appreciable, polymer physics theory (1) predicts $D \sim 1/R_G \sim L^{-\nu}$ with $\nu \cong 0.588$. The same scaling exponent has been calculated for both dynamic ($D \sim L^{-\nu}$) and static ($R_G \sim L^{\nu}$) quantities, with nearly identical results determined using a wide range of methods. Static scaling has been examined using Monte Carlo simulations (42), bead-rod simulations (43), and cylindrical self-avoiding polygon models (44). Renormalization group theory methods have been used in both static (42, 45) and dynamic (46) calculations, and bond-fluctuation simulations (47) were used to measure and compare

both scaling relationships. The predicted scaling exponent is also close to the previous experimental finding of $\nu = 0.61 \pm 0.016$ for linear DNA (48). Although the main purpose of the present study is to examine the effect of topology on diffusion, more accurate results on linear DNA were also obtained because we used DNA constructs of defined lengths, whereas previously (48), lengths of the longest molecules were only estimated.

Theoretical studies and numerical calculations further predict that the scaling exponent ν should be unaffected by a topological change from linear to circular form (42, 45, 49, 50). The two previous synthetic polymers experiments examining the dynamical scaling behavior of both linear and circular molecules in good solvent found such topological invariance; however, they did not find an exponent in accord with the predicted scaling of -0.588. Rather, reported exponents were in agreement with the -0.5 scaling predicted for a polymer in a theta solvent and thus not subject to excluded volume. Light scattering methods were used and scaling exponents of $\nu =$ 0.48 to 0.53 were reported (51, 52).

While the scaling exponent is predicted to be topologically invariant, the ratio of diffusion coefficients of circular and linear species $\chi = D_C/D_L$ is predicted to be greater than unity and independent of length for long molecules. However, the exact value is still debated and is found to be sensitive to how solvent conditions, hydrodynamic interactions, and excluded volume interactions are treated. Faster diffusion of circles compared to linear molecules can be qualitatively understood as being due to a reduced mean square end-to-end distance caused by the conformational

constraint of closure. However, it is important to note that increased hydrodynamic screening and an altered sensitivity to excluded volume effects are also expected to play a role (53).

Calculations based on classical Kirkwood hydrodynamic theory (54) predict $\chi = 3\pi/8 \cong 1.18$, while more recent renormalization group calculations using the Edwards Hamiltonian (46) predict $\chi = e^{3/8} \cong 1.45$. Three of the aforementioned experiments on synthetic polymer solutions (51, 52, 55) report values of $\chi = 1.11\text{-}1.2$, in reasonable agreement with the calculations using Kirkwood theory, while one (56) reports $\chi = 1.36$, in closer agreement with the renormalization group theory calculation. To our knowledge the ratio χ has only been measured for one relaxed circular DNA molecule, $ColE_1$ (~6.6 kbp), by light scattering, and a value of $\chi = 1.24$ was reported (57). An alternative approach for estimating χ has involved using R_G predictions for circles in an expression for hydrodynamic drag predicted by the Zimm model (58). Whether this approach leads to reasonable predictions will be considered below.

Traditionally, bulk methods such as light or neutron scattering have been used to determine D of isolated polymers. However, these methods are such that they usually need to be made at higher concentrations where the diffusion is concentration dependent, and thus extrapolation is required for determining the behavior of isolated molecules. In the present single-molecule experiments the average distance between molecules is hundreds of times R_G. Thus, imaging of the Brownian motion of single

DNA molecules provides the simplest and most direct way of determining the diffusion behavior of isolated polymers in the limit of infinite dilution.

3.3 Experimental Methods

Six samples of double stranded DNA (dsDNA) molecules were prepared by replication of plasmid, fosmid, and BAC constructs in *E. coli* as described in Chapter 2 (Table 3.1). It is well known that such DNA molecules replicated in *E. coli* adopt unknotted, negatively supercoiled configurations (59). Following purification ~50 to 80% of molecules were found to be in supercoiled form while the remainder were in the relaxed circular form. To prepare linear molecules, samples were digested with restriction endonucleases that cut at only one site (Table 2.1). To prepare relaxed circles, samples were digested with topoisomerase I under conditions where this enzyme is known to relax all supercoils in dsDNA without inducing knots (60). To verify that the molecules were fully relaxed after treatment with topoisomerase I we compared them with molecules treated with the nicking endonuclease Nt.Bst.NBI, which makes the DNA torsionally unconstrained and relaxes all supercoiling without inducing knots (60, 61). No difference was observed between these two samples in either gel electrophoresis measurements (which can resolve knots and supercoils (60)) or diffusion measurements, thus showing that the molecules treated by topoisomerase I were fully relaxed and unknotted.

DNA was labeled with YOYO-I and imaged in an aqueous buffer solution containing 10 mM Tris-HCl, pH 8, 1mM EDTA, 10 mM NaCl, 4% (v/v) β-

mercaptoethanol, 30% (w/v) glucose, 10 μg/ml glucose oxidase, and 120 μg/ml catalase, as described in Chapter 2. Gel electrophoresis and diffusion measurements were used to confirm that the dye did not cause supercoiling of the relaxed circular species, as discussed in further detail in section 3.4.3. Molecules were imaged with a custom-built epifluorescence microscope detailed in Figure 2.1.

The center of mass (x, y) coordinates of >1000 paths of >20 different molecules for each construct were tracked every 8/30 second and the Einstein relationship $\langle x^2 \rangle = \langle y^2 \rangle = 2Dt$ was used to determine the diffusion coefficient. Errors were estimated using the bootstrap method to calculate D for 1000 subensembles of molecules (62). To check the calibration of our apparatus, we measured D for a 0.87 μm diameter polystyrene microsphere in water and obtained a value within 1% of that predicted by the Stokes-Einstein law. We also measured D for our 45 kbp DNA molecule in five solutions of increasing viscosity and found that D decreased as the -0.99 ± 0.18 power of viscosity, in accord with theoretical expectations.

3.4 Results and Discussion

3.4.1 Linear and Relaxed Circular DNA

We have measured the scaling of D with L (Figure 3.1A) for both linear and relaxed circular molecules and find $\nu_L = 0.571 \pm 0.014$ and $\nu_C = 0.589 \pm 0.018$, respectively. These scaling exponents were determined by a linear fitting of log D vs log L and are in good agreement with the predicted value of $\nu \cong 0.588$. The present

value is also more accurate than the previously measured value of $\nu_L = 0.61 \pm 0.016$ for linear DNA (48) because here we used DNA constructs of defined lengths. To confirm the accuracy and precision of this power-law behavior we compared our results with the predicted scaling by plotting $D \cdot L^{0.588}$ versus L for both linear and circular molecules (Figure 3.1B). Linear fits to both data sets yield values of $6.27 \times 10^{-4} \pm 0.001$ and $-9.07 \times 10^{-4} \pm 0.001$ for linear and circular forms, respectively. The predicted power-law behavior is therefore within the error bars of these measurements and the relatively small errors in these fits show the accuracy of our reported scaling laws.

Figure 3.1 Scaling of diffusion coefficients for isolated DNA molecules. **(A)** Diffusion coefficient D vs. chain length L for isolated DNA molecules. The points are the data obtained by tracking fluorescently labeled linear (squares), relaxed circular (circles), and untreated (mostly supercoiled circular) DNA (triangles). The solid lines are power law fits having exponents of $\nu_L = 0.571 \pm 0.014$ and $\nu_C = 0.589 \pm 0.018$. The dashed line is a fit to the supercoiled DNA data with $\nu_S = 0.571 \pm 0.057$. The error bars indicate σ_D from bootstrap analysis. **(B)** Comparison of measured scaling of D with L to predicted scaling of -0.588. Plot of $D \cdot L^{0.588}$ vs. L (data points and error bars are the same as those in (A)). The solid lines are linear fits to the data which yield values of $6.27 \times 10^{-4} \pm 0.001$ and $-9.07 \times 10^{-4} \pm 0.001$ for linear and circular molecules, respectively.

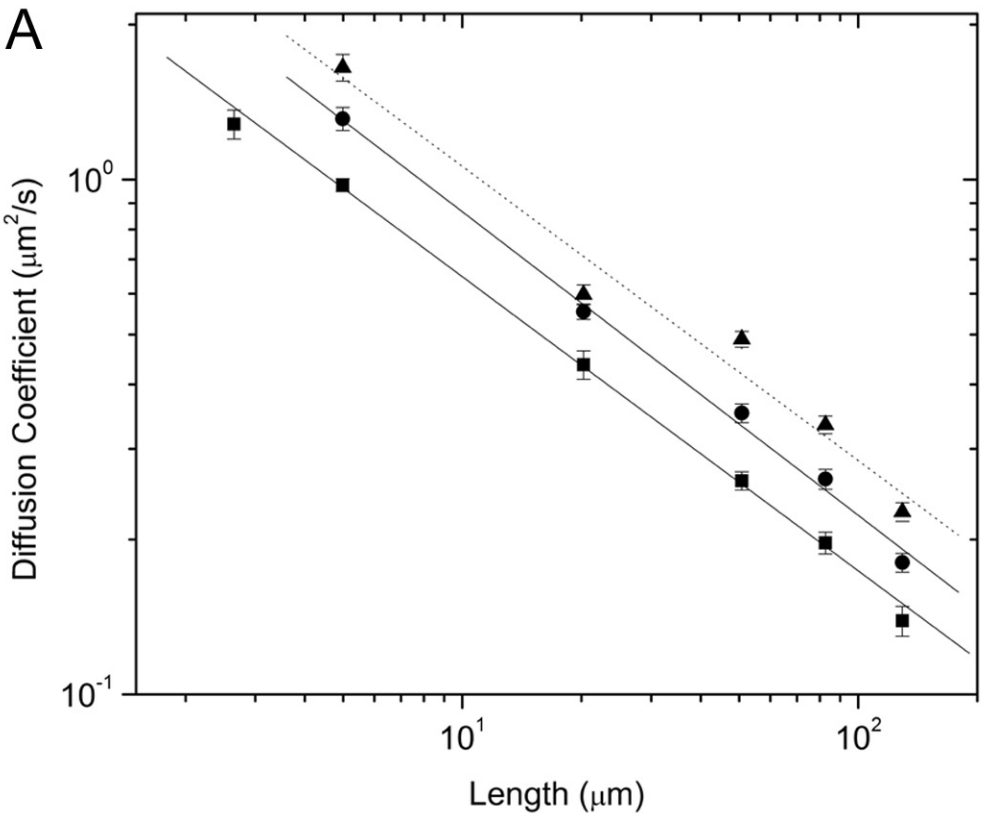
A
Diffusion Coefficient (μm²/s)
10⁰
10⁻¹
10¹
10²
Length (μm)

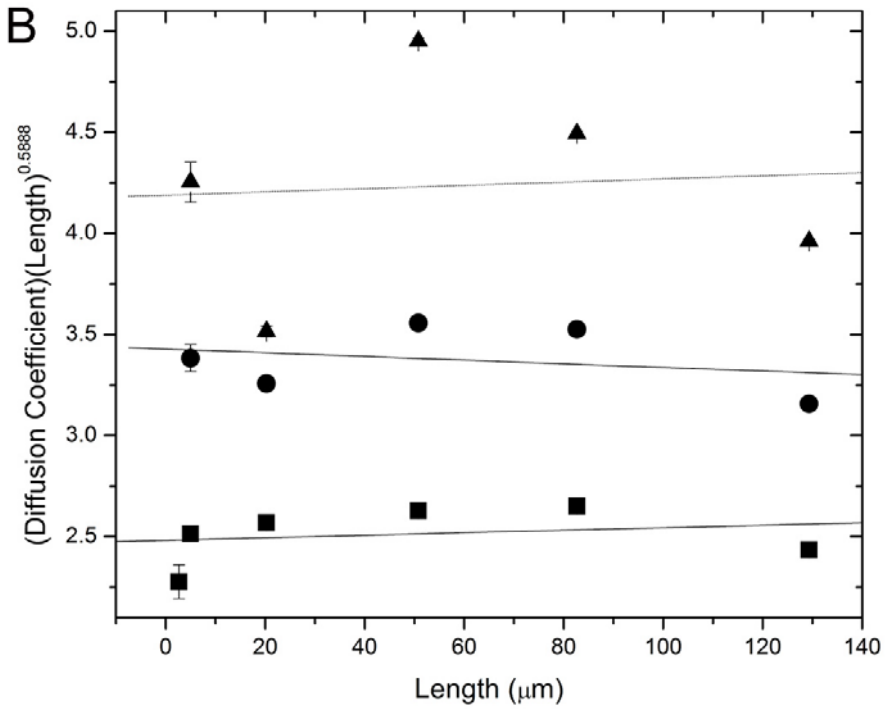
B
(Diffusion Coefficient)(Length)^0.5888
5.0
4.5
4.0
3.5
3.0
2.5
0
20
40
60
80
100
120
140
Length (μm)

Our ν_C value is higher than those previously reported for circular synthetic polymers ($\nu_C = 0.52 \pm 0.02$ and $\nu_C = 0.52$) (51, 52). Although these previous studies were done in good solvent conditions, the findings were noted to be in closer agreement with the value $\nu = 0.5$ expected for a theta solvent. It was proposed in Reference 51 that this difference could be due to a reduced excluded volume effect for low molecular weight polymers. Here, we covered a range of ~70 to 1900 persistence lengths ($N \cong 35 - 950$), which extends up to 5 times higher than that in Reference 51.

On the other hand, DNA differs from many synthetic polymers in that the persistence length is ~25 times larger than the double-helix diameter of 2 nm, which suggests that the excluded volume effect might be expected to be less significant for DNA than for typical synthetic polymers. However, we measure a scaling exponent of $\nu \cong 0.58$ extending to much shorter molecules. This value is in agreement with $\nu \cong 0.588$ predicted when including the excluded volume effect rather than that of $\nu = 0.5$ predicted with negligible excluded volume. The most likely explanation for our finding is the electrostatic self-repulsion of charged DNA molecules. It is often assumed that the effective diameter of DNA should correspond to the solvent-dependent Debye length rather than the natural helix diameter. Here, we use a solvent containing 10 mM NaCl which gives a Debye length λ_D of ~3nm ($\lambda_D = 0.3\text{nm}/[\text{NaCl}]^{1/2}$) (63), which is not much larger than the bare diameter of 2 nm. Using this Debye length, Marko and Siggia made a rough estimate based on the Flory condition for appreciable exclude volume ($L\lambda_D^2/2P^3 > 1$) which suggests that the excluded volume effect would only be expected to be marginally important for DNA

molecules of ~100 kbp and longer (64). However, early theoretical calculations by Stigter predict an effective diameter in 10 mM Na^+ of ~16 nm, which is much larger than the Debye length (65). Moreover, Toan and Micheletti have recently predicted that the electrostatic contribution is even larger and estimated an effective diameter of ~24 nm in 10 mM Na^+ (66). This value would imply a persistence length only ~2 times the effective diameter, leading to a much stronger excluded volume effect than that expected for bare dsDNA. In fact, according to the Flory condition for appreciable excluded volume, DNA molecules of ~5 kbp and greater would be subject to significant excluded volume effects. The shortest molecule used in this study is ~6 kbp. Thus, our present results, as well as recent studies of knotted DNA (67), provide experimental data in support of these theoretical predictions.

Our measured values for $\chi = D_C/D_L$, which were similar for all the molecules studied, yield a mean value of $\chi = 1.32 \pm 0.014$ (Table 3.1). This value is significantly higher than that predicted by first order perturbation theory based on the Kirkwood hydrodynamic model ($\chi \cong 1.18$) and those reported in scattering experiments on synthetic polymers ($\chi = 1.11$-1.2) (51, 52, 55). Our value is also higher than $\chi = 1.24$ reported for $ColE_1$ DNA (57) and is in closer accord with a pulsed-gradient-spin-echo NMR measurement on poly(ethylene oxide) of $\chi \cong 1.36$ (56). Our result along with that in Reference 56 is closer to the prediction of the most recent renormalization group calculation ($\chi \cong 1.45$) (49). Further, although this predicted value is higher than our finding, the authors note that their theory allows for knotted conformations and

could thus lead to a slightly overestimated value compared with that obtained experimentally with unknotted polymers.

Table 3.1 Diffusion Coefficients, Inferred Radii of Gyration, and Topology-Dependent Diffusion Ratios and Radius of Gyration Ratios for linear, relaxed circular and supercoiled DNA molecules.

DNA Construct	size (kbp)	Length* (μm)	D_L ($\mu m^2/s$)	$R_{G,L}$ (μm)	D_C ($\mu m^2/s$)	$R_{G,C}$ (μm)	D_S [§] ($\mu m^2/s$)	$\chi = D_C/D_L$	$G = R_{G,L}/R_{G,C}$
pYES[#]	5.9	2.65	1.28	0.213					
pPIC9K<TRL5>	11.1	4.99	0.976	0.279	1.31	0.173	1.65	1.35	1.61
pCC1FOS45	45	20.25	0.437	0.624	0.554	0.410	0.598	1.27	1.52
CTD-2342K16	112.8	50.81	0.260	1.05	0.35	0.645	0.490	1.36	1.63
CTD-2609C22	183.5	82.66	0.197	1.38	0.26	0.867	0.334	1.33	1.60
CTD-2657L24	287.1	129.32	0.139	1.96	0.18	1.26	0.226	1.30	1.56

*Accounting for the increase in length caused by YOYO-I, as described in Chapter 2.1.1

#Relaxed circular and supercoiled pYES2 moved too quickly to accurately track with our current setup.

§Samples had ~50-80% supercoiled molecules, as described in the text.

Although relatively few previous studies have considered the diffusion of circular versus linear polymers, a number of previous investigations have considered the effect of topology on the radius of gyration. The ratio $G = R_{G,L}/R_{G,C}$ has been calculated using a variety of models. The Bloomfield-Zimm model (68) predicts G = 1.45, renormalization field theory applied to Fixman's cluster expansion (45) gives G = 1.33, and, most recently, a modified Yu-Fujita model has been proposed (53) which predicts G = 1.54. The defining differences in these theories are the method of calculating the mean squared distance for cyclic polymers as well as the means of introducing excluded volume effects. In addition, a number of Monte Carlo simulations (69-74) have been performed and values ranging from G = 1.32 to 1.38 were reported. Finally, small-angle neutron scattering (75), light scattering (76, 77) and size exclusion chromatography (77) measurements on synthetic ring polymers reported values in the range $G \cong$ 1.37-1.39, while a light scattering measurement (57) on $ColE_1$ DNA found G = 1.39.

We are unable to accurately measure R_G with our experimental setup because of the limited resolution of optical microscopy. Other techniques such as static light scattering were considered but such measurements are extremely difficult for long molecules and become virtually impossible for molecules longer than ~60 μm (78). Therefore, while there is no apparent way to directly measure R_G for our entire range of molecular lengths, we can still examine whether our data is consistent with theories that relate R_G and D. The hydrodynamic radius R_H can be calculated from D using the Stokes-Einstein relation $D = kT/6\pi\eta_s R_H$, where k is Boltzmann's constant, $T \cong$ 297 K

is temperature and $\eta_s \cong 1.2$ cP is solvent viscosity. We may then combine predictions for G with the predicted relationship between R_H and R_G to test these predictions and compare our results to those previously reported. For linear polymers the ratio of these radii is predicted by the Zimm model (54) to be $R_{G,L}/R_{H,L} = 8/3\pi^{1/2} \cong 1.508$ while for circular polymers this ratio is predicted (58) to be $R_{G,C}/R_{H,C} = (\pi/2)^{1/2} \cong 1.253$, leading to a net prediction $G \cong 1.2C$. Within this estimate our results imply $G = 1.58 \pm 0.017$, which is in good agreement with the recent prediction of $G \cong 1.54$ based on a modified Yu-Fujita model (53). This model predicts less swelling of circles due to the excluded volume interaction than the Bloomfield-Zimm model.

Sedimentation measurements have also been reported for certain linear and circular DNA molecules in a limited length range. The ratio of sedimentation coefficients for circular and linear molecules S^0_C/S^0_L is theoretically predicted to equal D_C/D_L and thus can be compared to our measured ratio. $S^0_C/S^0_L = 1.23$ was measured for $ColE_1$ (57), while a ratio of 1.10 was reported for polyoma DNA (~4.8 kbp) (79). Lambda DNA (48.5 kbp) has also been measured and ratios of 1.18, 1.13, and 1.14 have been reported (80). These ratios are systematically lower than our finding of $D_C/D_L = 1.32$ and that of 1.45 predicted by renormalization group calculations.

3.4.2 Supercoiled DNA

We have also measured D for our untreated DNA samples containing ~50-80% supercoiled molecules (the remaining fraction being in relaxed circular form). The varying fractions of supercoiled species produced increased scatter in our data compared with data for the linear and relaxed circular samples. Also, we did not

attempt to characterize the degree of supercoiling of the molecules, although a single band was observed in gel electrophoresis. With these caveats in mind, we can still compare our results with previously reported theories and experiments. Interestingly, we find a scaling exponent of $\nu_S = 0.571 \pm 0.057$ which is similar to the scaling exponents we found for the linear and relaxed circular forms. Flow field-flow fractionation has previously been used to estimate *D* for three short supercoiled molecules (~2.7 - 7.4 kbp) and a value of $\nu_S = 0.66$ was reported (81), while light scattering measurements for five short supercoiled DNA molecules (2.1 - 10.2 kbp) found $\nu_S = 0.6$ (82). Theory of the conformation and hydrodynamics of supercoiled DNA is less developed than that of the relaxed circular form and multiple opposing models have been proposed (82-84). One model proposes a rod-like conformation for supercoiled DNA with $\nu_S \cong 0.8$ whereas another model predicts that supercoiled molecules would have a constantly changing conformation, like linear and relaxed circular molecules, and have the same scaling exponent of $\nu_S \cong 0.6$ as the other forms (84). Our findings and the previous findings with shorter DNA molecules appear to be in agreement with this latter model.

We also measured the ratios between the diffusion coefficients of the three different forms of our molecules. We found that the ratio between supercoiled and relaxed circular forms (D_S/D_C) ranged from ~1.1 to 1.4, while the ratios between supercoiled and linear forms (D_S/D_L) ranged from ~1.4 to 1.9. No systematic trend in these ratios with length was observed, so these variations may simply be due to the aforementioned sample variations. Previous measurements of diffusion coefficient

ratios have been limited to relatively short molecules (~1 - 10 kbp) and were made at finite concentrations using bulk methods. In light scattering studies $D_S/D_C = 1.251$ was reported for a 3.7 kbp DNA molecule (84) and $D_S/D_C = 1.18$ and $D_S/D_L = 1.46$ were reported for $ColE_1$ DNA (57). Photon correlation spectroscopy has also been used to study a 2.7 kbp molecule and a ratio of $D_S/D_L = 1.48$ was reported (85). Sedimentation ratios have been measured as well, finding $S^0_S/S^0_C = 1.26$ and $S^0_S/S^0_L = 1.56$ for $ColE_1$ DNA (57) and $S^0_S/S^0_C = 1.25$ and $S^0_S/S^0_L = 1.38$ for polyoma DNA (86). Surprisingly, although the presence of relaxed circular molecules in our samples would be expected to decrease both ratios our average values were actually slightly higher than previously reported experimental values, suggesting that the supercoiled form may be more compact than previously thought.

3.4.3 Fluorescent labeling effects

A potential concern in our measurements is whether the YOYO-I dye may alter the DNA twist. It is well known that the binding of certain dyes, such as ethidium bromide, may cause unwinding of DNA. As the dye:basepair ratio is increased, negatively supercoiled DNA stained with ethidium unwinds to a relaxed circular form and then begins to accumulate positive supercoils (87). Circular DNA relaxed by topoisomerase I is thus expected to become positively supercoiled when stained with ethidium. However, we have found that no such supercoiling occurs upon labeling with YOYO-I dye in the conditions used in our experiment. As many researchers now use this dye this observation constitutes an additional finding worthy of description.

We performed several experiments using pPIC9K<TRL5> DNA to examine the effect of YOYO-I. First, we carried out gel electrophoresis measurements on pre-labeled molecules. The high binding constant of YOYO-I ensures stability of the DNA-dye complex during electrophoresis (88), and YOYO-I fluorescence was observed on gel bands corresponding to labeled samples, confirming this stability. Furthermore, it has been shown that DNA supercoiling may be quantified by electrophoresis since the mobility increases with increasing supercoiling (89-91). We compared the supercoiled form, the relaxed circular form produced by treatment with topoisomerase I, and the relaxed circular form produced by nicking the DNA with a nicking endonuclease Nt.Bst.NBI (61). The relaxed circle produced by topoisomerase I has the potential to accumulate twist whereas the nicked form does not (60). As shown in Figure 3.2, we observed no change in mobility of any of the three forms of circular DNA at the level of YOYO-I staining used in our experiments.

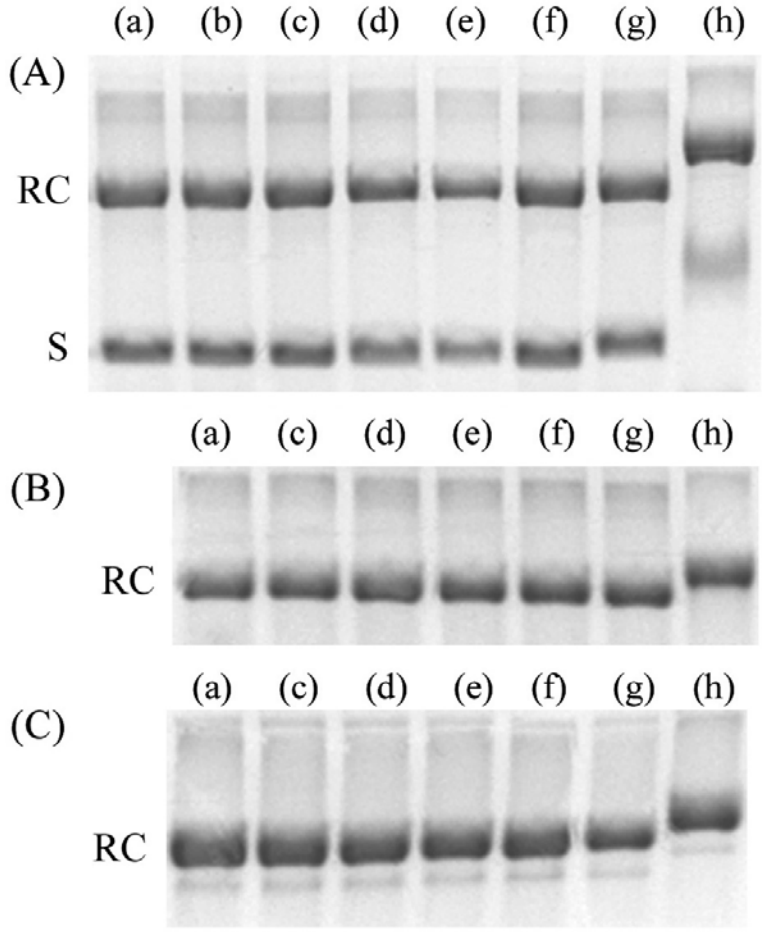

Figure 3.2 Agarose gel electrophoresis of YOYO-I labeled pPIC9K<TRL5> DNA samples containing **(A)** initial mixture of supercoiled (S) and relaxed circular (RC) species **(B)** relaxed circular form produced by treatment with topoisomerase I **(C)** nicked circular form. The staining level was varied as follows (in bp per dye molecule): (a) unlabeled DNA, (b) 500:1, (c) 50:1, (d) 5:1, (e) 1:2, (f) 1:20, (g) 1:200 and (h) 1:2000. The samples were incubated in the dark for 2 h at 50 °C to ensure homogeneous labeling. A 1% agarose gel was run using TAE buffer and post-stained with ethidium bromide to make the bands uniformly visible.

To confirm this finding, we also compared the diffusion of these different species. The value of D for molecules relaxed by topoisomerase I differed by less than 3% from the value for nicked molecules, whereas D measured for the sample containing supercoiled molecules was 20% higher. Thus, the relaxed circular DNA does not become supercoiled under the conditions of our experiments.

3.5 Conclusion

In conclusion, power-law scaling was observed for the relaxed circular, linear, and supercoiled DNA forms, in good agreement with certain theoretical predictions (45, 46, 84). We report the first measurement of the dependence of the diffusion coefficient on molecular length for relaxed circular DNA. Our observation of a scaling exponent of $\nu_C \cong 0.59$ is the first experimental finding for any circular polymer of an exponent that agrees with theoretical predictions for long molecules in a good solvent. Further, the findings provide evidence in support of several theories that predict an effective diameter of DNA much greater than the Debye screening length. We also report the first measurement for DNA of a length-independent ratio of diffusion coefficients for linear and circular relaxed molecules ($D_C/D_L \cong 1.32$). This measured ratio is significantly greater than that predicted by the classical Kirkwood theory and is in closer agreement with predictions of more recent renormalization group calculations.

3.6 Acknowledgements

Chapter 3, in part, is a reprint of the material as it appears in Proceedings of the National Academy of Sciences. Robertson, R. M., Laib, S. & Smith, D. E. *Proceedings of the National Academy of Sciences U.S.A.* **103**, 19, 7310-7314 (2006). The dissertation author was the primary investigator and author of this paper.

Chapter 4

Strong Effects of Molecular Topology on Diffusion of Entangled DNA Molecules

4.1 Abstract

When long polymers such as DNA are in a highly concentrated state they may become entangled, leading to restricted self-diffusion. Here we investigate the effect of molecular topology on diffusion in concentrated DNA solutions and find surprisingly large effects, even with molecules of modest length and concentration. We measured the diffusion coefficients of linear and relaxed circular molecules by tracking the Brownian motion of single molecules with fluorescence microscopy. Four possible cases were compared: linear molecules surrounded by linear molecules, circular molecules surrounded by linear molecules, linear molecules surrounded by circles, and circles surrounded by circles. In measurements with 45 kbp DNA at 1 mg/ml, we found that circles diffused ~100 times slower when surrounded by linear molecules than when surrounded by circles. In contrast, linear and circular molecules diffused at nearly the same rate when surrounded by circles, and circles diffused ~10 times slower than linears when surrounded by linears. Thus, diffusion in entangled DNA solutions is strongly dependent on topology of both the diffusing molecule and the surrounding molecules. This effect is also strongly dependent on DNA concentration and length. The differences largely disappeared when the concentration

was lowered to 0.1 mg/ml or when the DNA length was lowered to 6 kbp. Present theories cannot fully explain these effects.

4.2 Introduction

DNA is rather unique among polymers in that it is naturally found in a number of different topological forms, including linear, supercoiled circular, relaxed circular, knotted circular, and branched. DNA solutions handled *in vitro* in molecular biology research are often relatively concentrated (~1-10 mg/ml, for example, following lysis of bacterial cells during DNA isolation, or when DNA is re-dissolved following ethanol precipitation). According to classical theories and experiments in polymer physics, long flexible molecules form random coils that overlap and become entangled as the concentration of solution is increased (1, 12). In the field of polymer physics and rheology there is considerable fundamental interest in understanding the effect of molecular topology on entangled polymer dynamics (2, 92). In gel electrophoresis of DNA it is well known that molecular topology strongly affects the mobility of DNA. However, with few exceptions, most theories and experiments on diffusion in concentrated polymer solutions have examined only linear molecules. Here we investigate the effect of molecular topology on the diffusion of entangled DNA. Although relaxed circular molecules differ from linear molecules only by the presence of one additional pair of phosphodiester bonds (linking head to tail) and diffuse at nearly the same rate in dilute solution (see Chapter 3), we observe large differences in their diffusion rates with molecules of modest size and concentration.

4.3 Materials and Methods

A 45 kbp fosmid DNA construct (pCC1FOS45) was prepared as described in Chapter 2. It was treated with topoisomerase I to prepare the relaxed circular form and with ApaI to prepare the linear form (see Chapters 2 and 3). The DNA was concentrated by isopropanol precipitation and resuspended in TE buffer (Tris-HCl, EDTA, pH 8) with 10 mM NaCl. At this ionic strength it has been predicted and experimentally confirmed that intrinsic DNA charge is moderately screened (93), and that charge repulsion results in a ~5-fold increase in the effective diameter (distance of closest approach) of the DNA molecule from its bare diameter of 2 nm, as discussed in Chapter 3.4.1 (66, 67, 94). Since we only have monovalent counterions present, the DNA-DNA interactions are purely repulsive such that excluded volume considerations are important and there is no aggregation or condensation of the DNA (95, 96). Self-diffusion coefficients were measured by labeling a small fraction of molecules with YOYO-I and tracking Brownian motion with video microscopy, as described in Chapter 3. In all cases we found that the mean squared displacement increased linearly with time, indicating conventional diffusion.

4.4 Results and Discussion

Here we study all four possible topological combinations of linear and circular DNA molecules: linear molecules surrounded by linear molecules (L-L), circular molecules surrounded by linear molecules (C-L), linear molecules surrounded by

circles (L-C), and circles surrounded by circles (C-C). These cases are depicted schematically in Figure 4.1.

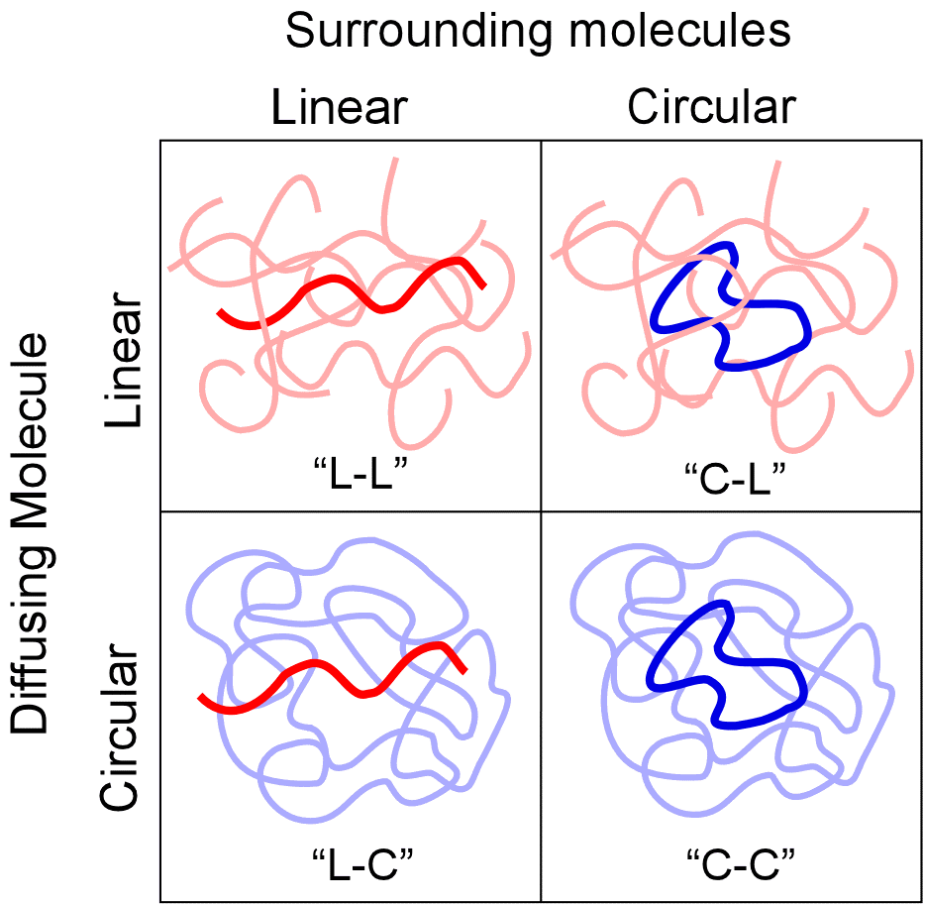

Figure 4.1 Schematic illustration of the possible topological combinations of concentrated linear and relaxed circular DNA molecules. The four cases depicted are: a linear diffusing molecule surrounded by linear molecules (labeled "L-L"), circular molecule surrounded by linear molecules ("C-L"), linear molecule surrounded by circular molecules ("L-C"), and circular molecule surrounded by circular molecules ("C-C"). Linear molecules are shaded red and circular molecules are blue. For clarity, the diffusing molecules are represented by brighter, thicker lines than the surrounding molecules.

At 1 mg/ml we observed dramatic differences in the diffusion coefficients (Figure 4.2 and Table 4.1). Changing the topology of the surrounding molecules had the largest overall effect. Most strikingly, the diffusion coefficient D of a circular molecule decreased by ~100-fold when the surrounding DNA was changed from circular to linear. A smaller though still quite significant decrease of ~6-fold was observed with linear DNA when the surrounding DNA was changed from circular to linear. The topology of the diffusing molecule also affected the result. When the surrounding DNA was circular the topology of the diffusing molecule made very little difference ($D_{C\text{-}C} \cong 1.3D_{L\text{-}C}$), but when the surrounding DNA was linear there was a sharp difference ($D_{L\text{-}L} \cong 10D_{C\text{-}L}$). In the dilute solution diffusion measurements described in Chapter 3 we found that the radius of gyration of the linear form was only 1.58 times that of the circular form, thus this 10-fold difference cannot simply be attributed to a size difference between circular and linear molecules of equal length, and must be attributed to the influence of topology on entanglement effects.

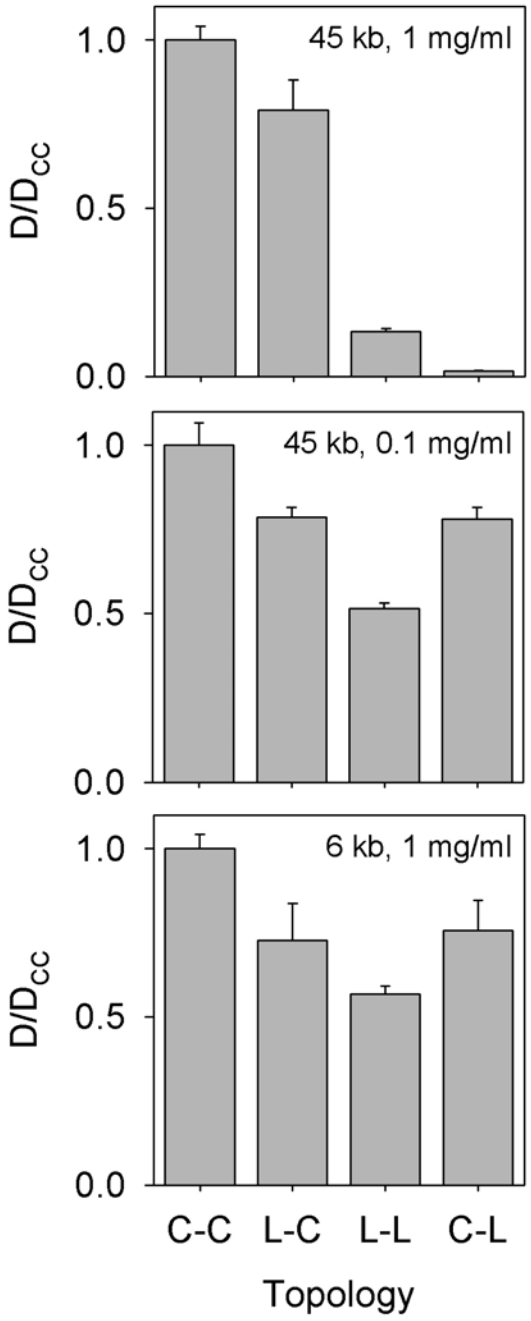

Figure 4.2 Dependence of DNA self-diffusion coefficients *D* on molecular topology. Bar graphs display normalized *D* values vs. topological case (depicted in Figure 4.1). All *D* values are normalized by the corresponding measured diffusion coefficient for a circular DNA surrounded by circular DNA ($D_{C\text{-}C}$) (the highest value of *D* in each case). The DNA length and concentration is listed at the top right of each plot.

To investigate the dependence of these topological effects on concentration we made additional measurements with the 45 kbp DNA diluted to 0.1 mg/ml. In this case we found that all four *D* values were within a factor of 2 of each other (Figure 4.2). Thus, these topological effects are only important at high concentration and the onset is between 0.1 and 1 mg/ml.

To investigate the dependence on DNA length we also made further measurements with a 6 kbp DNA construct at both 1 mg/ml and 0.1 mg/ml. This sample was digested with BamHI to prepare the linear form. With this shorter molecule there were only minor effects of topology, even at 1 mg/ml (Figure 4.2 and Table 4.1). Most conspicuously, while $D_{C\text{-}L}$ decreased only ~4-fold when DNA length was increased from 6 to 45 kbp at 0.1 mg/ml, it decreased by almost ~1000-fold at 1 mg/ml. Interestingly, the small differences in the four topological cases with the 6 kbp sample were almost identical at both concentrations and mimicked those measured with the 45 kbp DNA at 0.1 mg/ml. Thus, reducing the DNA length had an equivalent effect to reducing the concentration. Our interpretation is that the 6 kbp molecules are too short to effectively become entangled regardless of their topology.

Table 4.1 Measured DNA diffusion coefficients ($\mu m^2/s$) for the different length, concentration, and topological combinations of molecules.

	C-C	**L-C**	**L-L**	**C-L**
45 kbp, 1 mg/ml	0.026 ± 0.001	0.021 ± 0.002	0.0035 ± 3e-4	4.0e-4 ± 5e-5
45 kbp, 0.1 mg/ml	0.43 ± 0.03	0.33 ± 0.01	0.22 ± 0.01	0.33 ± 0.01
6 kbp, 1 mg/ml	0.46 ± 0.02	0.33 ± 0.05	0.26 ± 0.01	0.35 ± 0.04
6 kbp, 0.1 mg/ml	1.71 ± 0.19	1.22 ± 0.11	1.04 ± 0.07	1.45 ± 0.16

While several previous experiments, including those described in Chapter 3, have measured DNA diffusion in dilute solutions (24, 81, 97-100), very few have examined the effect of entanglements. Dynamic light scattering was used to study supercoiled 2.3 kbp DNA molecules at concentrations up to 4.0 mg/ml (100) and the results were in qualitative agreement with predictions for semi-dilute rigid rod polymers. This is a very different regime than considered here. Photobleaching recovery was used to study longer 48.5 kbp DNA solutions up to 0.3 mg/ml (101), but only a weak concentration dependence was observed and only the linear form was studied. 48.5 kbp linear DNA was also studied at higher concentrations (up to 0.8 mg/ml) and a sharp decrease in D was observed above ~0.5 mg/ml (39). In this regime, the dependence on length and concentration was found to be in accord with predictions of the reptation model for entangled polymer dynamics (12). The key postulate of this model is that the entangled molecule is confined to a tube-like region parallel to its contour. Diffusion occurs by a slithering motion of the molecule whereby it may escape head-first or tail-first from the tube. Motion in a direction perpendicular to the tube (and molecular contour) is highly restricted and can only occur if the surrounding molecules move out of the way, a process termed "constraint release" which is predicted to be very slow compared to reptation.

The reptation model was originally developed to describe polymer melts, i.e. molten synthetic polymers with a polymer volume fraction of 1. This situation is potentially very different than that of our DNA solutions, where the highest volume fraction is $\sim 10^{-3}$. While reptation models have been extended to describe polymer

solutions by the use of scaling arguments, the case of circular molecules has not been considered. Thus, we can only compare our results with predictions for melts. As circular molecules have no heads or tails by which to slither out of a tube-like constraint they cannot diffuse by normal reptation. Three configurations have been proposed for circular molecules in a melt of linear molecules (6). First, the circle could be pinned or threaded such that it can only move by constraint release (Figure 4.3c,d). Second, it could be unpinned but ramified by large loops (Figure 4.3b). Third, it could be unpinned with no large loops and move by reptation (similar to a linear molecule of half the length) (Figure 4.3a). Constraint release is predicted to dominate in the limit of long molecular length, leading to greatly hindered diffusion for a circular molecule. This prediction is thus consistent with our finding that $D_{C\text{-}L} << D_{L\text{-}L}$. It has also been speculated, though not proven, that constraint release would be negligible and that reptation would dominate the diffusion of circular polymers in a circular melt (6). This conjecture is consistent with our finding that $D_{C\text{-}C} >> D_{C\text{-}L}$. Several computer simulations have also predicted $D_{C\text{-}C} > D_{L\text{-}L}$ (102, 103). However, none of these analyses of melts can fully explain our results. None apply to solutions with low volume fraction, none predict concentration dependence, and none consider all four of the topological combinations that we have studied.

Surprisingly, most of the experimental findings for synthetic polymer melts differ quite dramatically from our findings with DNA. $D_{L\text{-}L} > D_{C\text{-}C}$, $D_{C\text{-}C} \cong D_{C\text{-}L}$, $D_{L\text{-}L} \cong D_{L\text{-}C}$, and $D_{L\text{-}L} > D_{C\text{-}L}$ have been reported (104-107). Only one of these results ($D_{L\text{-}L} > D_{C\text{-}L}$) was in qualitative agreement with our findings on DNA solutions. However,

in this study a smaller difference (of ~5-fold) was observed despite the use of melt with polymers of a greater number of persistence lengths and a 1000-fold higher volume fraction. Only one previous study, using pulsed-gradient NMR, has examined circular polymers in solution and found $D_{C\text{-}C} > D_{L\text{-}L}$ (108). However, in this study a theta solvent was used and the measured ratio $D_{C\text{-}C}/D_{L\text{-}L} \cong$ 1-2 was fairly constant over the entire concentration range, while in our measurements it increased from ~2 to 10. No previous experiments have investigated solutions where the diffusing and surrounding molecules had different topologies.

While such topological effects on diffusion in concentrated solutions of DNA have not been previously examined, strong effects of molecular topology on DNA mobility in gel electrophoresis are well known (41) and numerous theories have been put forward to explain these effects (109-111). When plasmid DNA of ~3-10 kbp is electrophoresed at constant voltage (DC) in 0.8% agarose the supercoiled form runs the fastest, followed by the linear and relaxed circular forms. However, with ~40-300 kbp fosmids and BACs the linear form migrates the fastest followed by the supercoiled form, while the mobility of the relaxed circle is practically zero (112, 113). More recently, fabricated nanostructures have been used to study transport and conformation of single DNA molecules of different lengths and topologies and have led to many insights into their dynamics in confined environments (114-116). The reptation model was originally used to explain DNA mobility in both DC and pulsed-field gel electrophoresis as well as other confined environments, however predictions did not always match experiment, and further contributions and corrections were

needed to account for the observed motion (109). Loop formation is predicted to play a large role in the migration of circular DNA as well as long linear DNA molecules (110) and the zero mobility phenomenon of long relaxed circular DNA has been attributed to the pinning of the relaxed circular DNA by free ends of the gel fibers or other impurities (111-113, 117). Further, because DNA is continually stretched by a driving electric field, tension plays an important role in its dynamics (118, 119). These studies shed light on the mechanism by which both linear and circular DNA move through fixed obstacles. However, while the mechanism of diffusion of DNA past rigid, fixed obstacles (gel fibers) may be compared to the case of an entangled DNA solution (where the obstacles formed by the surrounding molecules are dynamic), the two cases are still quite different. Gel electrophoresis not only involves fixed obstacles but the motion of the DNA is driven by an electric field, whereas in our experiment molecules are freely diffusing in all directions. Further, our examination of how the topology of the surrounding molecules affects diffusion has no analogy in gel electrophoresis as in that case the obstacles are not DNA molecules of varying topologies.

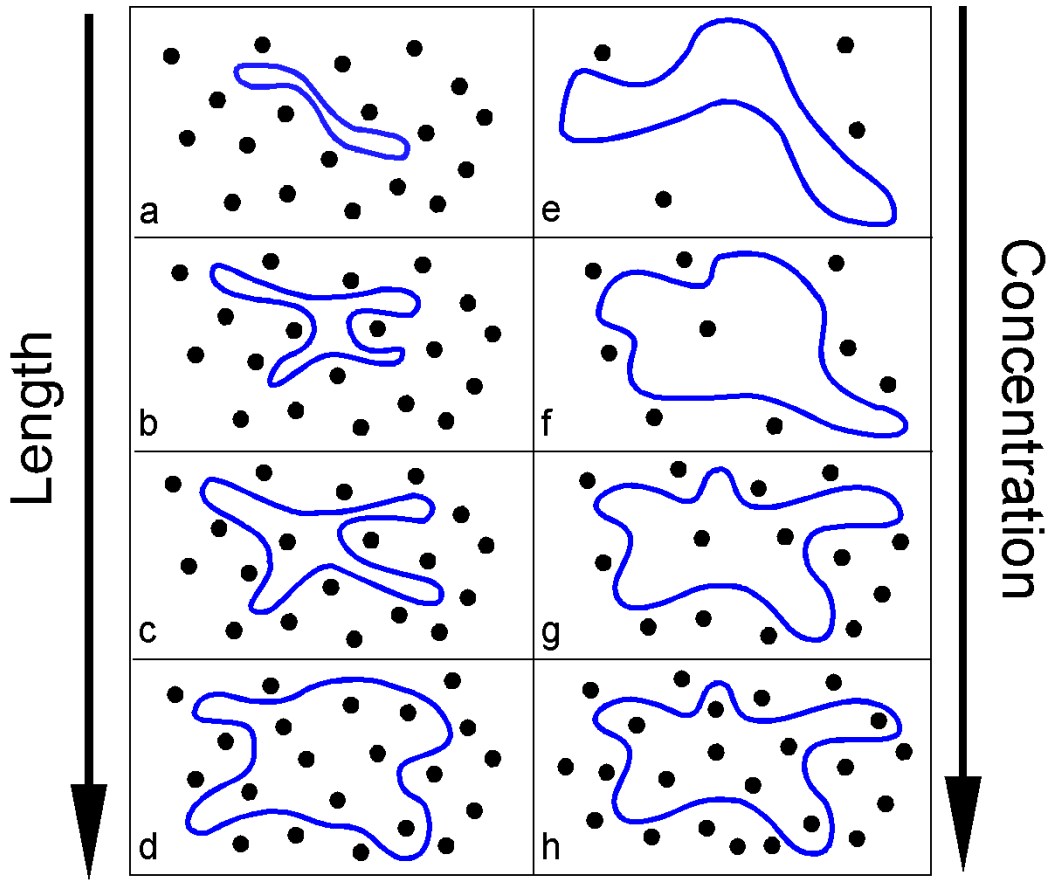

Figure 4.3 Schematic model of the effect of increasing length and concentration on the conformation and diffusion of a circular DNA molecule. Black dots represent "obstacles" formed by surrounding entangled DNA molecules and the blue loop represents a diffusing circular DNA. The left column [(a)-(d)] illustrates the effect of increasing the molecular length, as proposed in Reference 6. The right column [(e)-(h)] portrays the effect of increasing concentration. With short length (a) or low concentration (e) the molecule is most likely unthreaded and can diffuse by reptation. As length [(c),(d)] or concentration [(f)-(h)] increases DNA is increasingly likely to get threaded and can only diffuse by constraint release of the surrounding entangling DNA.

4.5 Conclusions

In summary, we report strong effects of molecular topology on the diffusion of entangled DNA molecules of modest size and concentration. We found that the topology of the surrounding molecules has a very strong influence and the topology of the diffusing molecule has a strong influence only when the surrounding molecules are linear. These findings suggest that free ends of molecules play a critical role in generating entanglements that retard diffusion. We propose that the strongly hindered diffusion of long circular DNA molecules surrounded by linear molecules is due to threading of the ends of the linear molecules through the circles, as predicted for polymer melts (6), which would prevent reptation. Diffusion would then likely be governed by constraint release, as proposed for melts, and the probability of threading would increase as either the length or concentration was increased (Figure 4.3). While the circular molecule never becomes completely unthreaded, the linear molecules that thread it are constantly changing, and we can determine the average time for a linear molecule to thread or unthread a circle. A linear molecule will become unthreaded in the time it takes to diffuse a distance equal to twice its radius of gyration. Thus, using our L-L diffusion measurement, previously determined radius of gyration (see Chapter 3) and Einstein's law, $R_G^2 = 6Dt$, we find the mean unthreading time to be 73 seconds. In contrast, in gels the obstacles are fixed, such that constraint release is prohibited. The comparatively high values of $D_{C\text{-}C}$ and $D_{L\text{-}C}$ are consistent with the conjecture that constraint release would be negligible in circular melts (6). However, the clear qualitative differences between our findings and those with melts suggest

caution in relating DNA solutions to synthetic polymer melts. In any case, our findings provide evidence of a previously unreported dramatic effect of topology on concentrated DNA molecules. Such effects are of fundamental interest in polymer physics and polymeric fluid rheology and may influence the molecular dynamics in *in vitro* molecular biology studies when long, concentrated DNA molecules are present.

4.6 Acknowledgements

Chapter 4, in part, is a reprint of the material as it appears in Proceedings of the National Academy of Sciences. Robertson, R. M. & Smith, D. E. *Proceedings of the National Academy of Sciences U.S.A.* **104**, 12, 4824-4827 (2007). The dissertation author was the primary investigator and author of this paper.

Chapter 5

Self-diffusion of Entangled Linear and Circular DNA Molecules: Dependence on Length and Concentration

5.1 Abstract

Self-diffusion coefficients D of DNA molecules of varying length and concentration were measured by tracking the Brownian motion of individual fluorescently labeled tracer molecules. Four possible cases were examined: linear tracer molecules surrounded by linear molecules (L-L), circular tracers surrounded by linears (C-L), linear tracers surrounded by circles (L-C), and circles surrounded by circles (C-C). With 6 and 11 kbp DNA D was largely insensitive to topology and varied consistent with Rouse scaling ($D \sim L^{-1}c^{-0.5}$). In contrast, with 25 and 45 kbp DNA topology had a strong influence. At 1 mg/ml we found $D_{C\text{-}C} > D_{L\text{-}C} >> D_{L\text{-}L} >> D_{C\text{-}L}$. In the L-L, L-C, and C-C cases a crossover from scaling consistent with the Rouse model to scaling consistent with the reptation model ($D \sim L^{-2}c^{-1.75}$) was observed at ~6 times the molecular overlap concentration. In contrast, $D_{C\text{-}L}$ decreased much more steeply with concentration, indicating that a process much slower than reptation governs that case.

5.2 Introduction

The physical behavior of entangled polymer solutions has been the subject of a plethora of theoretical and experimental studies. Entangled *linear* polymer solutions have been thoroughly investigated (2) and molecular diffusion and linear viscoelastic response in such systems have been found to be well described by the reptation model of de Gennes (12) and Doi and Edwards (1). The key assumption of this model is that on short time scales any given "tracer" molecule is confined by entanglements with the surrounding "matrix" molecules to move within a tube-like region parallel to its own contour. Such tube-like motion has been directly imaged by fluorescence microscopy (26, 39). In this regime, the predicted scaling of the self-diffusion coefficient D with molecular length L and concentration c in good solvent conditions is $D \sim L^{-2}c^{-1.75}$ (1). Below a certain concentration c_e or length L_e (but above the molecular overlap concentration, calculated as $c^* \cong (4/3)\pi M/N_A R_G^3$ where M is molecular weight and N_A is Avogadro's number (1)) entanglement effects should no longer dominate and D is expected to follow the predictions of the Rouse model (1, 120), $D \sim L^{-1}c^{-0.5}$. Below c^*, the Rouse model is no longer valid because hydrodynamic interactions become important, and D is predicted by the Zimm model to be independent of c and to scale as $D \sim L^{-0.588}$.

While the predicted scaling laws for both the Rouse and reptation regimes have been confirmed for linear polymers (121, 122), fewer studies have examined the crossover region. Most have used polymer melts, where the concentration is not variable, to achieve high degrees of entanglement. Further, there is no clear consensus

on the molecular length scales and concentrations over which this shift from the Rouse to the reptation regime occurs (123, 124), and no reliable way to calculate L_e and c_e based on molecular theory has been proposed.

Circular polymers (also referred to as cyclic or ring polymers) have been the subject of far fewer studies. As they have no ends by which to escape tube-like constraints, they seemingly could not undergo normal reptation and are thus an intriguing case. Furthermore, DNA is naturally found in both linear and circular forms, making this a case of practical interest. Constraint release, the shifting of the matrix chains constraining the tracer chain motion, has been predicted to play an important role in circular polymer diffusion, especially when the chains forming the entanglements are linear (6). Klein proposed three possible conformations for circular tracers in melts of linear polymers (C-L melts): (i) the circle is pinned or threaded by the surrounding chains, (ii) it is unpinned but ramified (large loops are present), or (iii) it is unpinned and linear (no large loops) (6). The probability of (ii) and (iii) to occur was predicted to be an exponentially decaying function of tracer chain length and the process by which (iii) diffuses is predicted to be similar to that for reptation of a linear chain of length *L/2*. Disregarding case (ii), which would have a lower self-diffusion coefficient than (iii), the predicted contribution from the unpinned cases for a circular tracer chain is $D_U \sim D_{rep}(L/2)e^{-\beta L}$, where β is a constant. Reptation is not possible in case (i) and the proposed mechanism is constraint release.

Graessley predicted that a polymer diffusing by constraint release would obey the scaling $D_{CR} \sim L^{-1}L_m^{-3}$ where L is the tracer chain length and L_m is the length of the

matrix chains (125). Klein modified this prediction, suggesting $D_{CR} \sim L^{-1}L_m^{-5/2}$, and further predicted the net self-diffusion coefficient for the C-L case to be $D_{C\text{-}L} = D_U + D_{CR}$. For small tracer chains the probability for (i) to occur was predicted to be extremely low, such that $D_{C\text{-}L} \sim D_U$. As L is increased D_{CR} is predicted to dominate. In addition, Mills considered a circle threaded only once by a linear chain (107), predicting $D_{P1} \sim L^{-1}L_m^{-1}$ for this conformation. The L-C and C-C cases were not addressed in these theories, although Klein conjectured that constraint release would be negligible in the C-C case and that reptation would dominate even at long chain lengths (6). What molecular geometries would allow for such behavior is unclear.

Several simulations of C-C and L-L polymer melts have been carried out and $D \sim L^{-\nu}$ was reported with ν ranging from 0.9 to 2, consistent with Rouse and reptation predictions. Three studies predicted $D_{C\text{-}C} > D_{L\text{-}L}$ for all lengths examined (102, 103, 126), whereas one predicted a crossover from $D_{C\text{-}C} < D_{L\text{-}L}$ to $D_{C\text{-}C} > D_{L\text{-}L}$ above a certain length (127, 128). One study also predicted that L_e would be ~2-5 times higher for the C-C case than for the L-L case (126). However, no theories are available for direct comparison, as none have considered the concentration dependence of D for solutions of circular polymers or combinations of circular and linear polymers.

The majority of previous experiments with circular polymers compared $D_{C\text{-}C}$ to $D_{L\text{-}L}$ for polymer melts. In disagreement with the simulations, three experimental studies found $D_{L\text{-}L} > D_{C\text{-}C}$ for all lengths examined (104, 105, 129), and two reported that L_e was roughly the same for *L-L* and *C-C* (130, 131). Scaling exponents of $\nu = 1$ to 2.34 were reported.

Three experimental studies have examined C-L melts. One reported $D_{C\text{-}L} \sim L^{-0.83}$, concluding that the length range used was too low to study entanglement effects (105). A second found $D_{C\text{-}C} \cong D_{C\text{-}L}$, with values in accord with the L-L case, concluding that both systems diffused by reptation (106). Threading or pinning of the tracer was thought to be unlikely in the C-L case due to the short length used. The third study found $D_{C\text{-}L} > D_{L\text{-}L}$ crossing over to $D_{L\text{-}L} > D_{C\text{-}L}$ as L was increased (107). These $D_{C\text{-}L}$ values lie between those predicted by reptation and constraint release models. For the longest matrix length $D_{C\text{-}L} \sim L^{-3.2} L_m^{-\sigma}$, with σ ranging from 0 to 1.6, was reported, in contradiction with the prediction of $D_{CR} \sim L^{-1} L_m^{-3}$ for simple constraint release (125), but in accord with the once-threaded circle model (107).

Only one experimental study has compared the L-C and L-L cases, finding $D_{L\text{-}C} \cong D_{L\text{-}L}$ for all lengths studied, in qualitative accord with the predicted result for a linear tracer undergoing reptation and constraint release in a linear matrix (106). Also, only one experimental study investigated concentration dependence with circular polymer solutions (108), finding a similar trend for C-C and L-L, but with $D_{C\text{-}C} > D_{L\text{-}L}$. Although a good solvent was used in this experiment, $D_{C\text{-}C} \sim D_{L\text{-}L} \sim c^{-3.0}$ was unexpectedly observed, which is the scaling predicted for a theta solvent (vs. $D_{L\text{-}L} \sim c^{-1.75}$ for good solvents).

Previously, four linear DNA constructs were studied with a length range of 6.6 to 48.5 kbp diffusing in solutions of linear λ DNA (48.5 kbp) (39). Results with 48.5 or 23.1 kbp tracer molecules were consistent with $D \sim c^{-1.75}$ for concentrations of 0.5 to 0.8 mg/ml. At 0.63 mg/ml $D \sim L^{-1.8\pm0.1}$ was found.

Here, we comprehensively examine how the self-diffusion coefficient of a tracer DNA molecule varies with concentration, length, and topology of both the tracer chain and the matrix chains. We examine all four possible topological cases: L-L, C-L, C-C, and C-L. For each case four different DNA lengths and ten different concentrations were studied, chosen to span the range from semi-dilute to concentrated (entangled) regimes.

5.3 Materials and Methods

Double-stranded DNA molecules of 5.9, 11.1, 25, and 45 kbp ($N \cong 20$ to 150, also see Table 5.1) were prepared by replication of cloned plasmid and fosmid constructs in *E. coli* as described in Chapter 2. The restriction enzymes BamHI and ApaI were used to prepare the linear form, and topoisomerase I was used to prepare the relaxed circular form (see Chapters 2 and 3). Tracer molecules were labeled with YOYO-I (dye molecule to base pair ratio of 1:6) and imaged with a custom-built epi-flourescence microscope (Figure 2.1) as described in Chapter 2. The samples were mixed with unstained DNA in an aqueous buffer solution (10 mM Tris-HCl (pH 8), 1 mM EDTA, 10 mM NaCl) by slowly pipetting ~20 times with a wide-bore tip, which has been shown to yield a homogeneous solution (132). Oxygen scavenging and anti-oxidant reagents were added to reduce photobleaching, as described in Chapter 2. Diffusion coefficients D were determined by tracking of Brownian motion, over a length scale of ~2-10R_G, as described in Chapter 3.3.3 (133). Briefly, the center of mass (x, y) coordinates of >1000 paths of >20 different molecules were tracked and

the Einstein relationship $\langle x^2 \rangle = \langle y^2 \rangle = 2Dt$ was used to determine the diffusion coefficient.

Table 5.1 Contour Lengths, Number of Kuhn Lengths (*N*), Radii of Gyration, and Overlap Concentrations for linear and relaxed circular DNA molecules.

DNA construct	size (kbp)	Contour Length* (μm)	*N***	$R_{G,L}$ (μm)	$R_{G,C}$ (μm)	c* (mg/ml)
pYES2	5.9	2.65	20	0.213	0.131	0.27
pPIC9K<TRL5>	11.1	4.99	37	0.279	0.173	0.22
pCC1FOS25	25	11.2	84	0.449	0.264	0.12
pCC1FOS45	45	19.8	150	0.624	0.554	0.08

*This length accounts for the ~1.35 increase in length caused by YOYO-1 (see Chapter 2)
**Kuhn length of dsDNA is ~100 nm at ionic strength used with ~1.35 increase upon staining

5.4 Results and Discussion

5.4.1 Concentration Dependence

The measured dependences of *D* on concentration are shown in Figures 5.1 & 5.2. First we compare the cases with circular matrix molecules. $D_{C\text{-}C} > D_{L\text{-}C}$ was observed for all concentrations and lengths. These two cases have not been directly compared in any previous study with any type of polymer. When the *D* values were normalized by their corresponding values at infinite dilution (Table 3.1) they approximately collapsed onto a single curve. With the shortest length (5.9 kbp) $D \sim c^{-\alpha}$ was observed, with $\alpha_{C\text{-}C} = 0.60 \pm 0.04$ and $\alpha_{L\text{-}C} = 0.56 \pm 0.04$, only slightly higher

than $\alpha = 0.5$ predicted by the Rouse model. With the three longer molecules $\alpha \cong 0.5$ was observed at low concentration, but a significant increase in α was noted starting at ~0.7, ~0.5, and ~0.3 mg/ml for L = 11.1, 25, and 45 kbp, respectively. The prediction $\alpha = 1.75$ of the reptation model, is approximately (tangentially) reached at ~0.9, ~0.7, and ~0.4 mg/ml for L = 11.1, 25 and 45 kbp, respectively, with both tracer topologies, indicating the onset of entanglement. Thus, c_e decreases with increasing L in both cases. Present theories have not considered these cases, so no comparison with theory is possible. We note that our finding differs from the aforementioned finding by pulsed-gradient NMR of $D_{C\text{-}C} \sim D_{L\text{-}L} \sim c^{-3.0}$ for poly(ethylene oxide) solutions (108).

Next we compare the cases where the matrix molecules are linear (Figures 5.1 & 5.2). While the trends in the L-L and C-L cases were similar to those observed in the L-C and C-C cases with 5.9 and 11.1 kbp molecules, dramatically different behavior was observed with the 25 and 45 kbp molecules. We observed a crossover from $D_{C\text{-}L} > D_{L\text{-}L}$ to $D_{L\text{-}L} > D_{C\text{-}L}$ at a concentration of ~4c^*. $D_{L\text{-}L}$ reached $\alpha \cong 1.75$ at roughly the same concentration as $D_{L\text{-}C}$ and $D_{C\text{-}C}$ leading to the relationship $c_e \cong 6c^*$ for the C-C, L-C and L-L systems. The finding that c_e is independent of topology is in qualitative accord with the topology-independent L_e found in rheology measurements on L-L and C-C polysterene and poly(dimthylsiloxane) melts (130, 131).

Figure 5.1 Self-diffusion rates vs. concentration plotted for each of the four molecular lengths. The diffusion coefficients D at each concentration are normalized by the values in the limit of zero concentration D_0 (see Table 3.1). The different point styles indicate the four different topological cases: circular molecules in a circular matrix (C-C) (open circles), linear molecules in a circular matrix (L-C) (open triangles), circular molecules in a linear matrix (C-L) (filled triangles), and linear molecules in a linear matrix (L-L) (filled squares). The dotted lines indicate the scaling laws $D \sim c^{-\alpha}$ predicted by the Rouse ($\alpha = 0.5$) and reptation ($\alpha = 1.75$) models for linear molecules.

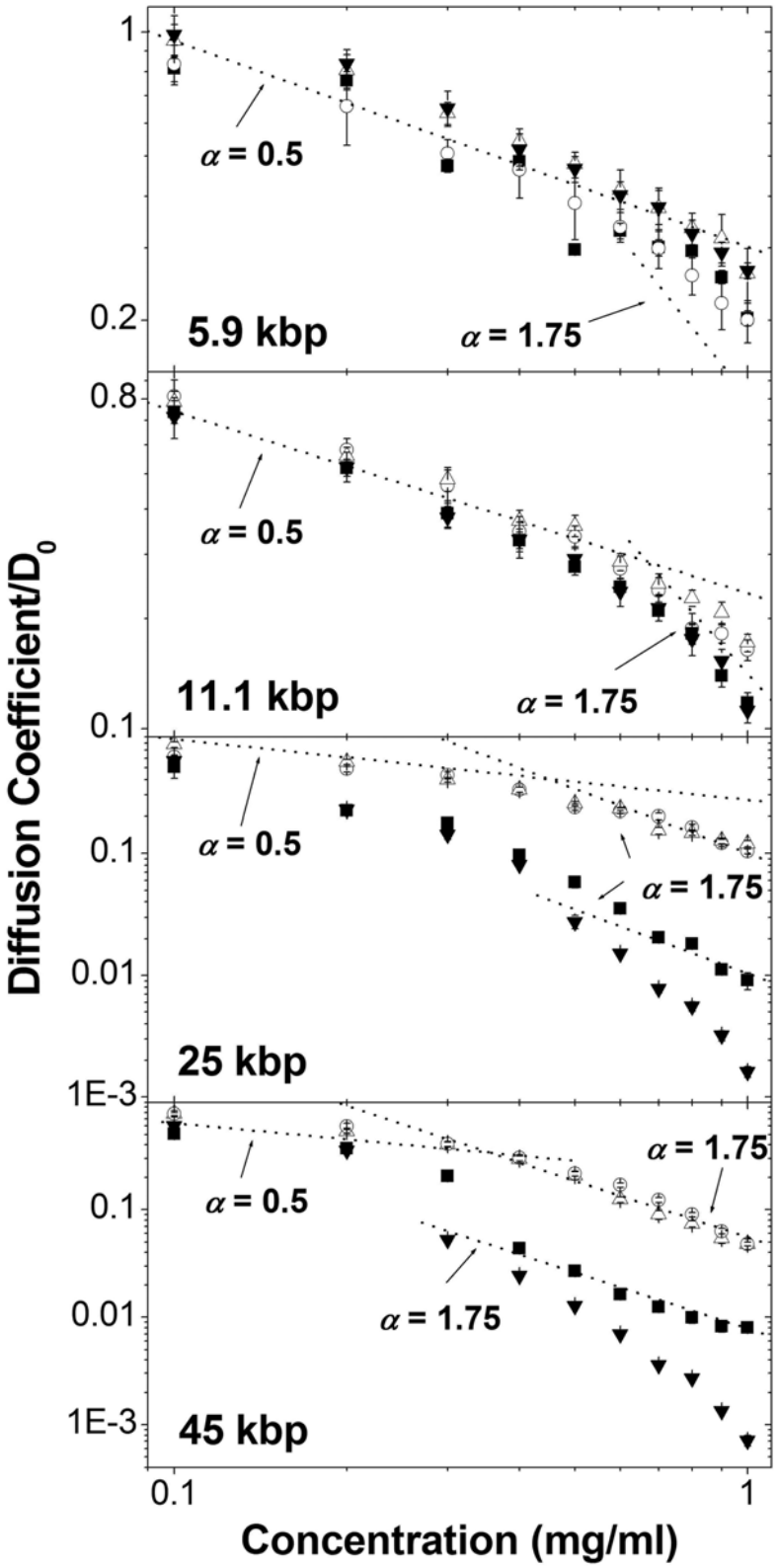
Diffusion Coefficient/D0
Concentration (mg/ml)
5.9 kbp
11.1 kbp
25 kbp
45 kbp
α = 0.5
α = 1.75
1
0.2
0.8
0.1
0.01
1E-3

Figure 5.2 Self-diffusion coefficients vs. concentration plotted for each of the four topological cases. These data are from the same set of measurements as Figure 5.1. The different point styles indicate the four different construct lengths: 5.9 kbp (open squares), 11.1 kbp (filled circles), 25 kbp (open hexagons), and 45 kbp (filled diamonds). The solid lines are power law fits to the 5.9 kbp data giving scaling exponents of $\alpha_{C\text{-}C} = 0.60 \pm 0.04$, $\alpha_{L\text{-}C} = 0.56 \pm 0.04$, $\alpha_{L\text{-}L} = 0.61 \pm 0.06$ and $\alpha_{C\text{-}L} = 0.63 \pm 0.05$. The dotted lines are as in Figure 5.1.

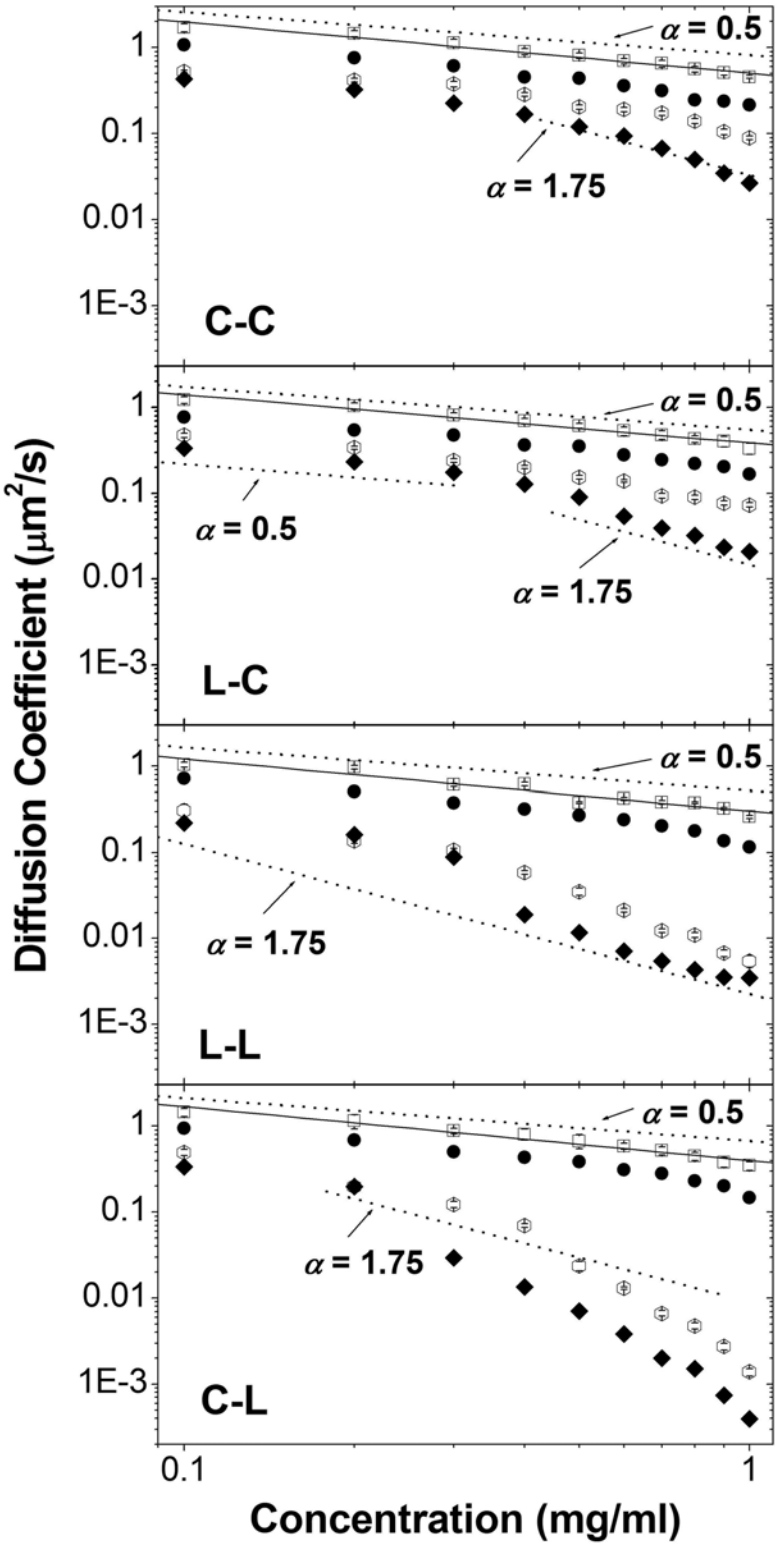
Diffusion Coefficient (μm²/s)
Concentration (mg/ml)
α = 0.5
α = 1.75
C-C
L-C
L-L
C-L
1
0.1
0.01
1E-3

Our results illustrate that the topologies of both the tracer and matrix molecules can have a strong effect on diffusion. At 1 mg/ml $D_{C\text{-}L}$ was ~10 fold smaller than $D_{L\text{-}L}$ and ~100-fold smaller than $D_{C\text{-}C}$. Our findings are qualitatively consistent with Klein's prediction for C-L melts that as the entanglement density is increased, constraint release, which is a much slower mode of diffusion than reptation, would dominate. Our findings are also consistent with Klein's conjecture that constraint release would be negligible for C-C melts and that reptation is the dominant diffusive mechanism. We note that circular polymers cannot diffuse by conventional reptation as they have no ends. However, in Klein's model (conformation (iii)) the circles were envisioned to adopt a collapsed form with the two antiparallel halves of the circle lying tangent to each other, and the reptation was envisioned to be analogous to that of a linear polymer of half the length. Our result of $D_{C\text{-}C} > D_{L\text{-}L}$ agrees qualitatively with the findings of the studies of poly(ethylene oxide) solutions by pulsed-gradient NMR (108). However, we find that $D_{C\text{-}C}/D_{L\text{-}L}$ increases from ~2 to ~10 as the scaling changes from Rouse-like to reptation-like, while in the NMR studies this ratio was found to have a constant value of ~1.5. One possible explanation for this discrepancy could be the difference in the relative concentrations examined. This NMR study probed concentrations up to ~6c^* while our highest concentration was ~12c^* for the 45 kbp molecule.

5.4.2 Length Dependence

The length dependences are shown in Figure 5.3. At low concentrations we find $D_{C\text{-}C} > D_{C\text{-}L} > D_{L\text{-}C} > D_{L\text{-}L}$ for all lengths. As the concentration was increased this relationship shifted to $D_{C\text{-}C} > D_{L\text{-}C} > D_{L\text{-}L} > D_{C\text{-}L}$ at ~4c* with the 25 and 45 kbp molecules. This is in agreement with the prediction $D_{C\text{-}C} > D_{L\text{-}L}$ of three Monte Carlo simulation studies (102, 103, 126), but in disagreement with one Monte Carlo study and findings on alkanes and PDMS by pulsed-gradient spin-echo NMR (104, 105, 127, 129).

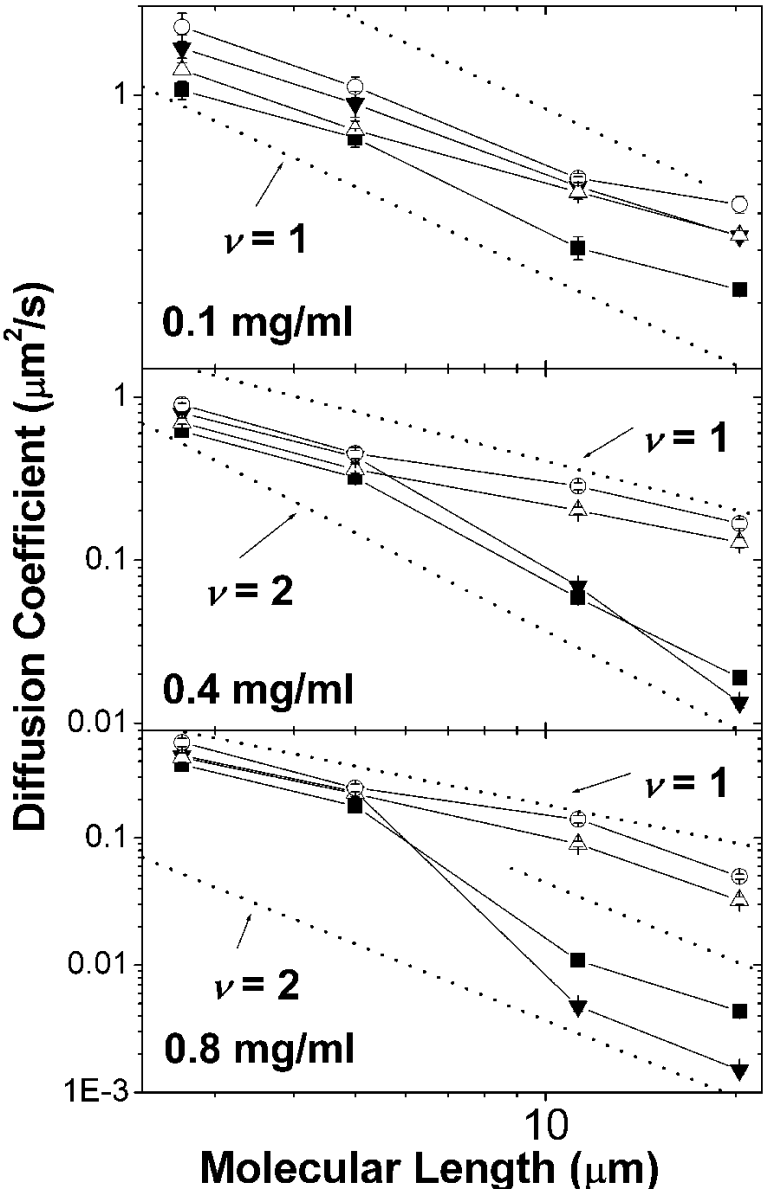

Figure 5.3 Self-diffusion coefficients vs. DNA length plotted for three different concentrations. These data are from the same set of measurements as Figure 5.1. The different point styles indicate the four different topological cases: C-C (open circles), L-C (open triangles), L-L (filled squares), and C-L (filled triangles). The dotted lines indicate the scaling laws $D \sim L^{-\nu}$ predicted by the Rouse ($\nu = 1$) and reptation ($\nu = 2$) models for linear molecules.

Here, in all cases the two shorter constructs showed a scaling exponent between ~0.5 and 1, showing that these solutions were in the dilute to semidilute regimes (with predicted exponents of 0.588 and 1, respectively). This behavior is similar to that found by NMR in the C-C and C-L cases ($\nu_{C\text{-}C} \cong 1$ and $\nu_{C\text{-}L} \cong 0.83$) (104, 105, 129). Scaling exponents with the 25 and 45 kbp molecules, in contrast, ranged from <1 to ~2 at high concentrations for all the topological cases. Similar behavior was reported previously for C-C and L-L melts in three simulation studies and one of the NMR studies (102, 103, 105, 127). A shift from Rouse ($\nu \cong 1$) to reptation ($\nu \cong 2$) scaling with these two constructs occurred at ~0.6 mg/ml with the circular solutions and earlier with the linear solutions (~0.3 mg/ml for C-L and ~0.4 mg/ml for L-L). This finding was quite unexpected for the C-L system. Constraint release is the only presently existing theory that can explain our finding of strongly hindered C-L diffusion, yet $D \sim L^{-4}$ predicted for constraint release (125) was not observed. Instead, the scaling was close to that predicted for reptation ($D \sim L^{-2}$). This result agrees qualitatively with predictions for relaxed circular DNA diffusing in a gel (109), in which DNA was proposed to move around obstacles via finger-shaped loops (akin to the unpinned configurations in Klein's model). However, this agreement is perhaps only fortuitous as this model neglected pinned configurations, which would presumably be important in an entangled polymer solution. Our results suggest that either the predicted scaling of D with L for constraint release is inaccurate or that a different diffusive process slower than reptation may be operating. Our finding of length scaling for $D_{C\text{-}C}$, $D_{C\text{-}L}$, and $D_{L\text{-}C}$ consistent with reptation is consistent with

previous findings of studies of polystyrene by forward recoil spectrometry (106), but their findings of $D_{C\text{-}C} \cong D_{C\text{-}L}$ and $D_{L\text{-}C} \cong D_{L\text{-}L}$, differ from ours. Our finding of $D_{L\text{-}L} > D_{C\text{-}L}$ is qualitatively consistent with one study of polystyrene by forward recoil spectrometry (107), but a higher scaling exponent ($\nu = 3.2$ to 4.8) for $D_{C\text{-}L}$ was found in that study. While similar scaling of D with L was found for all topological cases, there was a dramatic difference in the magnitudes of D. While the 45 kbp DNA diffused ~4 times slower than the 5.9 kbp DNA at 0.1 mg/ml in both the C-C and C-L cases, it diffused ~20 times slower at 1.0 mg/ml in the C-C case and ~1000 times slower in the C-L case. This finding was surprising, as the only previous experiment to compare C-C and C-L (in melts) had found $D_{C\text{-}C} \cong D_{C\text{-}L}$ (106).

Direct comparisons with previous studies of synthetic polymer melts may also be complicated by inherent physical differences between different types of synthetic polymers as well as DNA. In certain situations, a concentration or molecular weight dependent monomeric friction coefficient is thought to contribute to the diffusion coefficient, in addition to Rouse, reptation, and constraint release dynamics. In particular, chain-end free volume effects can lead to a monomeric friction coefficient dependent on molecular length for certain linear chains. However, such chain-end effects have only been found to contribute significantly to diffusion for relatively short, rigid chains (131) whereas they have been found to be negligible for poly(ethylene oxide) (108) and PDMS chains above $N \cong 14$ (131). Thus, our results for DNA of $N \cong 20$ to 150 are not expected to be influenced by such effects. Circular polymers are not subject to chain-end effects, as they have no ends, but packing

density effects can increase their diffusion rates in certain cases. In particular, small (low molecular weight) rings are likely to form flat disc-like structures that can pack more efficiently than the ellipsoid configurations of larger rings and linear chains (131). However, this effect has been shown (131) to be negligible for large rings ($N \geq 20$) such as those studied in our experiments.

5.5 Conclusions

We have shown that molecular topology can have an extremely strong effect on the diffusion of entangled polymers. This is the first study to systematically examine the four possible topological combinations of linear and circular molecules. Strong effects of topology were only apparent above a certain length and concentration. With the 5.9 and 11.1 kbp molecules the results were largely insensitive to topology. We observed concentration scaling exponents of ~0.5 over most of the concentration range, only approaching 1.75 at the highest concentrations. $D \sim L^{-1}$ scaling was evident over most of the length range. Our interpretation is that the 5.9 and 11.1 kbp molecules have lengths below the threshold for strong entanglement effects. With the 25 and 45 kbp DNA the normalized D values in the L-C and C-C cases fall approximately on the same curve, indicating that tracer topology has little effect in solutions of circular polymers. Both cases exhibit scaling close to that predicted by reptation ($D \sim c^{-1.75}$, $D \sim L^{-2}$), supporting the conjecture that constraint release is negligible when the matrix is circular (6). Because circular molecules are more compact than linear molecules it has been argued that circles

would form entanglements less effectively (102). However, while we found $D_{L\text{-}L} << D_{L\text{-}C}$, the concentration threshold c_e appeared to be insensitive to topology. In the linear DNA solutions the tracer topology played a critical role. While $D_{C\text{-}L}$ and $D_{L\text{-}L}$ behaved similarly at low concentration, $D_{C\text{-}L}$ decreased dramatically starting at ~4c^*. Thus, a mechanism much slower than reptation must be operating in the C-L case. Constraint release is the only model presently available to explain such slow diffusion; however, the measured scaling of D with L is weaker than that predicted for constraint release.

5.6 Acknowledgements

Chapter 5, in part, is a reprint of the material as it appears in Macromolecules. Robertson, R. M. & Smith, D. E. *Macromolecules* **40**, 9, 3373 –3377 (2007). The dissertation author was the primary investigator and author of this paper.

Chapter 6

Direct Measurement of the Intermolecular Forces Confining a Single Molecule in an Entangled Polymer Solution

6.1 Abstract

We use optical tweezers to directly measure the intermolecular forces acting on a single polymer imposed by surrounding entangled polymers (115 kbp DNA at 1 mg/ml). A tube-like confining field was measured, in accord with the key assumption of the reptation model. A time-dependent harmonic potential opposed transverse displacement, in accord with recent simulation findings. A tube radius of 0.8 μm was determined, close to the predicted value (0.5 μm). Three relaxation modes (~0.4, 5 and 34 s) were measured following transverse displacement, consistent with predicted relaxation mechanisms.

6.2 Introduction

Over the past several decades much effort has been directed at understanding the physical properties of entangled polymer solutions and melts. The reptation theory introduced by P. G. de Gennes and extended by Doi and Edwards and others has proven quite successful in describing many experimental findings (1, 2, 12, 13). The key assumption of the theory is that on short time scales each molecule is confined, due to entanglements with surrounding molecules, to move within a tube-like region parallel to its own contour. Motion transverse to the molecular contour is predicted to

be highly restricted compared with parallel motion. The advantage of the tube model is that it reduces a complex many-body problem to that of a single polymer moving in an effective mean field. While originally developed for melts, tube models have been successfully extended to polymer solutions using "blob" theory (12, 14), in which each chain is divided into correlation blobs of length ξ (see Chapter 1.3.2.3). The solution is then modeled as a melt of chains with monomer size ξ (15).

While tube theories have proven quite useful, the notion of a "tube-like constraint" has remained rather qualitative. No experiment has directly measured the intermolecular forces acting on a single entangled polymer. An expression for the tube radius has been predicted theoretically (1, 134), but in practice it has only been defined empirically via measurements of the plateau modulus $G_N^{(0)}$ (1, 132). Thus, the confining tube is present in most theories as an assumption rather than being derived from fundamental molecular properties. Elucidation of the nature of this entanglement field has been identified as one of the primary open challenges in the field (2). Recently, Zhou and Larson have presented a theoretical method for directly calculating the tube potential via molecular dynamics simulations (135).

In previous work, tube-like motion of single entangled DNA molecules was directly observed by fluorescence microscopy (26, 39), however the confining forces were not quantified. A simple picture of the confining potential would be a "hard-walled" square well of radius *a*. However, individual entanglements certainly lie at distances smaller and larger than *a*, and the surrounding polymers are able to reptate, stretch, and deform, causing individual constraints to constantly disappear, reappear,

and change locations (2, 136). Zhou and Larson predict that the tube radius actually increases gradually with time (135).

Behavior consistent with predictions of tube models has been observed in rheology experiments and these data have been analyzed to infer properties of the tube (1, 2). For example, when a polymeric fluid is sheared, polymers are stretched and experience elastic and orientational stress. In the Doi-Edwards (D-E) model, the stress on the polymer relaxes as it and the surrounding polymers return to equilibrium. At short times, or for small displacements, elastic relaxation is predicted to dominate, with the relevant time scale being the Rouse time τ_R. For $t > \tau_R$ the polymers are predicted to relax by reptation on time scales up to the disengagement time τ_D. Relaxation times have been measured in many rheology experiments but agreement with theory is not always good. Many efforts have been made to improve the theory by introducing various corrections such as contour length fluctuations, residual stretch relaxation, convective constraint release, etc. (1, 2, 136-138).

Here, we introduce a new experimental approach in which the forces imposed by entangled polymers to confine a single stretched DNA molecule are measured directly using optical tweezers (24, 26). We determine the form of the potential energy landscape restricting molecular displacement. We also characterize the time dependence of the forces by studying the dependence on displacement rate and the relaxation following displacement.

6.3 Materials and Methods

The probe molecule was a 25.3 kbp DNA (8.4 μm) construct prepared and labeled with biotin on one end and digoxygenin (DIG) on the other using PCR, as described previously (139). The probe was embedded in a 1 mg/ml (~40*c**) solution of linear 115 kbp (38 μm, $N \cong 380$) DNA, prepared as described in Chapter 2. Previous experiments confirm that we are in the well-entangled regime (26, 132).

The probe molecule was tethered by attaching the biotin end to an optically trapped streptavidin microsphere (1.4 μm radius) and the DIG end to an optically trapped anti-DIG coated microsphere (1.1 μm radius), and stretched with an applied tension of 10 pN (fractional extension ≅ 0.95) as described previously (139, 140) (Figure 6.1A&B). The surrounding molecules were allowed to relax. The optical traps were calibrated as described previously (140). 150 mW of laser power was used in each trap, which causes minimal local heating, from ~22 °C ambient temperature to ~27 °C (141). This increase is minor in that it does not cause any structural changes in the DNA (since it is only expected to melt at a much higher temperature of ~90 °C), and it changes the thermal energy kT (where T is in kelvin) by only 1.6%. To map the confining field, the sample chamber was displaced relative to the trapped probe molecule using a piezoelectric nanopositioning stage. Displacements were made either transverse or parallel to the probe chain contour at constant velocity. The force along the axis of displacement was measured by recording the deflection of the trapping laser at 1 kHz (140), and was low-pass filtered with a negative-exponential filter (0.1 sampling proportion in a 1 μm range). Measurements were also done

without the probe molecule to determine the contribution of the microspheres (~70%), and this force was subtracted from the total force to determine the force acting on the probe molecule. Measurements were repeated 20 times at different locations in the sample chamber to verify reproducibility and accurately determine the average induced force.

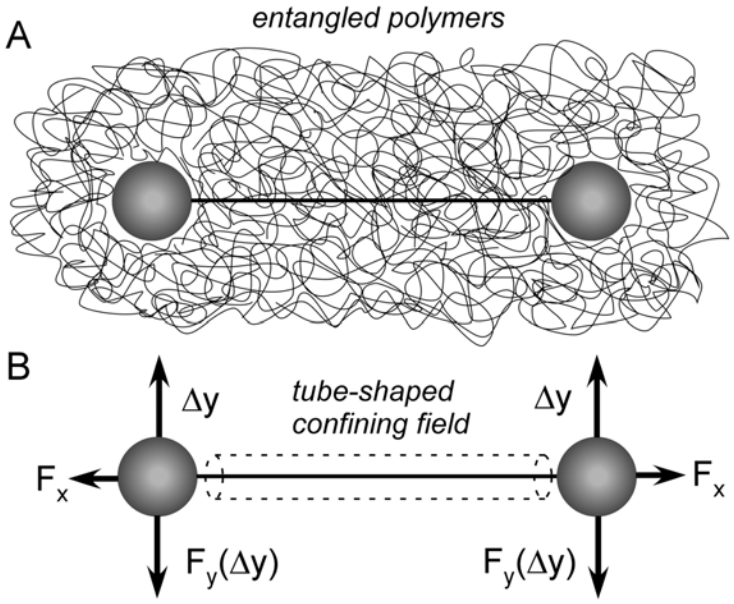

Figure 6.1 (A) Schematic diagram of experiment. A single DNA molecule is held stretched between two optically trapped microspheres and suspended in a concentrated solution of entangled DNA. **(B)** Reptation models postulate that collective intermolecular interactions give rise to a tube-like confining field (dashed lines). We measure the confining force per unit length (F_x and F_y) in response to an imposed displacement Δx or Δy.

DNA and numerous synthetic polymer solutions have been shown to exhibit universal rheological properties when scaled according to blob theory (15). Thus, we chose to scale our measured force by the correlation blob size $\xi = R_G(c/c^*)^{-\nu/3\nu-1} \cong 52$

nm where $\nu \cong 0.588$ is the Zimm scaling exponent (the R_G value used is listed in Table 3.1) (12, 132, 142). We divide the measured force by the number of correlation blobs spanning the probe (L/ξ = 8.4 μm/52 nm = 162, where L is the probe length) to determine the confining force per blob or unit length.

In traditional D-E theory the tube radius is defined as $a = (24/5(M_e/M)R_G^2)^{1/2}$, where $M_e = (4/5)cRT/G_N^{(0)}$ is the molecular weight between entanglements (1). Based on previous measurements of the plateau modulus $G_N^{(0)}$ for entangled DNA (20, 132), and the prediction that $G_N^{(0)}$ is independent of molecular weight M and proportional to c^2 (1), we estimate $G_N^{(0)} \cong 0.5$ Pa and calculate $a \cong 0.5$ μm. The accuracy of a is of course limited by the accuracy of the plateau modulus measurements.

Measurements were made with transverse displacements ranging from zero up to 15.5 μm. For large displacements (≥3 μm), the possibility of generating responses in the nonlinear or "strong flow" regime make the data difficult to interpret, so we focus most of our attention on analyzing the small displacement data relevant to probing the tube. According to reptation theory thermally diffusing chain segments reach the tube radius on the time scale of the equilibration time $\tau_e = a^4/24D_0R_G^2 \cong 0.02$ s where D_0 is the infinite dilution diffusion coefficient (Table 3.1) (1, 132, 142, 143). Thus, the characteristic rate at which chain segments are predicted to move a distance a via thermal motion is $v_{th} = a/\tau_e \cong 25$ μm/s. Therefore, we made displacements at 25 μm/s in addition to a range of higher and lower rates (0.01 to 65 μm/s).

6.4 Results and Discussion

For small transverse displacements the force increased linearly with distance (Figure 6.2A). The effective spring constant increased with increasing velocity. In contrast, negligible forces were induced in response to parallel displacements (Figure 6.3). A potential concern with parallel displacements is that the microsphere may partly disturb the surrounding chains through which the probe moves. However, the maximum displacement of 2.6 μm was much shorter than the 8.4 μm length of the probe molecule so ~70% of the probe was moving through surrounding chains that were undisturbed yet the force was negligible. Thus, we have shown by direct measurement that the collective intermolecular forces imposed by entangled polymers give rise to a tube-shaped confining field. By integrating the perpendicular force vs. displacement we can also determine the transverse confining potential per unit length $U(y)$ (Figure 6.2C&D).

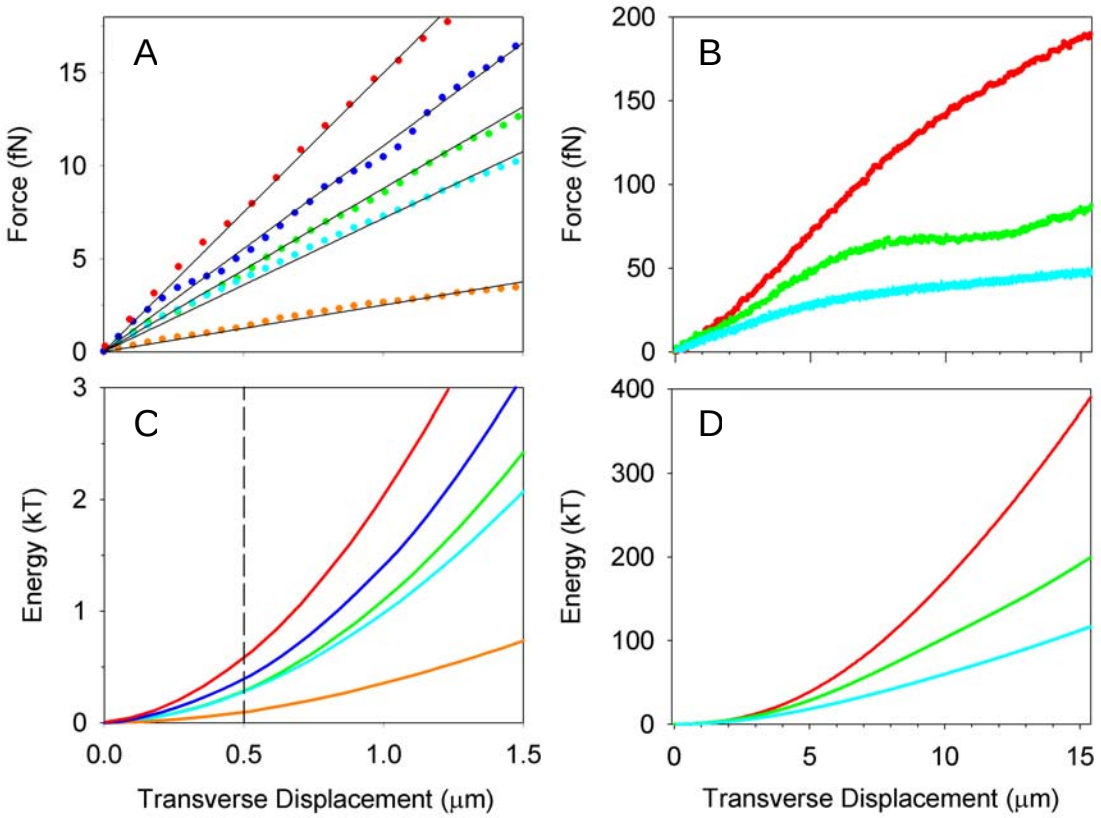

Figure 6.2 **(A)** F_y vs. Δy at rates of 65 μm/s (red), 25 μm/s (blue), 13 μm/s (green), 0.52 μm/s (cyan), and 0.10 μm/s (orange). **(B)** Results for Δy = 15.5 μm. **(C)** Confining potential per unit length *U(y)* determined by integration of force data in plot (A). The dashed line indicates the theoretically predicted tube radius. **(D)** *U(y)* determined by integration of force data in plot (B).

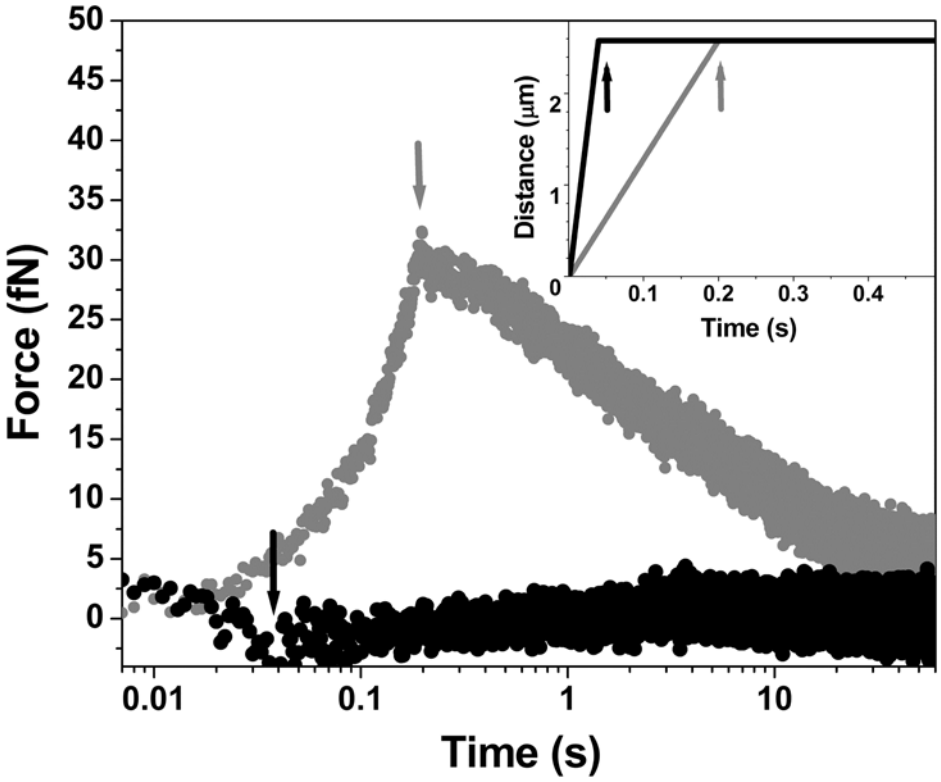

Figure 6.3 Average force induced by a displacement Δ*y* at 13 μm/s (gray) vs. a displacement Δ*x* at 65 μm/s (black). Arrows mark the maximum displacements. The inset graph shows the displacement profiles.

Zhou and Larson (135) calculated *U(y)* in simulations by determining the relative probability *P(y)* that a monomer fluctuates a certain transverse distance *y* from the primitive path and using the relationship $P(y) = e^{-U(y)/kT}$. Likewise, we can use this relationship to calculate *P(y)* from our measured *U(y)* (Figure 6.4). Although quantitative comparison with our results is not warranted because they simulated a melt rather than a solution, our findings are in qualitative agreement, as expected from blob theory. They find a time-dependent harmonic potential for short times, in accord with our findings. They also find that the tube radius calculated by conventional

theory is similar to the characteristic length at which $U(y) \cong kT$ ($P(y) \cong 1/e$) at time τ_e. Similarly, at the relevant $a/\tau_e \cong 25$ μm/s rate, we find $P(y) \cong 1/e$ at ~0.8 μm, similar to the theoretically predicted tube radius (0.5 μm) (Figure 6.4).

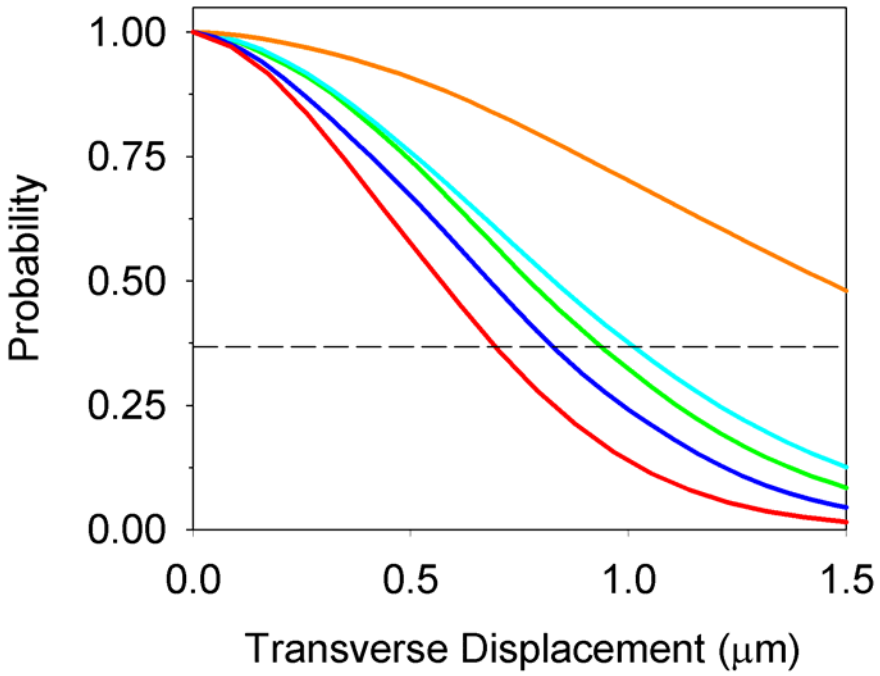

Figure 6.4 Relative probability for a transverse displacement y from the primitive path determined by $P(y) = e^{-U(y)/kT}$ where $U(y)$ is the transverse confining potential (Figure 6.2C). Colors indicate displacement rates as in Figure 6.2. Tube radius, defined as the distance where $P(y) = 1/e$, is indicated by the dashed line. Measured tube radii are: 0.65 μm, 0.82 μm, 0.94 μm, 1.0 μm and 1.8 μm for the 65 μm/s, 25 μm/s (a/τ_e), 13 μm/s, 0.52 μm/s, and 0.10 μm/s, respectively.

While the conventional tube model assumes that the tube radius is time-independent, our measurements and the recent simulation described above find a time-dependence (135). Zhou and Larson have suggested that this effect can help to

explain certain long-standing discrepancies between rheological data and theory. They calculate that the tube radius increases by ~10% on a time ranging from τ_e to $100\,\tau_e$. Similarly, our measured tube radius increases by ~20% with displacement rate decreasing from a/τ_e to $a/50\,\tau_e$.

The longest predicted relaxation time in D-E theory is the disengagement time $\tau_D = (18R_G^2/a^2)\,\tau_R \cong 40$ s, which is the time it takes a chain to completely diffuse out of its initial tube by reptation. On long times approaching τ_D we expect the tube constraints to weaken and eventually disappear. Indeed, at the lowest displacement rate in our experiment (0.1 μm/s), corresponding to $\sim 10a/\tau_D$, we find a potential of only 0.2 kT at the 0.8 μm tube radius. It rises to ~kT at ~2 μm, indicating ineffective tube confinement.

Our results for large displacements may be more difficult to interpret, as discussed above. We nevertheless present these findings (Figure 6.2B&D), since the tube model has been applied in many cases to nonlinear states generated by strong flows (1, 2). For all three rates a decrease in dF/dy was observed for $\Delta y > 7$ μm, which is close to the predicted equilibrium primitive path length of the entangled DNA ($L_0 \cong (M/M_e)a \cong 9$ μm) (1). This decrease may indicate displacement-induced slippage of entanglements off of the probe molecule. Such behavior may be related to that proposed to occur in "convective constraint release" models for non-linear responses in shear flow (132).

Further information came from the measured force relaxation following the displacements (Figure 6.4). Inverse Laplace transform analysis revealed three distinct

decay times for all datasets except the 0.1 μm/s case where only the two faster relaxation times were observed. The time constants and amplitudes were insensitive to the displacement rate and size. To accurately determine the time constants the averaged relaxation curves were fitted to a discrete sum of three decaying exponentials, yielding $\tau_1 = 0.45 \pm 0.34$ s, $\tau_2 = 5.4 \pm 2.8$ s, and $\tau_3 = 34 \pm 5.8$ s. The relative amplitudes of these decay times were all roughly equal (each ~1/3 of the total).

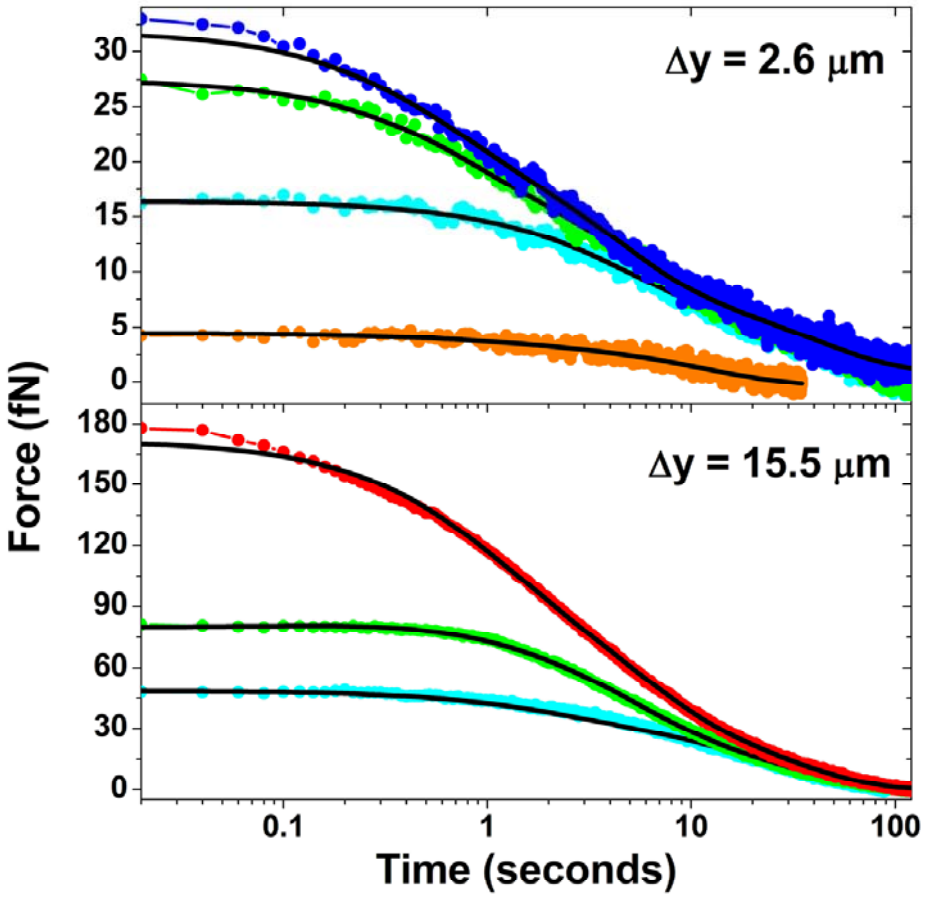

Figure 6.5 Force relaxation following transverse displacements of 2.6 or 15.5 μm. Colors indicate displacement rates as in Figure 6.2. The solid lines are fits to sums of decaying exponentials.

These measurements probe the relaxation of the distorted molecules surrounding the probe molecule. According to D-E theory (1), the shortest relaxation time is the Rouse time $\tau_R = 2R_G^2/\pi^2 D_0$ over which a deformed polymer elastically relaxes back to L_0. Using our measurements from Chapter 3 we calculate $\tau_R \cong 0.6$ s (132, 142), in good agreement with our measured τ_1. Theory also predicts that elastic relaxation accounts for only 1/5 of the total relaxation, attributing 4/5 to disengagement from the tube (144). However, we find a ~1/3 contribution for τ_1. It is possible that this larger amplitude is due to the contribution of unresolved higher order Rouse modes to τ_1 (144).

The longest predicted relaxation time, the disengagement time $\tau_D \cong 40$ s, is consistent with our measured value of τ_3. Its 1/3 contribution is much lower than the predicted 4/5, however we find a distinct intermediate decay time $\tau_2 \cong 12\,\tau_1$, not predicted by D-E theory, that also contributes, suggesting that reptation is occurring on this intermediate time scale τ_2 as well. A similar relaxation time was recently observed in nonlinear step shear experiments with polystyrene solutions (137, 145) and in flow deformation studies of DNA at $35c^*$ (132). Mhetar and Archer have proposed an explanation for this relaxation mode (138). They propose that the tube diameter shrinks during deformation, as its length is increased, prohibiting complete relaxation of chain extension to L_0 in time τ_R. An intermediate relaxation mode arises when the residual stretch relaxes as the tube expands back to its equilibrium diameter. Reptation is also predicted to occur on this time scale, although complete disengagement from the tube only occurs after a time τ_D. While the nature of the

deformation of the entangled polymers was different in the previous flow experiments than in our experiment, in both cases entangled polymers were deformed and allowed to relax. Our findings suggest that the relaxation mechanism proposed by Mhetar and Archer, which is the only model to our knowledge that proposes such an intermediate relaxation time, may apply in both cases.

Finally, we examine the dependence of the confining force on length and concentration of the surrounding chains. We made additional measurements using shorter 11 kbp DNA at 1 mg/ml (~7.5c^*, $\xi \cong 50$ nm) and 115 kbp DNA diluted to 0.1 mg/ml (~4c^*, $\xi \cong 300$ nm). The measured forces were similar for both cases and significantly lower than that for the 115 kbp, 1 mg/ml solution (Figure 6.5). With the most extreme deformation (15.5 μm at 65 μm/s) the maximum force per unit length was only ~50 fN for both cases compared with ~200 fN for the 115 kbp, 1 mg/ml solution. Also, both relaxations were well described by only a single time constant of ~0.5 s, which is close to the predicted value of τ_R. These findings suggest that at these lower concentrations or lengths the molecules are not yet entangled so there is no effective confining tube.

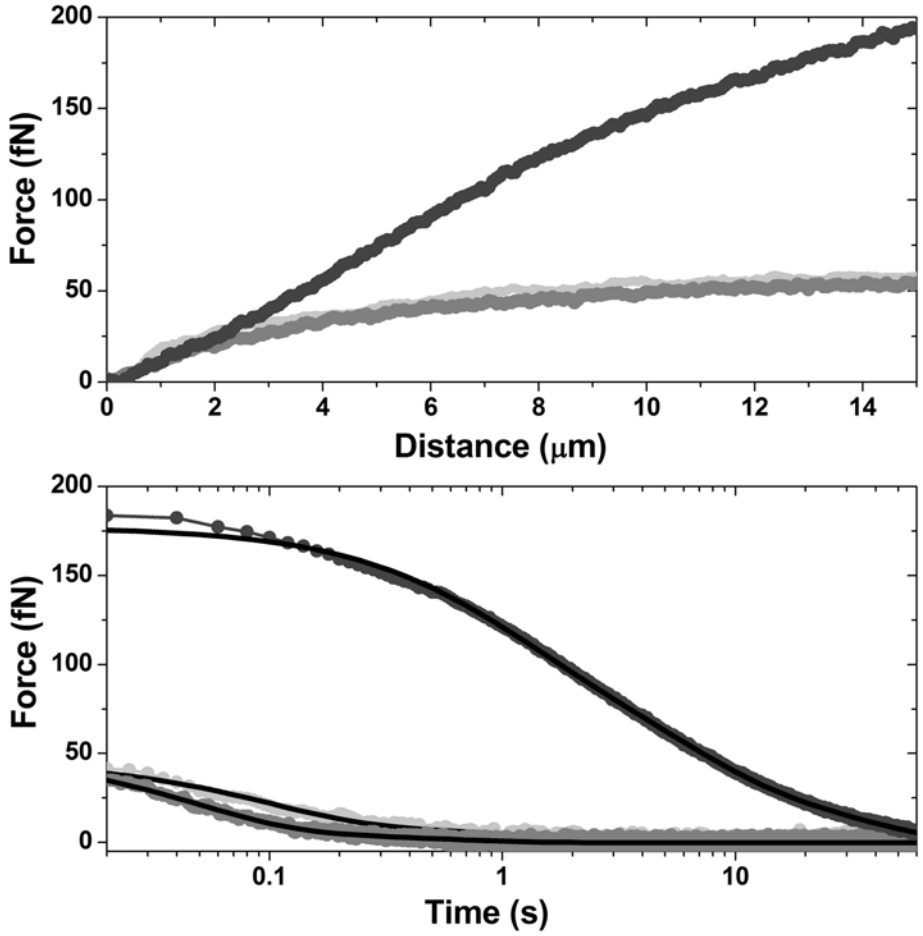

Figure 6.5 Dependence of confining forces on concentration and length of the surrounding molecules. **(top)** F_y vs. Δy at 65 μm/s with a high concentration of long entangled molecules (1 mg/ml, 115 kbp, dark grey); with a high concentration of shorter molecules (1 mg/ml, 11 kbp, grey); and with a lower concentration of long molecules (0.1 mg/ml, 115 kbp, light grey). **(bottom)** Corresponding force relaxations. The solid lines are fits to sums of decaying exponentials, yielding $\tau_{1,2,3}$ = 0.86, 4.8, 29 s for 1 mg/ml, 115 kbp; τ_1 = 0.5 s for 1 mg/ml, 11 kbp; and τ_1 = 0.6 s for 0.1 mg/ml, 115 kbp.

6.5 Conclusions

In conclusion, we have introduced a new method whereby we directly measure the forces confining an entangled polymer using optical tweezers. We have measured

for the first time the tube-like confining field underlying the predictions of the reptation model. We found that a harmonic barrier opposes displacement transverse to the molecular contour, and the effective spring constant increases with increasing displacement rate. We have determined a time-dependent tube radius from our measured forces and found that our value of $a \cong 0.8$ μm measured over the equilibration time scale is close to the classical prediction of $a \cong 0.5$ μm. It is important to note, however, that classical theory does not predict a time-dependent tube radius nor does it attempt to determine the actual form of the tube-like potential barrier. Only very recently has an attempt to quantify the tube potential been made, via a polymer melt simulation (136), and results of this study, namely a time-dependent tube radius and a harmonic confining potential, are in accord with ours. We have also measured the force relaxation following transverse displacement and found three distinct relaxation times. Two relaxation times were in accord with classical theory (1), while a third relaxation mechanism, in agreement with our measured intermediate relaxation time, has only recently been predicted for entangled polymeric fluids (139).

6.6 Acknowledgements

Chapter 6, in part, is a reprint of the material as it appears in Physical Review Letters. Robertson, R. M. & Smith, D. E. *Physical Review Letters* **99**, 12, 126001 (2007). The dissertation author was the primary investigator and author of this paper.

Chapter 7

Direct Measurement of the Confining Forces Imposed on a Single Molecule in a Concentrated Solution of Circular Polymers

7.1 Abstract

We measure the forces confining the transverse displacement of a single DNA molecule embedded within a concentrated solution of long relaxed circular DNA molecules (115 kbp at 1 mg/ml) using optical tweezers. We compare these measurements with our previous measurements of forces imposed by entangled linear DNA molecules of the same length and concentration. A tube-like confining field and three relaxation modes were observed, but the tube radius was 25% smaller (≅ 0.6 μm) and the longest relaxation time was ~3 times shorter (≅ 11 s) than with linear molecules, consistent with recent theoretical predictions by Iyer, Lele, and Juvekar. For displacements greater than the tube radius, the confining force imposed by circular polymers was substantially lower and shorter range than that measured with linear polymers.

7.2 Introduction

Intermolecular entanglements exert strong effects on the molecular dynamics and bulk fluid properties of concentrated polymer solutions. The reptation model, developed by de Gennes, Doi and Edwards and others, has been essential to understanding such effects, especially as applied to linear polymers (1, 2, 12). Circular polymers such as DNA present a more puzzling case, however. Their configurations and entanglements are less well understood, and it is not clear to what extent reptation theory applies. The key assumption of reptation theory is that entanglements act on short time scales to confine each molecule in a tube-like region parallel to its contour. While linear polymers can diffuse either head- or tail-first out of their tubes, forming new displaced tubes, circular polymers have no ends by which to escape tube constraints by conventional reptation.

Studies of synthetic circular polymers have, in some cases, found substantial differences in physical properties such as molecular diffusion and fluid rheology, as compared with linear polymers (104, 105, 129-131, 146, 147). However, a consensus understanding of the existing data has not been reached. In the case of DNA, we measured diffusion coefficients for entangled linear and relaxed circular molecules by tracking the Brownian motion of single molecules with fluorescence microscopy (see Chapters 4 and 5). We found that the scaling of the diffusion coefficient with concentration and length was consistent with the reptation model for both topologies, but relaxed circular DNA diffused up to 7 times faster than linear DNA of the same

length and concentration (45 kbp at 1 mg/ml). Thus, relaxed circular DNA appears to be less effective than linear DNA at producing restrictive entanglements.

We have developed a method for directly measuring the intermolecular forces imposed by entangled DNA molecules using optical tweezers, as described in Chapter 6. Our initial studies only examined linear molecules. Here, we extend this method to study entangled circular molecules, and report significantly different results than with linear DNA.

Some theories predict that entangled circles adopt a tree structure resembling a randomly branched polymer, and it has been conjectured that they could diffuse by reptation via protruding finger-shaped loops which continually thrust forward and back in an amoeba-like fashion (6, 92, 148, 149). Several simulations of circular polymer melts find evidence for a lower degree of entanglement and higher threshold length for entanglement than for linear molecules (102, 103, 126-128). Recently, Iyer et al. formulated a detailed dynamical theory for entangled circular polymers using concepts from the pom-pom model, originally developed to describe branched polymers within a tube model framework (7, 150). Within the pom-pom ring (PPR) framework of Iyer et al., an entangled circular polymer adopts a lattice-tree structure (akin to a randomly branched polymer but formed from loops) consisting of a primary/longest length ("trunk") and shorter, randomly positioned loops ("branches"). The longest time scale dynamics of such a structure is modeled as being governed by a reptation-type motion of the trunk (with predicted length $\sim N^{2/3}$) with added friction from the smaller loop branches, which are unentangled and able to relax more quickly

(8). We note that these existing theories have all been aimed at describing melts. However, tube models for linear polymer melts have been successfully extended to analyze solutions of entangled polymers using blob theory (12, 14, 15) in which each chain is divided into correlation blobs of length ξ and the solution is modeled as a melt of chains with effective monomer size ξ. However, blob theory has yet to be explicitly applied to circular polymers.

According to D-E theory the confining tube radius is given by $a = (24/5(N_e/N)R_G^2)^{1/2}$ where N_e is the molecular length between entanglements (1). A rigorous theoretical definition of N_e, specified in terms of molecular properties, has proven elusive so N_e is usually taken to be an empirically determined quantity inferred from measurements of the plateau modulus $G_N^{(0)}$. On the other hand, efforts have recently been made to define and quantify entanglements directly through molecular dynamics simulations (143, 151-154). Zhou and Larson have recently used such an approach to directly calculate the tube confining potential by analyzing an ensemble of simulated molecular trajectories (135), and our measurements on linear DNA, described in Chapter 6, compare favorably with some of their predictions.

According to the PPR model proposed by Iyer et al. the relative size of the tube radius for circular polymers compared with that for linear polymers depends on N as well as the ratio of the corresponding N_e values for both topologies (i.e., N_{eC}/N_{eL} where the "C" and "L" subscripts refer to the values for linear and circular polymers, respectively) (8). They derive the expression $a_C^2/a_L^2 = (N_{eC}/N_{eL})N^{2\nu-1}$, where $\nu \cong 0.3$ is the static scaling exponent predicted for semiflexible polymers such as DNA (103).

N_{eC}/N_{eL} has not been predicted theoretically, so Iyer et al. assume a value of $N_{eC}/N_{eL} \cong 5$, deduced from rheological measurements of $G_N^{(0)}$ for polystyrene melts (147). According to D-E theory, for linear DNA the tube radius is predicted to be $a = (24/5(N_e/N)R_G^2)^{1/2} \cong 0.5$ μm, using measured values of R_G (Table 3.1) and $G_N^{(0)}$ (see Chapter 6) (20, 132, 142). Thus, for circular DNA the theory of Iyer et al. predicts $a_C \cong 0.7a_L \cong 0.3$ μm. As will be described below, this prediction compares favorably with our measurements.

7.3 Materials and Methods

The details of our experiment are essentially the same as in our previous study discussed in Chapter 6, except that a solution of relaxed circular DNA was probed instead of linear DNA. Briefly, the probe molecule was a 25.3 kbp DNA (8.4 μm) construct prepared as described previously (139). The probe was suspended in a 1 mg/ml solution of 115 kbp (38 μm, $N \cong 380$) DNA molecules and attached to two optically trapped microspheres (1.1 μm and 1.4 μm radii) (139). The tethered probe was stretched with a tension of 10 pN. The 115 kbp molecules were prepared as described in Chapter 2. These molecules were treated with topoisomerase I to produce *torsionally-relaxed*, *non-interlinked* circles, as discussed in Chapter 3. Displacements were made by moving the sample chamber at constant velocity with a piezoelectric nanopositioning stage, and the induced force along the axis of displacement was measured by recording the deflection of the trapping laser at 1 kHz, as described previously (140). Previously, to obtain a confining force per unit length, independent

of the arbitrary probe length, we normalized the total induced force by the number of correlation blobs spanned by the probe molecule ($L/\xi = 162$, see Chapter 6). In order to directly compare our findings for circular DNA to those of linear we chose to normalize the data for circular DNA by the same quantity.

7.4 Results and Discussion

Transverse displacements were imposed at rates of 0.10, 0.52, 13, 25 and 65 μm/s as in Chapter 6. The results with circular and linear DNA are compared in Figure 7.1. For small displacements ($\Delta y < 0.4$ μm), the forces were approximately the same for both topological cases, and increased linearly with displacement for the higher displacement rates (13-65 μm/s). The induced force was rate dependent, as discussed in Chapter 6. A Hookean response was observed with the linear DNA for displacements up to ~1.5 μm, but the response with circular DNA deviated from linearity and was better described by a more slowly rising function of the form $F=\alpha(1-e^{-\beta\Delta y})$, where α and β are rate-dependent constants.

Figure 7.1 Measured force vs. transverse displacement and corresponding confining potentials and relative probabilities for entangled circular and linear DNA solutions. **(top-left)** Induced force per unit length F_y measured during a small displacement Δy at rates of 65 μm/s (red), 25 μm/s (blue), 13 μm/s (green), 0.52 μm/s (cyan), and 0.10 μm/s (orange); color schemes are the same for all panels. The lines are fits to the function $F_y = \alpha(1\text{-}e^{-\beta\Delta y})$. **(top-right)** Forces measured with linear DNA of the same length and concentration (see Chapter 6). The lines are linear fits. **(middle-left)** Confining potential per unit length $U(y)$ determined by integration of the force data for circular DNA. **(middle-right)** Potential measured with linear DNA. **(bottom-left)** Relative probability $P(y) = e^{-U(y)/kT}$ for the chain segments to fluctuate a transverse distance y from the primitive path. Inferred tube radii determined as the displacements where $P(y) = 1/e$ ($U = 1\ kT$), indicated by the positions where the curves cross the dashed line (0.70 μm, 0.76 μm, 0.95 μm, and 1.6 μm for the 65 μm/s, 25 μm/s, 13 μm/s and 0.52 μm/s rates, respectively). **(bottom-right)** Relative probability plotted for linear DNA. The inferred tube radii are: 0.65 μm, 0.82 μm, 0.94 μm, 1.0 μm and 1.8 μm for the 65 μm/s, 25 μm/s (a_L/τ_{eL}), 13 μm/s, 0.52 μm/s, and 0.10 μm/s rates, respectively.

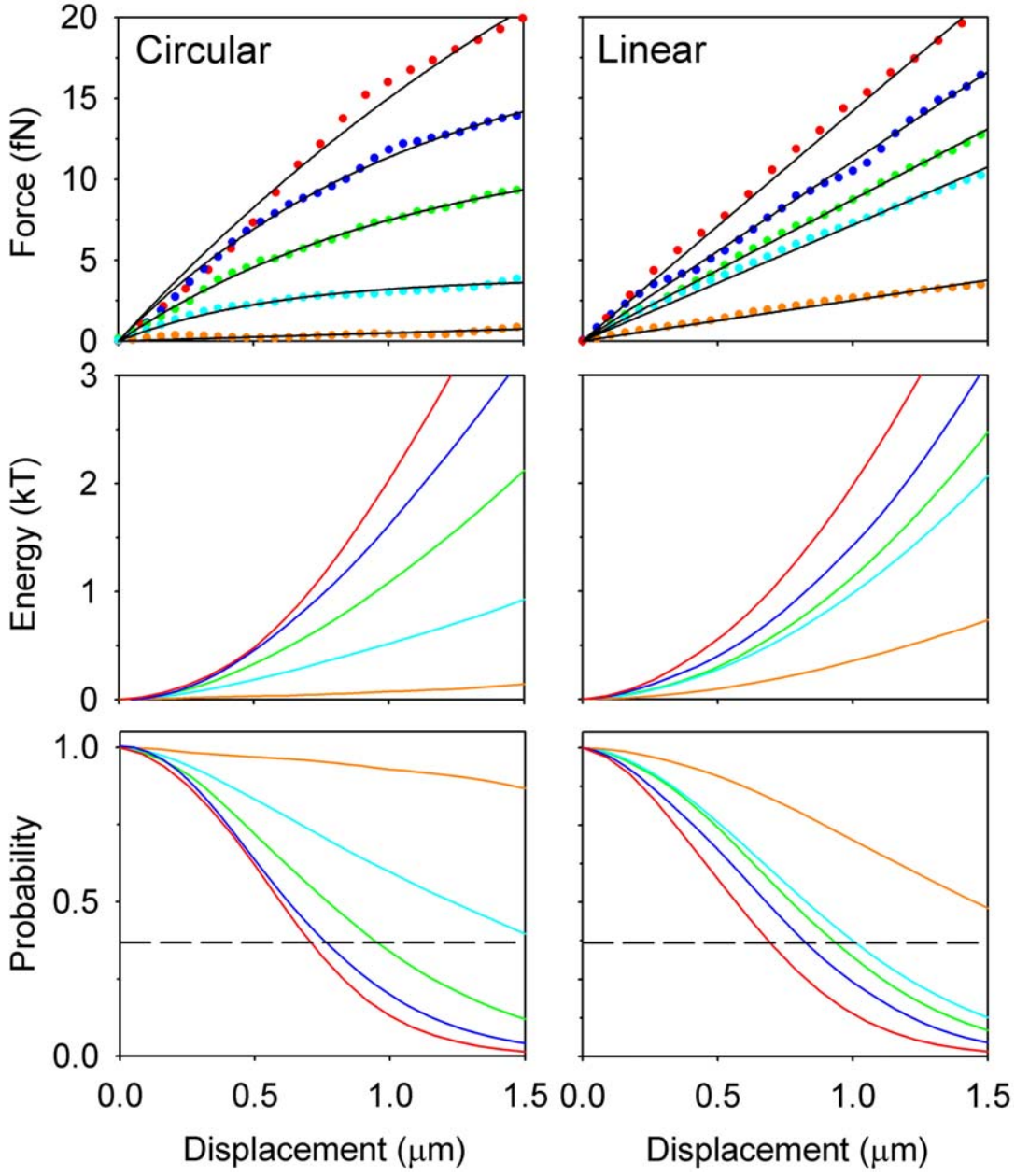
Circular
Linear
Force (fN)
Energy (kT)
Probability
Displacement (μm)
Displacement (μm)
0
5
10
15
20
0
1
2
3
0.0
0.5
1.0
0.0
0.5
1.0
1.5
0.0
0.5
1.0
1.5

By integrating the force versus displacement data we can determine the potential per unit length $U(y)$ confining transverse displacements (Figure 7.1). We can then use the approach described by Zhou and Larson to determine the relative probability $P(y)$ that a chain segment thermally fluctuates a certain transverse distance y from the primitive path via the relationship $P(y) = e^{-U(y)/kT}$ (Figure 7.1) (135). We can then define a characteristic confining distance corresponding to the displacement where $U \cong 1\ kT$ ($P(y) \cong 1/e$), as discussed in Chapter 6. For the three fastest displacement rates, the confining distance was nearly the same for both topologies. However, for 0.5 μm/s the characteristic confining distance was twice as large for the circular DNA, and at the slowest rate (0.1 μm/s) there was negligible confinement with circular DNA, in contrast to the case with linear DNA. Thus, we have shown that tube confinements are less persistent on long time scales with circular DNA than with linear DNA.

As discussed in Chapter 6, when comparing our results with the predicted tube radius in the D-E model one should probe the tube on a time scale close to the predicted thermal equilibration time $\tau_e = a^4/(24D_0R_G^2)$ (1). Using the value of a predicted by D-E theory we calculate $\tau_{eL} \cong 20$ ms for linear DNA, and using the prediction of Iyer et al. ($a_C \cong 0.7a_L$) we calculate $\tau_{eC} \cong 2.1$ ms for circular DNA. Thus, in our previous measurements with linear DNA we displaced the probe at $v_{thL} = a_L/(\tau_{eL} \cong 20\text{ ms}) \cong 25$ μm/s, as well as testing lower and higher rates (0.10-65 μm/s). Here, we made measurements at the same rates with circular DNA so as to directly compare the two cases. However, according to the calculation above the appropriate

displacement rate for circular DNA for probing the tube on the thermal equilibration time would be different, $v_{thC} = a_C/(\tau_{eC} \cong 2.1$ ms) $\cong 78$ μm/s. If we extrapolate our 13 to 65 μm/s force data to 78 μm/s, we find $a_C \cong 0.6$ μm $\cong 0.75a_L$, which is very close to the prediction of Iyer et al. of $a_C \cong 0.7a_L$.

While the small displacement data was similar for both topologies, in the circular case the force rose much more slowly with displacement for large displacements (Figure 7.2). The maximum force reached with circular DNA was ~2- to 10-fold smaller than that with linear DNA, depending on the rate of displacement. A decrease in dF/dy for $\Delta y > 1$ μm was also apparent with circular DNA for all displacements rates (Figure 7.2). With linear DNA we observed a decrease in dF/dy at a displacement of ~5-10 μm, which is similar to the predicted primitive path length of the entangled linear DNA ($L_{0L} \cong (N/N_{eL})a_L \cong 9$ μm) (1), and we attributed this decrease to displacement-induced slippage of some of the entanglements off of the probe (Figure 7.2). Our present results with circular DNA are also consistent with this interpretation because we see an earlier decrease in dF/dy at ~1-2 μm, and the predicted primitive path length for circular DNA is $L_{0C} \cong 2$ μm. Such behavior observed in the large-displacement regime may be related to the phenomenon of convective constraint release, predicted by certain theories to be important in understanding the nonlinear response of polymeric fluids (132, 155-158). With linear DNA we also observed a subsequent increase in dF/dy for the 13 μm/s rate, which may be due to the probe encountering new entanglements. No such feature was observed with the circular DNA, again suggesting that entanglements tend to more

easily slip off the probe as it is displaced. Based on our findings we would expect convective constraint release to occur more readily with circular polymers than with linear polymers.

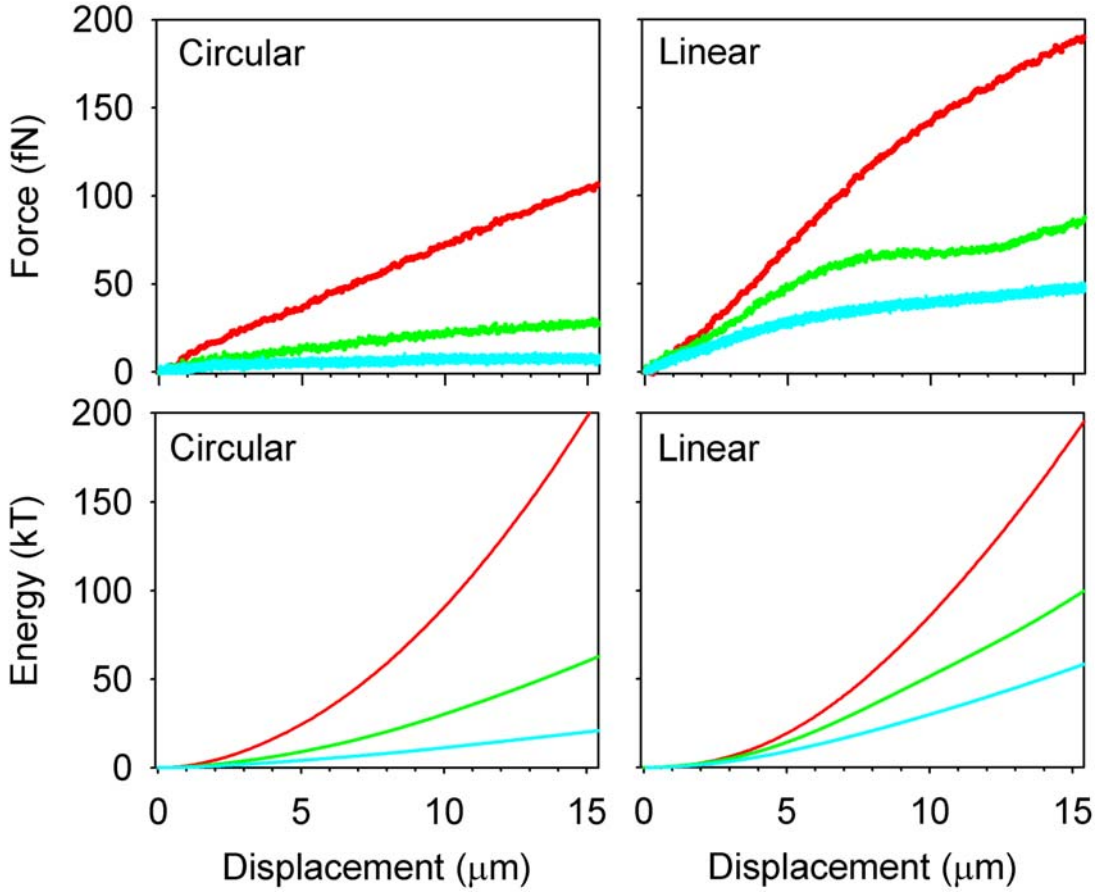

Figure 7.2 Induced force during a large displacement (Δy = 15.5 μm). The colors indicate different displacement velocities as defined in Figure 7.1. **(top-left)** Measurements with circular DNA. **(top-right)** Measurements with linear DNA (see Chapter 6). **(bottom-left)** Confining potential for circular DNA. **(bottom-right)** Confining potential for linear DNA.

Further information came from the measured force relaxation following the imposed displacements (Figure 7.3). These measurements probe the relaxation of the distorted molecules surrounding the probe molecule. In our previous studies with linear DNA, we found three distinct exponential decay times (see Chapter 6). Here, with circular DNA we found that the relaxations following a small displacement (Δy = 2.6 μm) were well fit by a sum of just two decaying exponentials, with similar time constants for both large and small displacements and the different displacement rates. The relaxations following a large displacement (Δy = 15.5 μm) (with the exception of the slowest, 0.1 μm/s dataset) also revealed a third, longer relaxation time. To accurately determine the relaxation times, we fit the averaged data to a discrete sum of three decaying exponentials, finding $\tau_{1C} = 0.3 \pm 0.1$ s, $\tau_{2C} = 4.1 \pm 1.6$ s, and $\tau_{3C} = 11 \pm 2.1$ s. In comparison, with linear DNA we obtained $\tau_{1L} = 0.4 \pm 0.3$ s, $\tau_{2L} = 5.4 \pm 2.8$ s, and $\tau_{3L} = 34 \pm 5.8$ s. Thus while τ_1 and τ_2 are similar for both topological cases, τ_3 is much shorter for the circular molecules and this mode was only observed with large displacements.

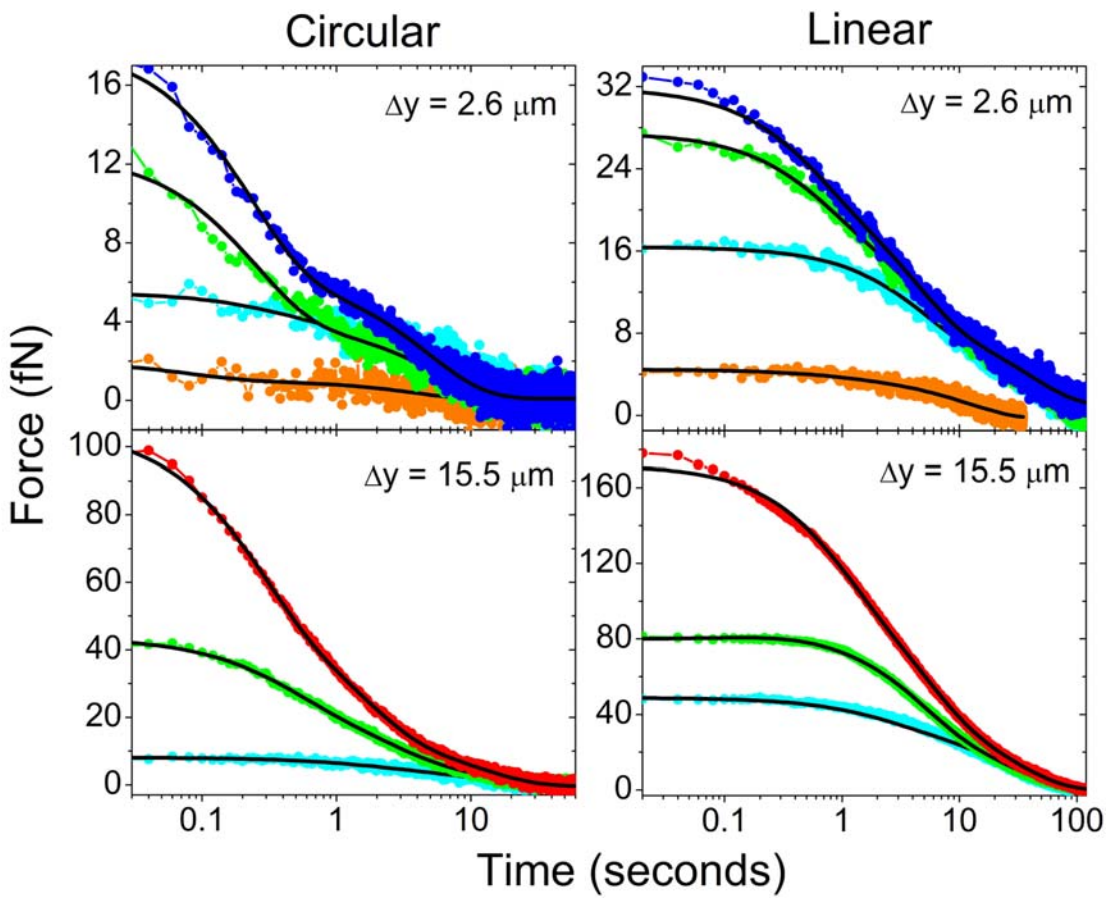

Figure 7.3 Measured force relaxation following the imposed transverse displacements of 2.6 or 15.5 μm. The colors indicate different displacement velocities as defined in Figure 7.1. The solid lines are fits to sums of two or three decaying exponentials. The linear DNA data is from our study described in Chapter 6.

According to D-E theory, the shortest relaxation time for an entangled polymer is the Rouse time (1) $\tau_R = 2R_G^2/\pi^2 D_0$, which is the time scale on which a deformed polymer elastically relaxes back to L_0. Using the values of D_0 and R_G from Table 3.1 (132, 142) we calculate $\tau_{RC} \cong 0.14$ s and $\tau_{RL} \cong 0.6$ s, for the circular and linear cases, respectively. These values are close to the measured values. The longest predicted relaxation time in D-E theory is the disengagement time $\tau_D = (18R_G^2/a^2)\tau_R$, over which a polymer is predicted to reptate out of its deformed tube. For linear DNA we

calculate $\tau_{DL} \cong 40$ s in agreement with our measured value of $\tau_{3L} = 34 \pm 5.8$ s. In the case of circular DNA, Iyer et al. (8) predict $\tau_{DC}/\tau_{DL} = (a_C^2/a_L^2)N^{2\nu-1} \cong 0.2$ implying $\tau_{DC} \cong 8$ s. Because the mechanism of reptation is usually discussed in the context of linear polymers, we emphasize here, as mentioned in the introduction, that reptation of a circular polymer in the PPR framework refers to the reptation of the tree trunk structure, slowed by the frictional constraints of the protruding loops. Because the length of the trunk ($\sim N^{2/3}$) is much shorter than a linear polymer of length N it follows that the time for a circular polymer to reptate out of its tube is predicted to be much shorter than that for a linear polymer.

Following a 2.6 μm displacement (~4 times the characteristic confining length) we observed two relaxation times. The first (~0.3 s) is consistent with Rouse relaxation and the second relaxation (~4 s) is an order of magnitude longer than the Rouse time. The observation of a transverse confining field that persists on a time scale much longer than the Rouse time is qualitatively consistent with reptation theory, which predicts that tube-like confinement would lead to two distinct relaxation time scales. However, the agreement with reptation theory is not quantitative since Iyer et al. predict a disengagement time of 8 s, which is a factor of two longer than the relaxation time we measure. The reason for this difference is unclear, however a model proposed by Mhetar and Archer in modeling the response of entangled polymeric fluids to non-linear step strains may provide a possible explanation (138). This model predicts that stress can be partially relaxed by reptation occurring on an intermediate time scale. The tube diameter is proposed to shrink during displacement

as its length is increased, prohibiting complete relaxation of chain extension to L_0 in time τ_R. An additional relaxation mode with decay time between τ_R and τ_D is associated with the relaxation of the residual stretch as the tube expands back to its equilibrium diameter. Reptation out of the deformed tube occurs on this time scale as well, although complete disengagement from the initial tube is still proposed to occur only after a time τ_D. As discussed in Chapter 6, evidence for a similar relaxation time has also been reported in nonlinear step shear experiments with linear polystyrene solutions (137, 145) and in flow deformation studies of linear DNA (132). While the nature of the deformation of the entangled polymers was different in the previous flow experiments than in our experiment, it is possible that this model may still be applied to the present case, since in both cases entangled polymers are deformed and allowed to relax.

The longer relaxation time scale of ~11 s observed following the larger displacement is in closer agreement with the predicted disengagement time of 8 s. The measured ratio $\tau_{3C}/\tau_{3L} \cong 0.3$ for circular versus linear polymers is also close to the predicted ratio of $\tau_{DC}/\tau_{DL} \cong 0.2$ for the disengagement times. It is not clear why this longer relaxation time only occurs following larger displacements, but within the context of the Mhetar-Archer model we can speculate that reptation occurring on an intermediate time scale may be sufficient for circular polymers to completely disengage from their deformed tubes following small (but not large) deformations. That a relaxation time corresponding to the disengagement time occurs with linear DNA for small displacements may be connected with the finding of larger confining

forces for linear DNA (≥2 times larger than with circular DNA at 2.6 μm). Perhaps a weaker, less persistent confining field leads to less deformation, and reduces the time needed for the polymer to reptate into an equilibrium tube configuration.

At long times approaching τ_D we expect the tube-like constraints to weaken and eventually disappear. Indeed, at the lowest displacement rate (0.1 μm/s) we found negligible forces resisting transverse displacement of the probe molecule. That this displacement rate corresponds to ~$10a_L/\tau_{DL}$ for the linear case but only ~$2a_C/\tau_{DC}$ for the circular case is consistent with our finding of a much lower confining force with circular DNA at this lowest displacement rate.

7.5 Conclusions

In conclusion, we directly measured the forces confining a polymer in an entangled circular DNA solution and compared our results with those for linear DNA of the same length and concentration. The confining forces were similar for both topologies for transverse displacements on the order of the tube radius; however, for larger displacements the force induced by the circular DNA rose more slowly than the Hookean response of the linear DNA. The determined tube radius for the circular DNA was 25% smaller than for the linear case ($a_C \cong 0.6$ μm $\cong 0.75a_L$) as predicted by the PPR model of Iyer et al. The measured force relaxations also differed in that the disengagement time for circular DNA was ~3 times shorter than that for linear DNA ($\tau_{3C}/\tau_{3L} \cong$ (11 s)/(34 s) $\cong 0.3$), in accord with predictions of the PPR model, and this predicted disengagement time was only apparent after large displacements for circular

DNA. Thus, we find that entanglements are present and induce tube-like constraints, in accord with the key concept of the reptation model, with both linear and circular DNA. However, the exact form of the confining potential and the time and length scales over which it persists differ for the two topologies.

7.6 Acknowledgements

Chapter 7, in part, is a reprint of the material as it appears in Macromolecules. Robertson, R. M. & Smith, D. E. *Macromolecules* **40**, 27, 8737-8741 (2007). The dissertation author was the primary investigator and author of this paper.

Chapter 8

Future Prospects

8.1 Introduction

The preceding chapters have described the use of single-molecule techniques to study the dynamics of and intermolecular forces that arise in DNA solutions of different concentrations, lengths, and topologies. Entangled DNA solutions as well as solutions of topologically-different DNA molecules have been the principal subjects of study. Video fluorescence microscopy and optical tweezers were used to study the diffusive behavior of DNA molecules and the forces that arise in entangled DNA solutions. These studies have led to much insight into entangled polymer dynamics, the restrictive nature of entanglements, and the effect that molecular topology has on polymeric fluids. However, there are still many unanswered questions, and these powerful techniques can be used to probe such questions that are of fundamental interest to polymer scientists and biologists alike.

8.2 Knotted DNA molecules

While DNA molecules are typically found in supercoiled, relaxed circular, and linear forms, knotted conformations have been found to occur both *in vivo* and *in vitro*. In fact, transiently knotted DNA configurations are believed to play an important role in DNA replication (159) as well as in DNA recombination (160).

Knotted configurations are usually formed by topoisomerases that act to wind and unwind circular DNA via strand passage. For example, topoisomerase I typically relaxes supercoils in double-stranded DNA molecules by cutting one strand, unwinding the supercoil (torsional stress) and reconnecting the strand. Because the other DNA strand remains uncut during the process the DNA is never in linear form (no free ends) and cannot form knots. However, if the DNA is nicked (one strand is cut), then as topoisomerase I cuts and reconnects the initially uncut strand near the cut segment of the nicked strand there is a possibility of knotting to occur. Previous studies have shown that indeed topoisomerase I does induced knots in nicked DNA molecules (161) and the number of nodes (strand crossings) can be resolved by gel electrophoresis (162).

The electrophoretic mobility of short (3.8 – 6.4 kbp) knotted DNA increases with increasing number of nodes suggesting that the equilibrium diffusion of these conformations would vary in the same manner (163). However, simulations of isolated knotted polymers have studied the dependence of the radius of gyration and diffusion coefficient on node number and have found that the R_G increases and D decreases with increasing node number (164-166). This expansion and decreased mobility was found to be dependent on excluded volume effects.

Thus, the effect of knots on DNA dynamics, which is important to both biologists and polymer scientists, is a nontrivial problem and is still debated. On one hand, one could imagine that the formation of knots would cause the DNA to become more compact and thus diffuse more quickly. However, one also has to consider the

repulsive intermolecular interactions that could cause the molecule to expand as it became knotted. Further, knots in larger molecules could lead to topologies similar to branched polymers, which display complex dynamics that are not yet fully understood (7, 150). The conflicting electrophoresis and simulation results suggest that there is not a simple universal relationship between node number and diffusion, so it would be of interest to study how the diffusion coefficients of knotted DNA molecules compare with those of other topologies, and how the number of nodes and the molecular length affect the diffusive behavior.

8.3 Polymer Blends

Classical polymer theory has focused on understanding the dynamics and properties of polymeric fluids consisting of linear polymers of exactly the same length. This makes sense as there are so many parameters and complex interactions that need to be considered in polymeric fluids that the task of considering blends of various lengths or topologies is quite daunting. In order to test these theories our studies thus far have focused on homogeneous DNA solutions of the same molecular length. However, in reality, most polymeric fluids used in industry are not homogeneous and consist of a blend of polymers of different lengths, so polymer blends are of fundamental interest to polymer chemists and engineers (167, 168). Numerous simulations and rheological experiments have focused on studying polymer blends; namely how the dynamics of entangled polymer melts are affected by the presence of polymers of more than one length (169). Traditional homogeneous polymer theories

have been extended to address blends of two polymer species (two different lengths), although the agreement with experiment is not always good and the correct method for considering both species is still debated. One difficulty that arises when considering polymer blends is miscibility. One cannot assume that the two species are homogeneously distributed in a blend. In fact, a homogenously mixed, or miscible, polymer blend, desired in industry, is often hard to produce (167), and much work has been devoted to determining the properties of species that could result in a miscible blend. Determining the miscibility of a blend has also proven to be a difficult experimental task (168, 170).

If one assumes a miscible blend, there are still numerous complex questions that arise. The reptation model assumes that the constraints (entangling polymers) surrounding the polymer of interest are fixed on the time scale of its motion, while in reality the constraints in a polymeric fluid are not fixed. While the reptation model has been successfully applied to homogenous entangled polymers of sufficient length, the approximation of fixed constraints begins to break down for polymer blends (170). Numerous theoretical attempts have been made to address the effect that a blend of constraints with different intrinsic time scales (lifetimes) has on the dynamics of an individual polymer (see Reference 170 and references within). Several corrections to the reptation model have been proposed, including concepts such as tube dilation, double reptation, constraint release and tube reorganization, and predictions have been made for the diffusion coefficients, terminal relaxation times, viscosity and other rheological parameters in binary blends. However, there are conflicting predictions

from the different models and systematic agreement with experiment has yet to be achieved.

It would be of interest to study binary blends of entangled DNA molecules to test predictions of the theories discussed above. Single-molecule measurements would be a valuable contribution as the miscibility of the solutions could be directly probed during measurements. Because measurements are carried out on a number of different molecules evenly spaced through out the sample, any inhomogeneities would be noticed as the data would fall into multiple groups corresponding to different "phases" in the solution. Diffusion measurements could elucidate how the diffusion coefficient of the individual molecules in blends depends on the ratio of species, the lengths of the species, and the overall concentration of the solution. Optical tweezers could also be used to measure the tube potential and relaxation times of blends and determine the effect that another species of altered length has on these parameters.

The same set of measurements could be done on blends of circular and linear polymers. In fact, several synthetic polymer studies have found that the addition of a small amount linear polymers to circular polymer melts dramatically alters the fluid properties (147, 171). While purely circular melts of polybutadienes have been found to have ~10 times lower viscosity than their linear counterparts ($\eta_C/\eta_L \cong 0.1$), upon addition of ~10% linear species to the circular melt the viscosity rises to $\eta/\eta_L \cong 0.5$. With 20-25% linear species the ratio of viscosities was $\eta/\eta_L \cong 1$, and a blend of 50% linear and 50% circular polybutadienes was found to actually be over twice as large as η_L. As the percent of linear species increases from 50% to 100% the viscosity begins

to decrease down to $\eta/\eta_L \cong 1$ again. These findings are predicted to be related to the difference in the entanglement spacing (M_e or N_e) of circular and linear polymers as well as the affinity for circular polymers to become threaded by their linear counterparts. However, a clear understanding of the molecular conformations and dynamics that give rise to the dramatic changes in fluid properties is not yet understood. Given that linear contaminants are essentially impossible to avoid when synthesizing circular polymers, their effect on the properties of a circular polymeric fluid is of much interest to polymer chemists and engineers. Further, because circular polymers have a strong affinity to become threaded by linear polymers, blends of circular and linear polymers are nearly always miscible. In fact, an inmiscible binary blend of different length polymers often becomes miscible upon cyclization of one species. Miscibility is a property sought in industrial polymeric fluids, and topological blends of circular and linear polymers provide an avenue for achieving this goal.

8.4 Rheology

While this thesis has focused solely on single-molecule measurements, the bulk of the data with which we have to compare our results are from rheological measurements. Further, until we introduced the direct method of measuring the tube potential in an entangled polymer solution, the only experimental method for determining the tube radius was via rheological measurements of the plateau modulus $G_N^{(0)}$. In order to compare our findings with predictions for the tube radius we had to assume a value for the plateau modulus based on previous rheological measurements

of DNA. Our measured relaxation times are also compared to those found in rheological measurements. However, it is not clear whether direct comparison between rheological flow experiments and our single-molecule method is warranted.

Thus, it would be of interest to determine rheological properties of our DNA samples in order to elucidate the similarities and differences between the molecular mechanisms, forces, and dynamics involved in rheological measurements and our single-molecule studies. In particular, one would like to know if the relaxation mechanisms and associated relaxations times measured in our optical tweezers experiments are the same as those measured in rheological experiments. Further, measurement of $G_N^{(0)}$ would allow us to directly compare our measured tube radius to that predicted by tube theory without relying on the predictions of how the plateau modulus varies with molecular length and concentration.

8.5 Blob Theory

Blob theory has extended the tube model to entangled polymer solutions, as discussed in Chapters 1.3.2.3 and 6. This model is essentially a coarse-grained scaling theory that replaces the monomer size b in a polymer melt with the correlation blob size ξ in a polymer solution. According to blob theory, above some critical length at which the polymers become well entangled, polymer solutions with the same blob size are essentially identical. In fact, Heo and Larson have shown that rheological data from a variety of entangled polymer solutions fall on the same curve when normalized

by their respective blob sizes (15). The prediction that polymer solutions with the same blob size have the same tube radius *a* follows.

In our initial study probing the tube potential of an entangled DNA solution (Chapter 6) we chose ξ to be our unit length and normalized our data accordingly. Our findings were in accord with classical predictions of the tube radius and the recent simulation that calculated the tube potential in a polymer melt (135). These results suggest that blob theory can indeed be applied to entangled DNA solutions. However, the evidence would be more compelling if entangled solutions of different lengths and concentrations could be measured as well. It would be of interest to apply our method to an entangled DNA solution of both larger and smaller molecular lengths with the concentrations adjusted so that all solutions had the same blob size. According to blob theory, the tube radius and relaxation times of these seemingly different solutions should be identical. Thus, this study would provide clear evidence either supporting or refuting the applicability of blob theory to entangled DNA solutions.

8.5 Conclusions

The avenues of research described above are just a few of many that one could pursue following the research described in this thesis. While polymer physics has been studied for over half of a century there are still innumerous questions that remain to be answered due to the complex nature of polymers and polymeric fluids. Single-molecule techniques and the use of DNA as a model system for studying polymer physics have opened the doors for directly probing many fundamental problems in

polymer science that previously could only be postulated or indirectly determined. Many advances in understanding have been made since the introduction of this approach; however, given the relative newness of these experimental techniques and the complexity of polymeric fluids, there are still many problems that beg to be addressed by such an approach.

References

1. Doi, M. & Edwards, S. F. (1986) *The theory of polymer dynamics* (Oxford University Press, Oxford).

2. McLeish, T. C. B. (2002) *Advances in Physics* **51,** 1379-1527.

3. Hu, X. D., Jenkins, S. E., Min, B. G., Polk, M. B. & Kumar, S. (2003) *Macromolecular Materials and Engineering* **288,** 823-843.

4. Winkler, R. G., Mussawisade, K., Ripoll, M. & Gompper, G. (2004) *J. Phys.: Condens. Matter* **16,** S3941-S3954.

5. Tao, Y.-G., Otter, W. K. d. & Padding, J. T. (2005) *Journal of Chemical Physics* **122,** 244903.

6. Klein, J. (1986) *Macromolecules* **19,** 105-118.

7. McLeish, T. C. B. & Larson, R. G. (1998) *Journal of Rheology* **42,** 81-110.

8. Iyer, B. V. S., Lele, A. K. & Juvekar, V. A. (2006) *Physical Review E* **74,** 021805.

9. Rouse, P. E. (1953) *Journal of Chemical Physics* **21**, 7, 1272-1280.

10. Zimm, B. H. (1956) *Journal of Chemical Physics* **24**, 2, 269-278.

11. Flory, P. J. (1949) *Journal of Chemical Physics* **17**, 3, 303-310.

12. de Gennes, P. G. (1979) *Scaling concepts in polymer physics* (Cornell University Press, Ithaca, N.Y.).

13. Larson, R. G. (1998) *The Structure and Rheology of Complex Fluids* (Oxford University Press, Oxford).

14. Colby, R. H. & Rubinstein, M. (1990) *Macromolecules* **23,** 2753-2757.

15. Heo, Y. & Larson, R. G. (2005) *Journal of Rheology* **49,** 1117-1128.

16. Longuethiggins, H. C. & Zimm, B. H. (1960) *Journal of Molecular Biology* **2,** 1-4.

17. Zimm, B. H. & Crothers, D. M. (1962) *Proc. Natl. Acad. Sci. U.S.A.* **48,** 905-911.

18. Crothers, D. M. & Zimm, B. H. (1960) *Journal of Molecular Biology* **2,** 1-4.

19. Pecora, R. (1991) *Science* **251,** 893-898.

20. Jary, D., Sikorav, J. L. & Lairez, D. (1999) *Europhysics Letters* **46,** 251-255.

21. Bustamante, C., Marko, J. F., Siggia, E. D. & Smith, S. (1994) *Science* **265,** 1599-1600.

22. Marko, J. F. & Siggia, E. D. (1995) *Physical Review E* **52,** 2912-2938.

23. Invitrogen Technical Note #Y3601.

24. Smith, D. E., Perkins, T. T. & Chu, S. (1996) *Macromolecules* **29,** 1372-1373.

25. Shaqfeh, E. S. G. (2005) *Journal of Non-Newtonian Fluid Mechanics* **130,** 1-28.

26. Perkins, T. T., Smith, D. E. & Chu, S. (1994) *Science* **264,** 819-822.

27. Rickgauer, J. P. & Smith, D. E. (2007) in *Soft Matter: Scattering, Imaging and Manipulation*, eds. Pecora, R. & Borsali, R. (Springer, New York).

28. Perkins, T. T., Smith, D. E., Larson, R. G. & Chu, S. (1995) *Science* **268,** 83-87.

29. Quake, S. R., Babcock, H. & Chu, S. (1997) *Nature (London)* **388,** 151-154.

30. Meiners, J. C. & Quake, S. R. (2000) *Physical Review Letters* **84,** 5014-5017.

31. Schroeder, C. M., Babcock, H. P., Shaqfeh, E. S. G. & Chu, S. (2003) *Science* **301,** 1515-1519.

32. Schroeder, C. M., Teixeira, R. E., Shaqfeh, E. S. G. & Chu, S. (2005) *Macromolecules* **38,** 1967-1978.

33. Gerashchenko, S., Chevallard, C. & Steinberg, V. (2005) *Europhysics Letters* **71,** 221-227.

34. Maniatis, T., Sambrock, J. & Fritsch, R. (1989) *Molecular Cloning: A Laboratory Manual* (Cold Spring Harbor Laboratory, Cold Spring Harbor, NY).

35. Shizuya, H., Birren, B., Kim, U. J., Mancino, V., Slepak, T., Tachiiri, Y. & Simon, M. (1992) *Proc. Natl. Acad. Sci. U.S.A.* **89,** 8794-8797.

36. Epicentre-Biotechnologies Technical Note #179: EZ-Tn5 <oriV/KAN-2> Insertion.

37. Wild, J., Hradecna, Z. & Szybalski, W. (2002) *Genome Res.* **12,** 1434-1444.

38. Kent, W. J. (2002) *Genome Res.* **12,** 656-664.

39. Smith, D. E., Perkins, T. T. & Chu, S. (1995) *Physical Review Letters* **75,** 4146-4149.

40. Smith, S. B., Aldridge, P. K. & Callis, J. B. (1989) *Science* **243,** 203-206.

41. Alberts, B. (2002) *Molecular biology of the cell* (Garland Science, New York).

42. Jagodzinski, O., Eisenriegler, E. & Kremer, K. (1992) *J Phys I France* **2,** 2243-2279.

43. Koniaris, K. & Muthukumar, M. (1991) *Journal of Chemical Physics* **95,** 4, 2873-2881.

44. Shimamura, M. K. & Deguchi, T. (2001) *Phys Rev E* **64,** 020801.

45. Prentis, J. J. (1982) *Journal of Chemical Physics* **76,** 3, 1574-1583.

46. Schaub, B. & Creamer, D. B. (1987) *Phys Lett A* **121,** 9, 435-442.

47. Muller, M., Wittmer, J. P. & Cates, M. E. (1996) *Phys Rev E* **53,** 5, 5063-5074.

48. Smith, D. E., Perkins, T. T. & Chu, S. (1996) *Macromolecules* **29**, 4, 1372-1373.

49. Johannesson, H., Creamer, D. B. & Schaub, B. (1987) *J Phys A: Math Gen* **20,** 5071-5078.

50. Moore, N. T., Lua, R. C. & Grosberg, A. Y. (2004) *Proc. Natl. Acad. Sci. U.S.A.* **101,** 37, 13431-13435.

51. Duval, M., Lutz, P. & Strazielle, C. (1985) *Makromol Chem, Rapid Commun* **6,** 71-76.

52. Hodgson, D. F. & Amis, E. J. (1991) *Journal of Chemical Physics* **95,** 10, 7653-7663.

53. Bensafi, A., Maschke, U. & Benmouna, M. (2000) *Polym Int* **49,** 175-183.

54. Fukatsu, M. & Kurata, M. (1966) *Journal of Chemical Physics***, 44**, 12, 4539-4545.

55. Higgins, J. S., Ma, K. & Nicholson, L. K. (1983) *Polymer* **24**, 793-799.

56. Griffiths, P. C. & Stilbs, P. (1995) *Journal of Physical Chemistry* **99,** 16752-16756.

57. Voordouw, G., Kam, Z., Borochov, N. & Eisenberg, H. (1978) *Biophysical Chemistry* **8,** 171-189.

58. Burchard, W. & Schmidt, M. (1981) *Macromolecules* **14,** 210-211.

59. Vologodskii, A. V. & Cozzarelli, N. R. (1994) *Annu Rev Biophys Biomol Struct* **23,** 609-643.

60. Dean, F. B., Stasiak, A., Koller, T. & Cozzarelli, N. R. (1985) *J Biol Chem* **260,** 4975-4983.

61. Morgan, R., Calvet, C., Demeter, M., Agra, R. & Kong, H. (2000) *Biological Chemistry* **381,** 1123-1125.

62. Efron, B. & Tibshirani, R. (1991) *Science* **253,** 390-395.

63. Cocco, S., Marko, J. F., Monasson, R., Sarkar, A. & Yan, J. (2003) *Eur Phys J E Soft Matter* **10,** 249-263.

64. Marko, J. F. & Siggia, E. D. (1995) *Physical Review E* **52,** 2912-2938.

65. Stigter, D. (1977) *Biopolymers* **16,** 1435-1448.

66. Toan, N. M. & Micheletti, C. (2006) *Journal of Physics-Condensed Matter* **18,** S269-S281.

67. Bao, X. Y. R., Lee, H. J. & Quake, S. R. (2003) *Physical Review Letters* **91,** 265506.

68. Bloomfield, V. & Zimm, B. H. (1966) *Journal of Chemical Physics* **44,** 1, 3104-3108.

69. Naghizadeh, J. & Sotobayashi, H. (1974) *Journal of Chemical Physics***, 60,** 8, 3104-3108.

70. Chen, Y. (1981) *Journal of Chemical Physics* **75,** 10, 5160-5163.

71. Chen, Y. (1981) *Journal of Chemical Physics* **74,** 3, 2034-2038.

72. Bernal, J. M. G., Tirado, M. M., Freire, J. J. & Torre, J. G. d. l. (1991) *Macromolecules* **24,** 593-598.

73. Zifferer, G. & Preusser, W. (2001) *Macromolecular Theory and Simulations* **10,** 5, 397-407.

74. Shen, Y. & Zhang, L. (2005) *Journal of Polymer Science: B* **43,** 223-232.

75. Higgins, J. S., Dodgson, K. & Semlyen, J. A. (1979) *Polymer* **20,** 553-558.

76. Roovers, J. (1985) *Journal of Polymer Science: B* **23,** 1117-1126.

77. Lutz, P., McKenna, G. B., Rempp, P. & Strazielle, C. (1986) *Makromol Chem, Rapid Commun* **7,** 599-605.

78. Harpst, J. A. & Dawson, J. R. (1989) *Biophysical Journal* **55,** 1237-1249.

79. Vinograd, J. & Lebowitz, J. (1966) *Journal of General Physiology* **49,** 103-125.

80. Dawson, J. R. & Harpst, J. A. (1971) *Biopolymers* **10,** 2499-2508.

81. Liu, M. K. & Giddings, J. C. (1993) *Macromolecules* **26,** 3576-3588.

82. Langowski, J. & Giesen, U. (1989) *Biophysical Chemistry* **34,** 9-18.

83. Seils, J. & Pecora, R. (1995) *Macromolecules* **28**, 3, 661-673.

84. Fishman, D. M. & Patterson, G. D. (1996) *Biopolymers* **38,** 535-552.

85. Langowski, J., Geisen, U. & Lehmann, C. (1986) *Biophysical Chemistry* **25,** 191-200.

86. Weil, R. & Vinograd, J. (1963) *Proceedings of the National Academy of Sciences U.S.A.* **50,** 730-738.

87. Larsson, A., Carlsson, C., Jonsson, M. & Albinsson, N. (1994) *Journal of the American Chemical Society* **116,** 8459-8465.

88. Rye, H. S., Yue, S., Wemmer, D. E., Quesada, M. A., Haugland, R. P., Mathies, R. A. & Glazer, A. N. (1992) *Nucleic Acids Research* **20,** 2803-2812.

89. Bauer, W. & Vinograd, J. (1968) *Journal of Molecular Biology* **33,** 141-171.

90. Keller, W. & Wendel, I. (1974) *Cold Spring Harbor Symposia on Quantitative Biology* **39,** 199-208.

91. Espejo, R. T. & Lebowitz, J. (1976) *Analytical Biochemistry* **72,** 95-103.

92. McLeish, T. (2002) *Science* **297,** 2005-2006.

93. Manning, G. S. (1978) *Quarterly Reviews of Biophysics* **11,** 179-246.

94. Stigter, D. (1977) *Biopolymers* **16,** 1435-1448.

95. Rau, D. C. & Parsegian, V. A. (1992) *Biophysical Journal* **61,** 246-259.

96. Baumann, C. G., Bloomfield, V. A., Smith, S. B., Bustamante, C., Wang, M. D. & Block, S. M. (2000) *Biophysical Journal* **78,** 1965-1978.

97. Voordouw, G., Kam, Z., Borochov, N. & Eisenberg, H. (1978) *Biophys Chem* **8,** 171-89.

98. Langowski, J. & Giesen, U. (1989) *Biophysical Chemistry* **34,** 9-18.

99. Fishman, D. M. & Patterson, G. D. (1996) *Biopolymers* **38,** 535-552.

100. Seils, J. & Pecora, R. (1995) *Macromolecules* **28,** 661-673.

101. Scalettar, B. A., Hearst, J. E. & Klein, M. P. (1989) *Macromolecules* **22,** 4550-4559.

102. Brown, S. & Szamel, G. (1998) *Journal of Chemical Physics* **109,** 6184-6192.

103. Muller, M., Wittmer, J. P. & Cates, M. E. (2000) *Physical Review E* **61,** 4078-4089.

104. Cosgrove, T., Turner, M. J., Griffiths, P. C., Hollingshurst, J., Shenton, M. J. & Semlyen, J. A. (1996) *Polymer* **37,** 1535-1540.

105. von Meerwall, E., Ozisik, R., Mattice, W. L. & Pfister, P. M. (2003) *Journal of Chemical Physics* **118,** 3867-3873.

106. Tead, S. F., Kramer, E. J., Hadziioannou, G., Antonietti, M., Sillescu, H., Lutz, P. & Strazielle, C. (1992) *Macromolecules* **25,** 3942-3947.

107. Mills, P. J., Mayer, J. W., Kramer, E. J., Hadziioannou, G., Lutz, P., Strazielle, C., Rempp, P. & Kovacs, A. J. (1987) *Macromolecules* **20,** 513-518.

108. Griffiths, P. C., Stilbs, P., Yu, G. E. & Booth, C. (1995) *Journal of Physical Chemistry* **99,** 16752-16756.

109. Alon, U. & Mukamel, D. (1997) *Physical Review E* **55,** 1783-1793.

110. Smith, S. B., Heller, C. & Bustamante, C. (1991) *Biochemistry* **30,** 5264-5274.

111. Mickel, S., Arena, V. & Bauer, W. (1977) *Nucleic Acids Research* **4,** 1465-1482.

112. Serwer, P. & Hayes, S. J. (1987) *Electrophoresis* **8,** 244-246.

113. Levene, S. D. & Zimm, B. H. (1987) *Proceedings of the National Academy of Sciences U.S.A.* **84,** 4054-4057.

114. Lin, Y. W., Huang, M. F. & Chang, H. T. (2005) *Electrophoresis* **26,** 320-330.

115. Tegenfeldt, J. O., Prinz, C., Cao, H., Huang, R. L., Austin, R. H., Chou, S. Y., Cox, E. C. & Sturm, J. C. (2004) *Analytical and Bioanalytical Chemistry* **378,** 1678-1692.

116. Turner, S. W., Perez, A. M., Lopez, A. & Craighead, H. G. (1998) *Journal of Vacuum Science & Technology B* **16,** 3835-3840.

117. Wang, M. & Lai, E. (1995) *Electrophoresis* **16,** 1-7.

118. Duke, T. A. J. & Viovy, J. L. (1992) *Physical Review Letters* **68,** 542-545.

119. Volkmuth, W. D., Duke, T., Wu, M. C., Austin, R. H. & Szabo, A. (1994) *Physical Review Letters* **72,** 2117-2120.

120. von Meerwall, E. D., Amis, E. J. & Ferry, J. D. (1985) *Macromolecules* **18,** 260-266.

121. Amis, E. J. & Han, C. C. (1982) *Polymer* **23,** 1403-1406.

122. von Meerwall, E. D., Grigsby, J., Tomich, D. & Vanantwerp, R. (1982) *Journal of Polymer Science Part B-Polymer Physics* **20,** 1037-1053.

123. Kolinski, A., Skolnick, J. & Yaris, R. (1987) *Journal of Chemical Physics* **86,** 7164-7173.

124. Kreer, T., Baschnagel, J., Muller, M. & Binder, K. (2001) *Macromolecules* **34,** 1105-1117.

125. Graessley, W. W. (1982) *Advances in Polymer Science* **47,** 67-117.

126. Muller, M., Wittmer, J. P. & Cates, M. E. (1996) *Physical Review E* **53,** 5063-5074.

127. Ozisik, R., Doruker, P., Mattice, W. L. & von Meerwall, E. D. (2000) *Computational and Theoretical Polymer Science* **10,** 411-418.

128. Ozisik, R., von Meerwall, E. D. & Mattice, W. L. (2002) *Polymer* **43,** 629-635.

129. Cosgrove, T., Griffiths, P. C., Hollingshurst, J., Richards, R. D. C. & Semlyen, J. A. (1992) *Macromolecules* **25,** 6761-6764.

130. McKenna, G. B., Hadziioannou, G., Lutz, P., Hild, G., Strazielle, C., Straupe, C., Rempp, P. & Kovacs, A. J. (1987) *Macromolecules* **20,** 498-512.

131. Orrah, D. J., Semlyen, J. A. & Rossmurphy, S. B. (1988) *Polymer* **29,** 1452-1454.

132. Teixeira, R. E., Dambal, A. K., Richter, D. H., Shaqfeh, E. S. G. & Chu, S. (2007) *Macromolecules* **40,** 2461-2476.

133. Because D_0 and thus R_G were measured for stained molecules which have a contour length ~1.35 times that of native DNA (24), the R_G values used in the equation for c^* had to be scaled to the length of a native DNA molecule to achieve an accurate c^* value for the unstained molecules. This was done by using the relationship $(R_{G,unstained}/R_{G,stained}) = (L_{unstained}/L_{stained})^{\nu}$ where $\nu \cong 0.58$ is the measured scaling exponent from Chapter 3.

134. Kremer, K. & Grest, G. S. (1990) *Journal of Chemical Physics* **92,** 5057-5086.

135. Zhou, Q. & Larson, R. G. (2006) *Macromolecules* **39,** 6737-6743.

136. Montfort, J. P., Marin, G. & Monge, P. (1984) *Macromolecules* **17,** 1551-1560.

137. Archer, L. A., Sanchez-Reyes, J. & Juliani (2002) *Macromolecules* **35,** 10216-10224.

138. Mhetar, V. & Archer, L. A. (1999) *Journal of Non-Newtonian Fluid Mechanics* **81,** 71-81.

139. Fuller, D. N., Gemmen, G. J., Rickgauer, J. P., Dupont, A., Millin, R., Recouvreux, P. & Smith, D. E. (2006) *Nucleic Acids Research* **34,** e15.

140. Rickgauer, J. P., Fuller, D. N. & Smith, D. E. (2006) *Biophysical Journal* **91,** 4253-4257.

141. Mao, H., Arias-Gonzalez, J. R., Smith, S. B., Tinoco, I. & Bustamante, C. (2005) *Biophysical Journal* **89,** 1308-1316.

142. Hur, J. S., Shaqfeh, E. S. G., Babcock, H. P., Smith, D. E. & Chu, S. (2001) *Journal of Rheology* **45,** 421-450.

143. Putz, M., Kremer, K. & Grest, G. S. (2000) *Europhysics Letters* **49,** 735-741.

144. Likhtman, A. E. & McLeish, T. C. B. (2002) *Macromolecules* **35,** 6332-6343.

145. Sanchez-Reyes, J. & Archer, L. A. (2002) *Macromolecules* **35,** 5194-5202.

146. Roovers, J. (1985) *Macromolecules* **18,** 1359-1361.

147. Roovers, J. (1988) *Macromolecules* **21,** 1517-1521.

148. Cates, M. E. & Deutsch, J. M. (1986) *Journal De Physique* **47,** 2121-2128.

149. Obukhov, S. P., Rubinstein, M. & Duke, T. (1994) *Physical Review Letters* **73,** 1263-1266.

150. Karayiannis, N. C. & Mavrantzas, V. G. (2005) *Macromolecules* **38,** 8583-8596.

151. Everaers, R., Sukumaran, S. K., Grest, G. S., Svaneborg, C., Sivasubramanian, A. & Kremer, K. (2004) *Science* **303,** 823-826.

152. Kremer, K., Sukumaran, S. K., Everaers, R. & Grest, G. S. (2005) *Computer Physics Communications* **169,** 75-81.

153. Sukumaran, S. K., Grest, G. S., Kremer, K. & Everaers, R. (2005) *Journal of Polymer Science Part B-Polymer Physics* **43,** 917-933.

154. Sen, S., Kumar, S. K. & Keblinski, P. (2005) *Macromolecules* **38,** 650-653.

155. Marrucci, G. (1996) *Journal of Non-Newtonian Fluid Mechanics* **62,** 279-289.

156. Mead, D. W., Larson, R. G. & Doi, M. (1998) *Macromolecules* **31,** 7895-7914.

157. Ianniruberto, G. & Marrucci, G. (1996) *Journal of Non-Newtonian Fluid Mechanics* **65,** 241-246.

158. Muller, R., Pesce, J. J. & Picot, C. (1993) *Macromolecules* **26,** 4356-4362.

159. Sundin, O. & Varshavsky, A. (1981) *Cell* **25,** 659-669.

160. Crisona, N. J., Kanaar, R., Gonzalez, T. N., Zechiedrich, E. L., Klippel, A. & Cozzarelli, N. R. (1994) *Journal of Molecular Biology* **243,** 437-457.

161. Dean, F. B., Stasiak, A., Koller, T. & Cozzarelli, N. R. (1985) *Journal of Biological Chemistry* **260,** 4975-4983.

162. Wasserman, S. A. & Cozzerelli, N. R. (1991) *Journal of Biological Chemistry* **266,** 20567-20573.

163. Stasiak, A., Katritch, V., Bednar, D., Michoud, D. & Dubochet, J. (1996) *Nature* **384,** 6605, 122.

164. Shimamura, M. K. & Deguchi, T. (2001) *Physical Review E* **64,** 020801.

165. Shimamura, M. K. & Deguchi, T. (2002) *Physical Review E* **65,** 051802.

166. Lai, P.-Y. (2002) *Physical Review E* **66,** 021805.

167. Paul, D. R. & Barlow, J. W. (1980) *Polymer Reviews* **18,** 109-168.

168. Zhao, L. & Choi, P. (2006) *Materials and Manufacturing Processes* **12,** 135-142.

169. Utracki, L. A. & Kamal, M. R. (2002) *Polymer Blends Handbook* (Kluwer Academic Publishers, Dordrecht, Netherlands).

170. Haley, J. C. & Lodge, T. P. (2005) *Journal of Rheology* **49,** 1277-1302.

171. McKenna, G. B. & Plazek, D. J. (1986) *Polymer Communications* **27,** 304-306.